Active Site Studies of a Thermophilic Dehydrogenase

Natascha Hotz

A Thesis

In the Department

of

Chemistry and Biochemistry

Presented in Partial Fulfillment of the Requirements

For the Degree of Master of Science at

Concordia University

Montreal, Quebec, Canada

December 2010

CONCORDIA UNIVERSITY

School of Graduate Studies

This is to certify that the thesis prepared

By: Natascha Hotz

Entitled: Active Site Studies of a Thermophilic Dehydrogenase

and submitted in partial fulfillment of the requirements for the degree of

Master of Science (Chemistry)

complies with the regulations of the University and meets the accepted standards with respect to originality and quality.

Signed by the final examining committee:

______________________ Chair

______________________ Examiner
Dr. Peter Pawelek

______________________ Examiner
Dr.Paul Joyce

______________________ Supervisor
Dr. Joanne Turnbull

Approved by ______________________
Chair of Department or Graduate Program Director

______________ Date

______________________ Dean of Faculty

Abstract

Active Site Studies of a Thermophilic Dehydrogenase

Natascha Hotz

Prephenate dehydrogenase (PD) is one enzyme within the family of TyrA proteins dedicated to the biosynthesis of L-tyrosine (L-Tyr). It catalyzes the NAD^+-dependent oxidative decarboxylation of prephenate to hydroxyphenylpyruvate (HPP), which then undergoes transamination to L-Tyr, a feedback inhibitor of the enzyme. Guided by the recent crystal structures of a monofunctional PD from the hyperthermophilic bacterium *Aquifex aeolicus* in complex with active site ligands (63), residues were targeted for mutagenesis and the variant proteins were characterized by kinetic, biophysical and computational methods as an attempt to provide insight into how these residues participate in the catalytic mechanism and mode of regulation of *A. aeolicus* PD. We identified H205, a highly conserved residue, as an important catalytic group which likely maintains H147 in a catalytically competent conformation via a hydrogen bonding network, whereas electrostatic interactions afforded by D206 appear critical for the overall stability of the enzyme. We demonstrated that S254 is critical for feedback inhibition by L-Tyr, likely mediated by a hydrogen bonding network involving S254, T152, H217 and water. Moreover, R250 and K246 act in an additive fashion to facilitate the binding of prephenate to the enzyme. The combination of substrates and L-Tyr with the enzyme was further probed using fluorescence emission quenching, equilibrium dialysis and isothermal titration microcalorimetry. The latter technique revealed that L-Tyr binds with very high affinity to the native enzyme and that the combination is enthalpy driven. Perturbations in the binding of L-Tyr are further highlighted for selected variant proteins. .

Acknowledgments

I would like to thank my supervisor Dr. Joanne Turnbull for her guidance, support and excellent advice throughout the last two years. It was great having you as supervisor because you trusted me, respected me and constantly pushed me to be the best I can be. Working with you enhanced my educational but also my personal development in many ways. I am grateful to Concordia University and to PROTEO for graduate scholarships to ease the financial burden of international tuition fees.

I would also like to thank my committee members Drs. Paul Joyce and Peter Pawelek for their suggestions, help and support with my research. Additionally, Drs. Judith and Jack Kornblatt were invaluable for assistance with ITC experiments and Dr. Lamoureux with the docking experiments. I would like to thank all the members of my lab and I am honoured that I had the chance to get to know you and to work with you, and I am grateful for all the fun times we had together. I would like to take the opportunity to sincerely thank my parents and all my family who loved and encouraged me throughout my whole life and who supported my decision to do my masters studies in Montreal even if this meant being separated by 6000 km. A special thank you for my “Babily” who was my home and family here and gave me all the support I needed when I was ready to give up. Lastly, I would like to thank all my friends--the ones I left behind, for their continuous interest and support, but also those I got to know here and who made my time in Montréal a very special experience.

Table of Contents

List of Figures .... **vii**

List of Tables .... **viii**

List of Abbreviations .... **ix**

Chapter 1: Introduction **1**

1.1 Aromatic Amino Acids Biosynthesis 1

1.2 The TyrA Protein Family 6

1.3 PD within the Bifunctional CM-PD from *E. coli* 8

1.4 Proposed Mechanism for Prephenate Dehydrogenase 9

1.5 L-Tyr Feedback Inhibition in *E. coli* CM-PD 14

1.6 Crystallographic Studies of Different TyrA proteins 15

1.7 Prephenate Dehydrogenase from *Aquifex aeolicus* 18

1.8 Research Objective 24

Chapter 2: Materials and Methods **27**

2.1. Materials 27

2.2. Strains and Plasmids 28

2.3. Bacterial Growth Media 28

2.4. Site-Directed Mutagenesis 29

2.5. Transformation 32

2.6. Agarose Gel Electrophoresis 33

2.7. Expression and Purification of Δ19PD Proteins 33

2.8. Determination of Protein Concentration 35

2.9. Polyacrylamide Gel Electrophoresis 35

2.10. ESI-ToF Mass Spectrometry 36

2.11. Determination of Enzyme Activities and Kinetic Parameters 37

2.12. Determination of the Effect of L-Tyr on Δ19PD Activity 39

2.13. Far-UV Circular Dichroism Spectroscopy 41

2.14. Fluorescence Spectroscopy 42

2.15. Determination of Dissociation Constants for Substrates and Substrate Analogs by Intrinsic Fluorescence Emission 43
2.16. Equilibrium Dialysis 46
2.17. Isothermal Titration Calorimetry 48
2.18. Molecular Modelling 49

Chapter 3: Results 51
3.1 Site-Directed Mutagenesis 51
3.2 Expression and Purification of *A. aeolicus* Δ19PD Variant Proteins 51
3.3 Electrospray Ionization Mass Spectrometry 55
3.4 Far-UV Circular Dichroism Spectra of Δ19PD Proteins 57
3.5 Kinetic Studies of Native Δ19PD and Variants 59
3.5.1. Determination of Steady-State Kinetic Parameters...59
3.5.2. Effects of L-Tyr on PD activity of Native and Variant *A. aeolicus* Δ19PD proteins 63
3.5.3. Pattern of Inhibition by L-Tyr of Native Δ19PD and T152P.................................66
3.6 Dependence of pH on the Ionization of Active Site Residues..............................69
3.7 Determination of Dissociation Constants for Substrates and Inhibitor 73
3.7.1. Isothermal Titration Calorimetry (ITC) 73
3.7.2. Fluorescence Quenching Assays..76
3.7.3. Equilibrium Dialysis 80
3.8 Molecular Docking of Prephenate in the Active Site of Δ19PD from *A. aeolicus* 82

Chapter 4: Discussion..89

Chapter 5: Summary and Future Work 110

References 114

List of Figures

Figure 1: The pathway for aromatic amino acid biosynthesis. 2
Figure 2: Biosynthesis of L-Tyr and L-prephenate via the common pathway....................4
Figure 3: Proposed mechanism for the prephenate dehydrogenase-catalyzed reaction. 10
Figure 4: Multiple sequence alignment of PD domains of TyrA proteins. 13
Figure 5: Crystal structure of *A. aeolicus* Δ19PD complexed with $NADH^+$ and HPP, pH 7.8..........17
Figure 6: Selected active site residues of A. aeolicus Δ19PD complexed with NAD+ at pH 3.2 with prephenate modeled in the active site. 22
Figure 7: Selected active site residues of A. aeolicus Δ19PD complexed with NAD+ and (A) HPP or (B) L-Tyr at pH 7.8....................23
Figure 8: SDS-PAGE analysis of a native Δ19PD purification 53
Figure 9: SDS-PAGE analysis of purified Δ19PD proteins....................54
Figure 10: SDS-PAGE analysis of Δ19 PD D206A purification....................55
Figure 11: Deconvoluted ESI-MS spectra of the native Δ19 PD thrombin-treated protein...............55
Figure 12: Far-UV CD spectra of native and variant Δ19PDs....................58
Figure 13: Effect of L-Tyr on PD activity of Δ19PD proteins....................65
Figure 14: Double reciprocal plot of the inhibition of *A. aeolicus* Δ19PD by L-Tyr at 55ºC 68
Figure 15: Fluorescence emission spectra for selected Δ19PD proteins. 70
Figure 16: pH dependence of kinetic parameters and L-Tyr inhibition of the PD activity of Δ19 PD from *A. aeolicus*....................72
Figure 17: Isothermal titration calorimetry analysis of select Δ19PD proteins. 74
Figure 18: Changes in fluorescence intensity of Δ19PD upon binding of (A) NAD^+ and (B) HPP...78
Figure 19: Determination of K_d using intrinsic fluorescence quenching. 79
Figure 20: Equilibrium dialysis analysis for dissociation constant and solution stoichiometry for native Δ19PD 82
Figure 21: Active site of *A. aeolicus* Δ19PD with docked prephenate showing possible complexes 87
Figure 22: Active site of *A. aeolicus* Δ19PD W259Y complexed with NAD^+ and L-Tyr at pH 7.8..96
Figure 23: Mechanism for partial competitive inhibition observed for inhibition of T152P by L-Tyr....................98
Figure 24: Surface view of *A. aeolicus* Δ19PD-NAD^+ complex with prephenate modeled into the active site, pH 7.5....................104

List of Tables

Table 1: Primer sequences for site-directed mutagenesis of *A. aeolicus* Δ19PD................................30

Table 2: Temperature cycling parameters for PCR using *PfuTurbo* DNA polymerase......................31

Table 3: Temperature cycling parameters for PCR using *Phusion*® *HF* DNA polymerase................31

Table 4: Representative purification table for native Δ19PD 53

Table 5: Summary of molecular weights of native and variant Δ19PD proteins. 56

Table 6: Kinetics parameters for the reactions catalyzed by Δ19PD proteins 60

Table 7: Summary of IC_{50} and K_i values for the interactions of Δ19PD proteins with L-Tyr 64

Table 8: Binding parameters for native Δ19PD and selected variants obtained by ITC.....................75

List of Abbreviations

Å	Angstrom
AD	Arogenate dehydrogenase
ADT	Arogenate dehydratase
Ala (A)	Alanine
Arg (R)	Arginine
Asn (N)	Asparagine
Asp (D)	Aspartic acid
ANS	1-anilino-8-naphthalene sulfonic acid
bp	Base pair
BSA	Bovine serum albumin
CD	Circular dichroism
CM	Chorismate mutase
Da	Dalton
DNA	Deoxyribonucleic acid
EDTA	Ethylenediamine tetra-acetic acid
ESI-Q-ToF	Electrospray ionization Quadrupole Time-of-Flight
FA	Formic acid
Gdn-HCl	Guanidinium hydrochloride
Gln (Q)	Glutamine
Glu (E)	Glutamic acid
Gly (G)	Glycine
H-bond	Hydrogen bond
HEPES	4-(2-hydroxyethyl)-1-piperazineethanesulfonic acid
His (H)	Histidine
HPP	4-hydroxyphenyl pyruvate
HPpropionate	4-hydroxyphenyl propionate
Ile (I)	Isoleucine
ITC	Isothermal titration calorimetry
IPTG	Isopropyl-β-D-thiogalactopyranoside

k_{cat}	Turnover number
K_d	Dissociation constant
K_i	Inhibition constant
K_m	Michaelis constant
LB	Luria-Bertani broth
Leu (L)	Leucine
Lys (K)	Lysine
MS	Mass spectrometry
MW	Molecular weight
$NAD(P)^+$/ NAD(P)H	Oxidized/reduced nicotinamide adenine dinucleotide (phosphate)
MES	N-morpholino ethane sulphonic acid
Ni-NTA	Nickel-nitrilotriacetic acid
PCR	Polymerase chain reaction
Phe (F)	Phenylalanine
PD	Prephenate dehydrogenase
PDT	Prephenate dehydratase
PMSF	Phenylmethylsulfonyl fluoride
PP	Phenylpyruvate
Pre	Prephenate
Pro (P)	Proline
SDS-PAGE	Sodium dodecyl sulfate- polyacrylamide gel electrophoresis
Ser (S)	Serine
Thr (T)	Threonine
Tris	Tris(hydroxymethyl)aminomethane
Trp (W)	Tryptophan
Tyr (Y)	Tyrosine
U	Units
UV	Ultraviolet
Val (V)	Valine
V_{max}	Maximum velocity
WT	Wild-type

Chapter 1: Introduction

1.1 Aromatic Amino Acids Biosynthesis

The aromatic amino acids L-tyrosine (L-Tyr), L-tryptophan (L-Trp) and L-phenylalanine (L-Phe) are critical for the growth and survival of all living organisms. These compounds are not only used as building blocks for protein synthesis but also act as precursors for many important aromatic metabolites such as flavonoids (1), quinones (2,3), cyanogenic glycosides (4) and alkaloids (5,6). Archae- and eubacteria, fungi and plants are able to synthesize the aromatic amino acids via metabolic pathways denoted as the "shikimate" and "common" pathways, whereas mammals must take up these essential amino acids from their diet. Therefore, the enzymes involved in these two consecutive pathways are key targets for the design of inhibitors that can act as herbicides, fungicides or antimicrobial agents (7,8). Additionally these enzymes are widely used in bioengineering since all the aromatic amino acids are commercially valuable in the food, pharmaceutical and agricultural industries either as products themselves or as precursors for the synthesis of important compounds that include drugs and biodegradable polymers (9, 10, 11, 12).

The shikimate pathway (Figure 1) links carbohydrate metabolism to the biosynthesis of aromatic compounds (13,14). It comprises seven metabolic steps that terminate with the synthesis of the branch point intermediate chorismate. The first reaction in the shikimate pathway is the condensation of derivatives of 6-carbon sugars such as glucose, namely erythrose-4-phosphate and phosphoenol-pyruvate, to yield a 7-carbon compound 3-deoxy-D-*arabino*-heptulosonate 7-phosphate (DAHP). The reaction is catalyzed by 3-deoxy-D-*arabino*-heptulosonate 7-phosphate synthases (DAHP synthase), which is a highly regulated enzyme. During the following steps the seven carbon compound is cyclised to yield shikimate which is then converted to chorismate. Chorismate is the end product of the shikimate pathway and it serves as a precursor not only for the biosynthesis of L-Tyr and L-Phe but also for aromatic vitamins, quinones, aromatic amino acids and folates (15).

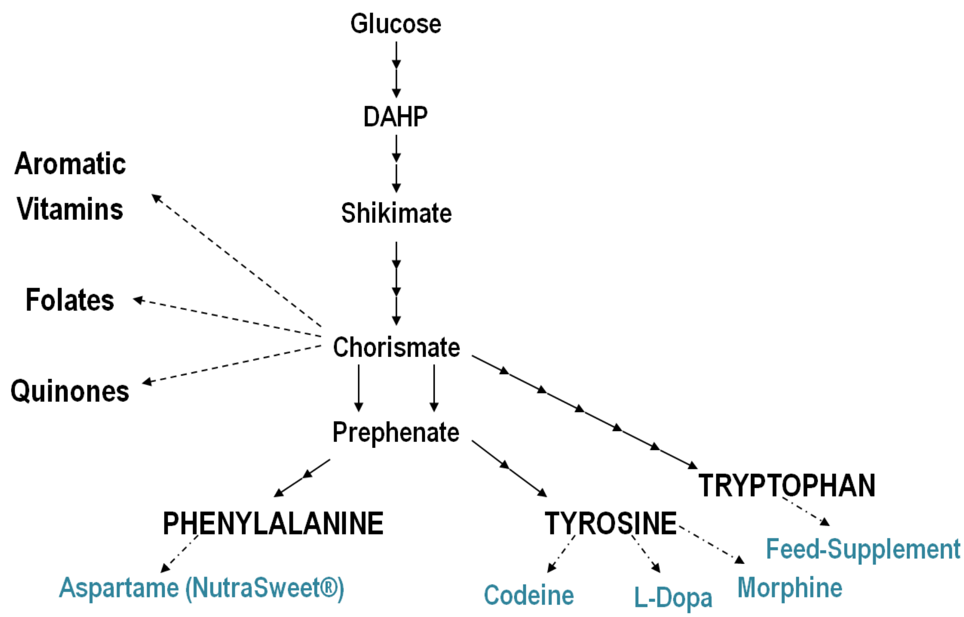

Figure 1: The pathway for aromatic amino acid biosynthesis. The shikimate pathway consisting of the first seven enzyme-catalyzed steps ending in the production of chorismate; DHAP denotes 3-deoxy-D-arabino-heptulosonate

The biosynthesis of L-Tyr and L-Phe occurs via the common pathway (Figure 2). First, chorismate undergoes a Claisen rearrangement to prephenate, catalyzed by chorismate mutase (CM). Depending on the end product, prephenate is then either oxidatively decarboxylated by prephenate dehydrogenase (PD) in the presence of NAD^+ to form *p*-hydroxyphenylpyruvate (HPP) and carbon dioxide or is dehydrated and decarboxylated by prephenate dehydratase (PDT) to form phenylpyruvate. HPP is subsequently transaminated to form L-Tyr, whereas phenylpyruvate yields L-Phe.

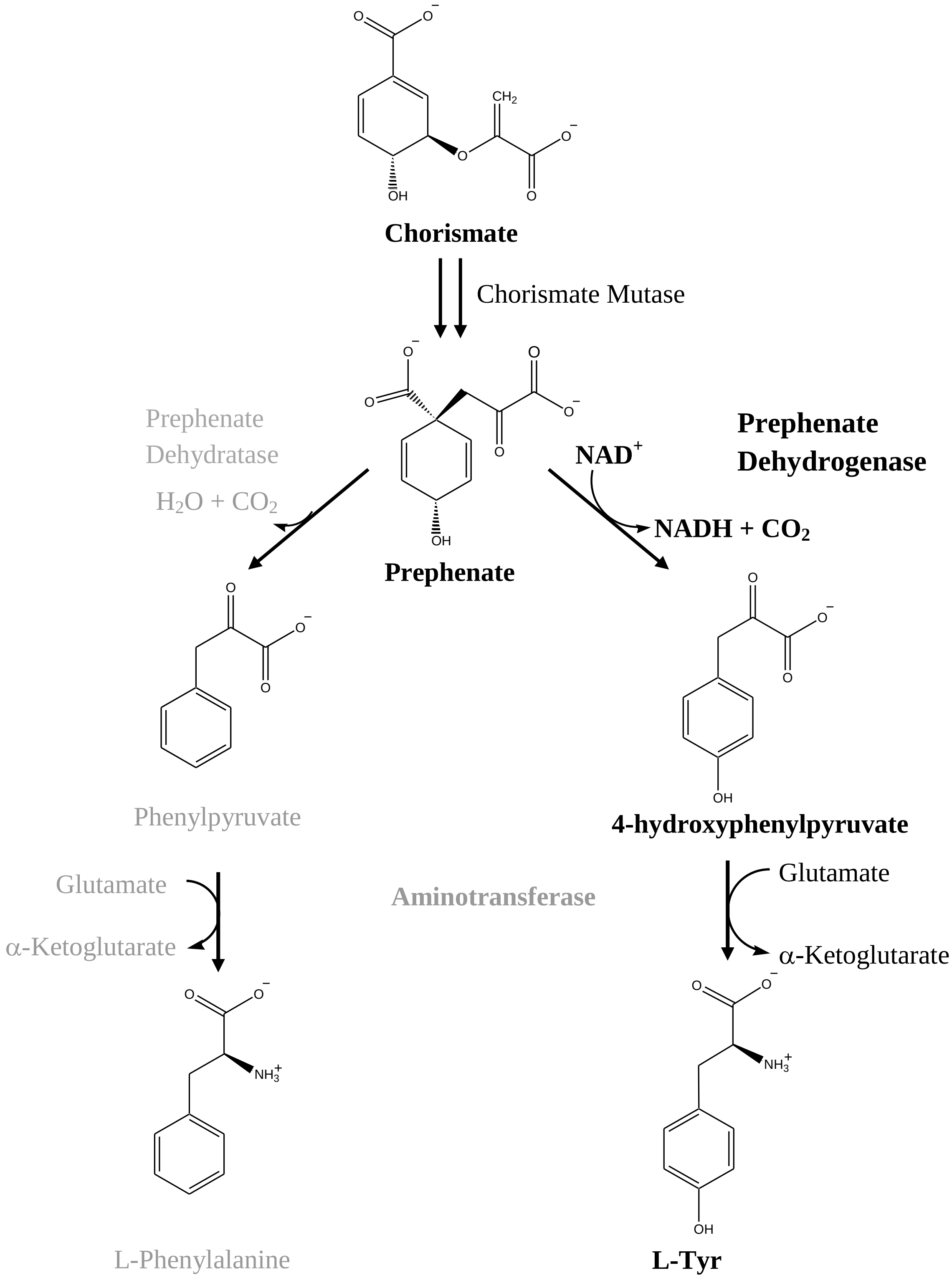

Figure 2: Biosynthesis of L-Tyr and L-prephenate via the common pathway.

Both end-products act as feed-back inhibitors of the CM-catalyzed reaction; additionally L-Tyr and L-Phe inhibit PD and PDT activities, respectively. This study focuses on the enzyme prephenate dehydrogenase, shown in bold (Figure 2).

The aromatic amino acid biosynthesis pathway is regulated at both the genetic and protein levels. Since many of the genes encoding the enzymes in the shikimate and common pathways are organized in operons they can be regulated by only three regulatory genes, tyrR, trpR and pheR (16, 17, 18). The proteins encoded by these repressors, together with the appropriate amino acid acting as co-repressors, form complexes which bind at the operator loci and therefore inhibit transcription. Additionally the pathway can be regulated through attenuation at the level of charged tRNA(s) (19). However, the most important mode of regulation is through feedback inhibition by L-Phe, L-Tyr and L-Trp. The aromatic amino acids are able to inhibit DAHP synthase at the beginning of the shikimate pathway. This enzyme exists in three isoenzyme forms, DAHP Phe, Tyr or Trp, each specific for its appropriate amino acid feedback inhibitor. As mentioned previously, at the protein level CM and PD activities can be inhibited by L-Tyr. This offers the possibility of engineering bacterial strains which lack tyrR and/or are resistant to feedback inhibition leading to over-expression of L-Tyr. As of today several L-Tyr overproduction strains have been generated. These include strains of *Corynebacterium glutamicum* and *E. coli* which express tyrosine-resistant variants of DAHP and CM-PD (20, 21). Another approach was to use an L-Phe producing strain of *E. coli* which was converted into an L-Tyr producing strain by replacing the native tyrA promoter with the trc promoter (22, 23). Chávez-Béjar *et. al.* (24).used an engineered *E. coli* strain which expressed the chorismate mutase domain of the native CM-PD and a cyclohexadienyl dehydrogenase (Tyr_C) from *Zymomonas mobilis*.

1.2 The TyrA Protein Family

The TyrA protein family is dedicated to L-Tyr biosynthesis. It consists of homologous dehydrogenases that are classified into three categories depending upon their specificities for the cyclohexadienyl substrate selected for the oxidative decarboxylation reaction (25, 26). Prephenate dehydrogenase ($TyrA_p$) uses prephenate as the sole substrate, yielding HPP which then can undergo transamination to yield L-Tyr. Another cyclohexadienyl substrate is L-arogenate which differs structurally from prephenate by the replacement of the pyruvyl side chain with an alanyl group. Formed from the transamination of prephenate, L-arogenate can be oxidatively decarboxylated to L-Tyr by arogenate dehydrogenases ($TyrA_a$) that are specific only for this substrate. The third class of dehydrogenases are cyclohexadienyl dehydrogenases ($TyrA_c$) which can efficiently utilize both, prephenate and L-arogenate, as substrates. Additionally, TyrA proteins use NAD^+ and/or $NADP^+$ as nucleotide cofactor (25). Generally, prephenate-specific dehydrogenases prefer NAD^+ as a co-substrate while arogenate-specific enzymes prefer $NADP^+$ (27, 28, 29). TyrA classes are also generally linked to distinct organisms as deduced through extensive phylogenetic analysis and sequence alignments (reviewed by Jensen and colleagues (26)): bacteria and yeast are believed to possess $TyrA_p$ or $TyrA_c$ activity while plants and a few bacteria such as cyanobacteria are $TyrA_a$ specific.

TyrA proteins always catalyze an irreversible step in L-Tyr biosynthesis, regardless of the organism in which they are found. They all share a core catalytic domain of about 30 kDa and maintain the same fundamental reaction chemistry. However, many TyrA proteins are multi-functional due to fused domains. In the following, several examples of monofunctional and multifunctional TyrA proteins will be cited. PDs from *Aquifex aeolicus* (30) and *Bacillus subtilis* (31), ADs from *Nicotiana silvestris* (32) and *Synechocystic sp.* (33), and the cyclohexadienyl dehydrogenases from *Pseudomonas stutzeri* (31) and *Zymomonas mobilis* (39) are monofunctional TyrA proteins. In contrast, prephenate dehydrogenases from *E. coli* and *Haemeophilus influenzae* are bifunctional enzymes with CM activity associated with the N-terminal region of the protein (42) while PDs from *Pseudomonas fluorescens* and *Acinetobacter calcoaceticus* are bifunctional with phosphoshikimate carboxyvinyltransferases activity at the proteins' C-terminal portion (56). Recently two trifunctional PDs have been identified, one in *Nanoarchaem equitans* and the other in *Archaeoglobus fulgidus* (34). Both enzymes possess a PD, a CM and a PDT domain. The trifunctional enzyme from the latter organism has been recombinantly expressed and purified.

While many enzymes within the TyrA protein family have been tentatively classified in a phylogenetic context using bioinformatic tools (25, 35), only a few have been purified and preliminarily characterized. These include monofunctional $TyrA_a$ from *Synechocystis sp.* (25 36), $TyrA_P$ from *Streptococcus mutans* (37) and *Mycobacterium tuberculosis* (38), $TyrA_c$ from *Z. mobilis* (39) and genetically engineered monofunctional prephenate dehydrogenases from *E. coli* (40) and *E. herbicola* (41). The most well characterized TyrA protein to date is the bifunctional CM-PD from *E. coli* which has been extensively studied using kinetic, biochemical and biophysical tools. Accordingly, this bifunctional enzyme has served as a model for the study of other TyrA proteins. (42, 43, 44, 45, 46, 47, 50).

1.3 PD within the Bifunctional CM-PD from *E. coli*

E. coli CM-PD is a homodimer with a monomer molecular weight of ~ 42 kDa (48, 49, 50). The enzyme is considered bifunctional since chorismate mutase and prephenate dehydrogenase activities are associated with each of the polypeptide chains. Alignment of the primary sequence of *E. coli* CM-PD with that of CM-PDT (the bifunctional enzyme involved in L-Phe biosynthesis) indicates that the first one-third of the polypeptide encodes the CM domain while the remaining residues specify PD activity (49). Regrettably, the crystal structure of bifunctional *E. coli* CM-PD has never been solved and therefore the exact geometry of the active site(s) at which the two reactions occur is unknown. Evidence through kinetic studies conducted under a variety of physiochemical conditions suggests that there is one active site supporting both activities (49, 50). More recent results, however, have shown selective inhibition of one activity by putative transition state analogues for each reaction which suggest that the CM and PD active sites are distinct (43, 50). Mutagenesis studies further support this latter model; single amino acid replacements of *E. coli* CM-PD can selectively eliminate mutase (K37A) or dehydrogenase activity (H197N) (46, 47). Interestingly, if the sites are separate, they may be in close proximity or within regions of the polypeptide that are structurally interdependent. This is manifested by the fact that single amino acid substitutions in the PD domain can impair both CM and PD activities (K187R, R286A/H) (47). Additionally, attempts to generate two monofunctional enzymes from the bifunctional *E. coli* parent have also been met with limited success. Ganem and colleagues (40) found that expressing the two domains independently resulted in unstable enzymes with reduced activities, again highlighting the structural interplay between different regions of the bifunctional protein. More encouraging examples of genetic engineering come from Jensen and coworkers, who reported the first characterization of an active engineered monofunctional PD from a bifunctional CM-PD in *Erwinia herbicola* (*Pantoaea agglomerans*) (41).The engineered monofunctional PD still contained over 60% of the mutase domain providing stabilizing interactions yet the kinetic parameters and response to feedback inhibition by L-Tyr were considerably altered compared to the full length CM-PD. Additionally, recent findings in the Turnbull lab have shown that purified Δ80 CM-PD from *H. influenzae* (a construct lacking the first 80 amino acids of the bifunctional protein) functions as a highly active monofunctional PD although the mutase domain appears important for the thermal and chemical stability of the engineered monofunctional enzyme (51).

1.4 Proposed Mechanism for Prephenate Dehydrogenase

A catalytic mechanism for the dehydrogenase reaction of *E. coli* CM-PD **(**Figure 3) has been proposed, supported by the results of isotope effects studies (52), peptide mapping (45), pH profiles (42, 52) and site-directed mutagenesis (46, 47). Selected studies are described below.

Prephenate dehydrogenase catalyzes the NAD^+-dependent oxidative decarboxylation of prephenate to HPP. The formation of the aromatic product, HPP, is the driving force behind this irreversible reaction. The two chemical steps of the reaction, hydrid transfer and decarboxylation, are believed to occur concomitantly, as deduced by using ^{13}C and deuterium kinetic isotope effect studies which probe the cleavage of the C-C bond in the decarboxylation step in the presence of deuterated or non-deuterated deoxyprephenate (52).

The kinetic mechanism of the dehydrogenase reaction catalyzed by *E. coli* CM-PD has also been determined. Through the analysis of steady-state initial velocity patterns, product and dead-end inhibition studies, and isotope trapping experiments, SampathKumar and Morrison showed that PD conforms to a rapid equilibrium random kinetic mechanism with catalysis as the rate-determining step in the reaction (27).

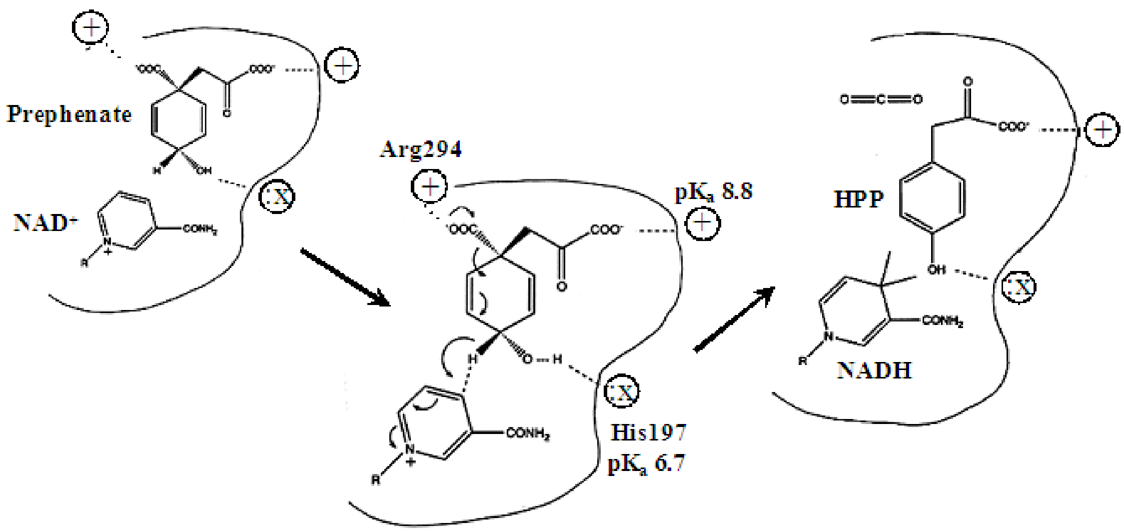

Figure 3: Proposed mechanism for the prephenate dehydrogenase-catalyzed reaction. Prephenate and NAD^+ bind to distinct sites in the active site of PD domain. The driving force for the reaction is the formation of an aromatic compound, HPP. A deprotonated group, H197, (pK_a 6.5), is believed to assist hydride transfer from the 4-hydroxyl group of prephenate to NAD^+ and concomitant decarboxylation by polarizing the 4-hydroxyl group. R294 was proposed to interact with the ring carboxylate of prephenate bound to the enzyme-NAD+ complex leaving a third protonated group (pK_a 8.8) which would likely interact with side chain carboxylate of prephenate to lock prephenate in the active site. Mechanism proposed by Christendat and Turnbull (47).

In addition, pH rate studies have been performed by Hermes *et. al.* (52) and Turnbull and colleagues (44, 46) to determine the pK_a values of residues involved in the dehydrogenase reaction of *E. coli* CM-PD. The profile for the variation of log V/E_t as a function of pH identified one ionisable group which must be deprotonated for maximum activity and is involved in catalysis and/or product release (52). In contrast, log $(V/E_t)/K_{prephenate}$ vs. pH displayed the titration of an additional residue (pK_a value ~ 8.8) which was assigned to the binding of prephenate to the enzyme-NAD^+ complex. Further studies on the effects of temperature and solvent on the pK_a values supported the hypothesis that the catalytic residue is a histidine (52). Chemical modification and peptide mapping studies confirmed that a histidine residue was located near the dehydrogenase active site, but only the results of site-directed mutagenesis guided by the analysis of multiple sequence alignments (Figure 4) successfully identified H197 as the catalytic H-bond acceptor (45, 46, 53). Conversion of H197 to asparagine completely eliminated PD activity while having little effect on the binding of prephenate and NAD^+. Additionally, this amino acid replacement did not affect chorismate mutase activity of the bifunctional enzyme nor the K_m for chorismate (46). Results from site-directed mutagenesis also revealed that an evolutionary conserved residue, R294, was important for prephenate binding since a conversion to glutamine reduced the affinity of prephenate for the enzyme-NAD^+-complex by 120-fold without affecting the catalytic activity (47). Additionally, studies on the inhibition of PD activity by several HPP analogues, modified at the C-1 position, led to the hypothesis that R294 might interact electrostatically with the ring carboxylate; all compounds which lacked the ring carboxyl group exhibited similar dissociation constants for native enzyme and the R294Q variant (47). These results are in conflict with the hypothesis of Hermes *et. al.* (52) who proposed that the ring carboxyl group might reside in a hydrophobic pocket within the enzyme to promote rapid decarboxylation in the concerted mechanism.

```
A. aeolicus              RSGFKGKIYGYDINPESISKAVDLGIIDEGTTSIAKVEDFSPDFVMLSSP 100
B. subtilis              KNHPGKRIIGIDISDEQAVAALKLGVIDDRADSFISGVKEAATVIIATPV 75
S. thermophilus          RDHPDYEILGYNRSDYSRNIALERGIVDRATGDFKEFAPLADVIILAVPI 73
H. pylori                EWGRFKSVIGYDHNALHAKLALTLGLVDECVG--FEKILECDVIFLAIPV 58
M. tuberculosis          HGARSDGFDAITDLNQTLTRAAAT-----------------EALIVLAVPM 55
E. coli                  LSGYQVRILEQHDWDRAADIVAD-----------------AGMVIVSVPI 152
H. influenzae            ASGYPISILDREDWAVAESILAN-----------------ADVVIVSVPI 154
Synechocystis sp.        RRG--HYLIGVSRQQSTCEKAVERQLVDEAGQD-LSLLQTAKIIFLCTPI 67
S. cerevisiae            DAGWGVICCDREEYYDELKEKYASAKFELVKNG-HLVSRQSDYIIYSVEA 82
                                                                    ..

A. aeolicus              VRTFREIAKKLSYILSEDATVTDQGSVKGKLVYDLENILGKR---FVGGH 147
B. subtilis              EQTLVMLEELAHSGIEHELLITDVGSTKQKVVDYADQVLPSR-YQFVGGH 124
S. thermophilus          KQTMAYLKELADLDLKDNVIITDAGSTKREIVEAAERYLTGKNVQFVGSH 123
H. pylori                EGIIGCLKKMTS--IKKSATIIDLGGAKAQIIRNIPKSIRKN---FIAAH 103
M. tuberculosis          PALPGMLAHIRKS--APGCPLTDVTSVKCAVLDEVTAAGLQAR--YVGGH 101
E. coli                  HVTEQVIGKLPP--LPKDCILVDLASVKNGPLQAMLVAHDGP---VLGLH 197
H. influenzae            NLTLETIERLKPY-LTENMLLADLTSVKREPLAKMLEVHTGA---VLGLH 200
Synechocystis sp.        QLILPTLEKLIPH-LSPTAIVTDVASVKTAIAEPASQLWSGF----IGGH 112
S. cerevisiae            SNISKIVATYGPS-SKVGTIVGGQTSCKLPEIEAFEKYLPKD-CDIITVH 130
                               :             : .  . *                  :  *

A. aeolicus              PIAGTEKSGVEYSLDNLYEGKKVILTPTKKTDKKRLKLVKRVWEDVGGVV 197
B. subtilis              PMAGSHKSGVAAAKEFLFENAFYILTPGQKTDKQAVEQLKNLLKGTNAHF 174
S. thermophilus          PMAGSHKSGAIAADVTLFENAYYIFTPTSLTKETTIPELKDILSGLKSRY 173
H. pylori                PMCGTEFYGPKASVKGLYENALVILCDLEDSGTEQVEIAKEIFLGVKARL 153
M. tuberculosis          PMTGTAHSGWTAGHGGLFNRAPWVVSVDDHVDPTVWSMVMTLALDCGAMV 151
E. coli                  PMFGPDSGSLAKQVVVWCDGRK----------PEAYQWFLEQIQVWGARL 237
H. influenzae            PMFGADIASMAKQVVVRCDGRF----------PERYEWLLEQIQIWGAKI 240
Synechocystis sp.        PMAGTAAQGIDGAEENLFVNAPYVLTPTEYTDPEQLACLRSVLEPLGVKI 162
S. cerevisiae            SLHGPKVNTEGQPLVIINHRSQY---------PESFEFVNSVMACLKSKQ 171
                         .: *.
```

```
A. aeolicus                 EYMSPELHDYVFGVVSHLPHAVAFA----LVDTLIHMSTP--EVDLFKYP 241
B. subtilis                 VEMSPEEHDGVTSVISHFPHIVAAS----LVHQTHHSENL--YPLVKRFA 218
S. thermophilus             VEIDAAEHDRVTSQISHFPHLLASG----LMEQAADYAQA--HEMTNHFA 217
H. pylori                   IKMKSNEHDTHVAYISHLPHVLSYA-----LANSVLKQND--PEMILSLA 196
M. tuberculosis             VPAKSDEHDAAAAAVSHLPHLLAEA--------LAVTAAE--VPLAFALA 191
E. coli                     HRISAVEHDQNMAFIQALRHFATFAYGLHLAEENVQLEQL--LALSSPIY 285
H. influenzae               YQTNATEHDHNMTYIQALRHFSTFANGLHLSKQPINLANL--LALSSPIY 288
Synechocystis sp.           YLCTPADHDQAVAWISHLPVMVSAA--LIQACAGEKDGDI--LKLAQNLA 208
S. cerevisiae               VYLTYEEHDKITADTQAVTHAAFLSMGSAWAKIKIYPWTLGVNKWYGGLE 221
                                   **     . .      .

A. aeolicus                 GGGFKDFTRIAKSDPIMWRDIFLENKENVMKAIEGFEKSLNHLKELIVRE 291
B. subtilis                 AGGFRDITRIASSSPAMWRDILLHNKDKILDRFDEWIREIDKIRTYVEQE 268
S. thermophilus             AGGFRDMTRIAESEPGMWASILMTNGPAVLDRIEDFKKRLDHVADLIKAE 267
H. pylori                   GGGFRDMSRLSKSSPLMWKDIFKQNRDNVLEAIKKCEKEIVQAKAWIENN 246
M. tuberculosis             AGSFRDATRVAATAPDLVRAMCEANTGQLAPAADRIIDLLSRARDSLQSH 241
E. coli                     RLELAMVGRLFAQDPQLYADIIMSS-ERNLALIKRYYKRFGEAIELLEQG 334
H. influenza                RLELAMIGRLFAQDAELYADIIMDK-SENLAVIETLKQTYDEALTFFENN 337
Synechocystis sp.           SSGFRDTSRVGGGNPELGTMMATYNQRALLKSLQDYRQHLDQLITLISNQ 258
S. cerevisiae               NVKVNISLRIYSNKWHVYAGLAITNPSAHQQILQYATSATELFSLMIDNK 271
                               .    *:      :   :   .        .            .

A. aeolicus                 -AEEELVEYLKEVKIKRMEID----------------------------- 311
B. subtilis                 -DAENLFRYFKTAKDYRDGLPLRQKGAI---------------------- 295
S. thermophilus             -DESAIWEFFDNGRKKRKEMEIHKKGGVESAFDIFVDVPDREDVILSIME 316
H. pylori                   -DYESLAEWMAQANKLQEFM------------------------------ 265
M. tuberculosis             GSIADLADAGHAARTRYDSFPRSDIVTVVIGADKWREQLAAAGRAGGVIT 291
E. coli                     -DKQAFIDSFRKVEHWFGDYAQRFQSES---------------------- 361
H. influenza                -DRQGFIDAFHKVRDWFGDYSEQFLKES---------------------- 364
Synechocystis sp.           -QWPELHRLLQQTNGDRDKYVE---------------------------- 279
S. cerevisiae               --EQELTDRLLKAKQFVFGKHTGLLLLDDTILEKYSLSKSSIGNSNNCKP 319
                                 :       .
```

Figure 4: Multiple sequence alignment of PD domains of TyrA proteins. Alignment includes sequences from several bacterial species. It includes monofunctional PDs from *Aquifex aeolicus*, *Streptococcus thermophilis, Bacillus subtilis, Heliobacter pylori*, *Mycobacterium tuberculosis* and *Saccharomyces cerevi*siae, bifunctional CM-PDs from *Escherichia coli* and *Haemophilus influenzae* and the monofunctional AD from *Synechocystis sp.* The catalytic H-bond acceptor is highlighted in yellow and the cationic Arg interacting with prephenate's carboxylate group is in green. Residues studied in this thesis are highlighted in light blue. The multiple sequence alignment was performed using ClustalW2.

1.5 L-Tyr Feedback Inhibition in *E. coli* CM-PD

L-Tyr, the end product of the pathway, acts as a feedback inhibitor of both the dehydrogenase and mutase activities of *E. coli* CM-PD. Additionally, feedback inhibition of *E. coli* CM-PD is dependent on the presence of NAD^+. Double reciprocal plots of velocity at varying prephenate concentration and fixed, increasing concentrations of L-Tyr are notably concave upward, suggestive of cooperative interactions in the binding of the end product (28, 43, 48, 50). Accordingly, there have been several models proposed to explain the effects of L-Tyr on CM-PD activity. Analytical ultracentrifugation experiments performed by Hudson *et. al.* (48) showed that dimeric *E. coli* CM-PD could exist in equilibrium with a tetrameric form, the latter stabilized by the binding of NAD^+ and L-Tyr. Additionally, the presence of NAD^+ promotes the binding of L-Tyr to the enzyme and *vice-versa* (50). In this model, prephenate was assumed to combine with the same site as prephenate and the tetramer was inactive. In contrast, kinetic and biophysical studies by Christopherson and coworkers suggested that L-Tyr combines at the same site as does prephenate but does not prompt tetramer formation. The concave upward kinetics could be explained by tertiary structural changes in the enzyme whereby the binding of an inhibitor molecule to one subunit influences the binding of a second inhibitor molecule to the other subunit (54, 28). Turnbull et. al. (44) proposed an alternate mechanism based on the results of fitting initial velocity data to several models and by analyzing the patterns of inhibition in the presence of both HPP and L-Tyr. They proposed that L-Tyr binds to an allosteric site and that an active tyrosine-enzyme-prephenate complex yields product at a much slower rate than does the enzyme-prephenate complex. Inherent in these models was the assumption that NAD^+ and L-Tyr do not induce tetramer formation at concentrations of enzyme used in kinetic assays. Interestingly, the inhibition of *A. aeolicus* PD by L-Tyr does not appear to accompany the formation of a tetramer which strengthens the hypotheses of Christopherson & Morrison (28) and Turnbull (55).

Possible residues that are involved in feedback inhibition of *E. coli* CM-PD by L-Tyr have been identified only recently. By introducing random mutations into *E. coli tyrA* using error-prone PCR and then selecting for growth on media containing the potent inhibitory L-Tyr analogue, m-fluoro-D,L-Tyr, Lütke-Eversloh and Stephanopoulos (21) identified site-specific mutations that appeared to encode variants insensitive to fluorotyrosine. These included Tyr263H, A354V and F357L within the PD domain. Follow-up studies were performed by Turnbull's group using site-directed mutagenesis guided by a model of *E. coli* PD generated from a structure for *H. influenzae* TyrA in complex with NAD^+ and L-Tyr (56, 58). Through the analysis of kinetic data, inhibition studies with L-Tyr and fluorescence binding studies with m-fluoro-D,L-Tyr, residues Tyr285 and Tyr303 were identified as the most critical for the enzyme's interaction with L-Tyr followed by H257, Q298, A354, then F357. Interestingly, those variants that were the most L-Tyr insensitive resisted tetramerization in the presence of L-Tyr and NAD^+, as deduced by size exclusion chromatography (56).

1.6 Crystallographic Studies of Different TyrA proteins

As previously mentioned, although *E. coli* CM-PD is the best characterized TyrA protein, its crystal structure has yet to be reported. Only recently have there been structures solved for TyrA--all from recombinant proteins heterologously expressed in *E. coli*. In 2006 the first structure of a prephenate dehydrogenase was reported; an Nterminally deleted form of the monofunctional PD from the hyperthermophilic bacterium *A. aeolicus* (Δ19PD) was co-crystallized with NAD^+ at pH 3.2 and yielded crystals that diffracted to 1.9 Å resolution (30, 57). Later that year, the structure of AD from *Synechocystis sp* in complex with $NADP^+$ was reported (36). Only three years later did liganded structures of Δ19PD from *A.aeolicus* become available following co-crystallization studies at pH 7.8 in the presence of NAD^+ plus either prephenate, hydroxyphenyl proprionate, a product analog, or L-Tyr (63). Most recently, the structure of the PD domain of bifunctional CM-PD from *H. influenzae* in complex with NAD^+ and L-Tyr has been published (58). Now an unpublished crystal structure of an unliganded prephenate dehydrogenase from *Streptococcus thermophilus* has also been released into the Protein Data Bank (3dzb).

Comparisons of the amino acid sequences of the PD domains of all four proteins show only 18% sequence identity between the enzymes from *A. aeolicus* and *E. coli*, a value of 32% between *A. aeolicus* and *S. thermophilus* and 29% between the PD of *A. aeolicus* and the AD of *Synechocystis sp. E. coli* and *H. influenzae PDs* show the highest sequence identity at 57%. In spite of these low to moderate primary sequence correlations the overall fold of all four crystallized enzymes is very similar. A representative structure of Δ19PD from *A. aeolicus* in complex with NAD^+ and HPP is shown in Figure 5. The enzyme is dimeric and contains within each monomer a C-terminal dimerization domain and an N-terminal nucleotide binding domain. The active site (one for each monomer) is at the interface of the two domains and encompasses amino acid residues from both monomers. Interestingly, the overall geometry of the active site of all four proteins also appears fairly well conserved including the presence of those residues that have been identified to be important for substrate binding and catalysis in *E. coli* CM-PD.

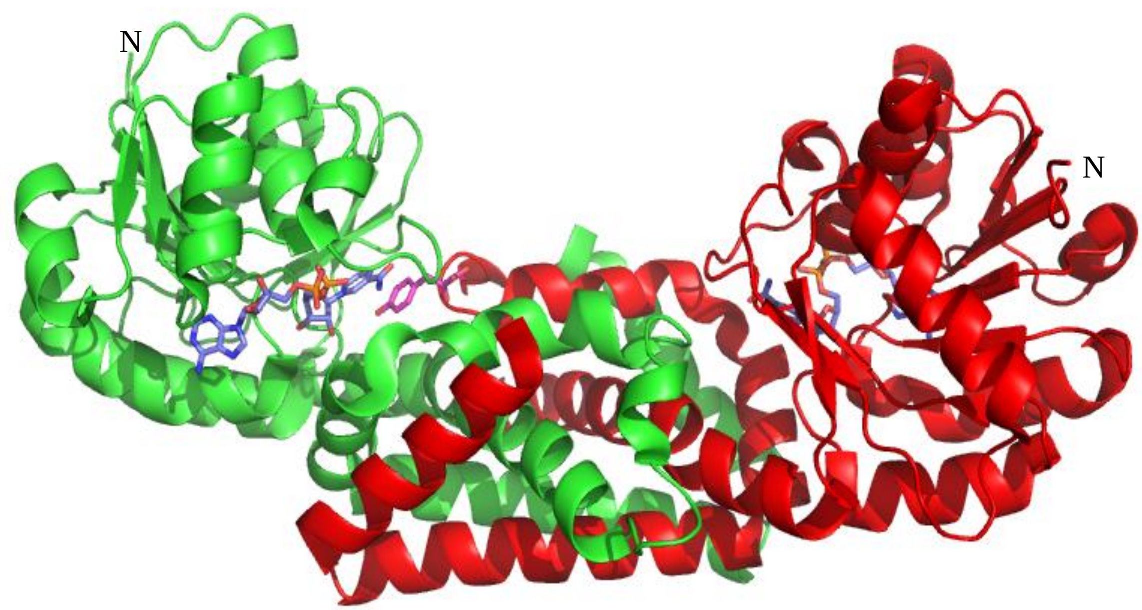

Figure 5: Crystal structure of *A. aeolicus* ∆19PD complexed with NADH^{+} and HPP, pH 7.8.
The two monomers are coloured in green and red. Each monomer can be divided into a N-terminal dinucleotide-binding domain and a C-terminal dimerization domain. NADH is represented as light blue sticks and HPP as pink sticks. This picture was created using PyMOL (62) with the coordinates derived from ref (63).

As mentioned above, H197 in *E. coli* CM-PD has been identified as the catalytic H-bond acceptor. The equivalent residue in *A. aeolicus* PD, H147, is located adjacent to the cofactor's nicotinamide ring and the C-4 position of HPP thus implicating this residue in hydride transfer from prephenate to NAD^{+}. Additionally, R250 in *A. aeolicus* PD (R294 in *E. coli* CM-PD), is located in a highly polar environment and in close proximity to the pyruvyl side chain of HPP, ideally poised to lock the product, and by inference also the substrate, in the active site. The findings of the crystallographic data are currently being probed in solution by mutagenesis studies and will be mentioned later (63).

Legrand *et. al.* (36) reported that AD from *Synechocystis* sp. strictly uses arogenate and $NADP^+$ as substrates and is presumably insensitive to feedback inhibition by L-Tyr. Crystallographic analysis of this enzyme bound with $NADP^+$ at pH 8.0, combined with amino acid sequence comparisons led these same authors to propose H112 as the catalytic H-bond acceptor, although no confirmatory mutagenesis studies have been reported. Interestingly R217, the equivalent to R294 in *E. coli* CM-PD, appears to be too far from the active site to be involved in arogenate binding. A group of five basic residues including R213 (equivalent to K246' in *A. aeolicus* PD) has also been identified in AD's crystal structure. These residues are located at the interface of the two monomers and have been proposed by Legrand and colleagues to help electrostatically guide L-arogenate to the active site. Additionally, H179, G219, G226, M228 and Tyr232 and notably G221 were proposed to participate in substrate selectivity.

The crystal structure of the PD domain of bifunctional CM-PD from *H. influenzae* bound with NAD^+ and L-Tyr (58) has also identified H200 (equivalent to H147 in *A. aeolicus* PD) and R297 (equivalent to R250 in *A. aeolicus* PD) as well as other important active residues and their roles are currently being examined by site-directed mutagenesis (51, 58).

1.7 Prephenate Dehydrogenase from *Aquifex aeolicus*

A. aeolicus is a microaerophilic, hydrogen-oxidizing, obligate chemolithautotroph organism, originally isolated from thermal vents found in Yellowstone National Park and can thrive at temperatures up to 95 °C. The entire genome has been sequenced (59) and was shown through bioinformatics analysis to contain a putative *tyrA* gene encoding a monofunctional PD. Interestingly, a gene, encoding CM-PDT (*pheA*) was identified but not a gene for a monofunctional CM.

Prephenate dehydrogenase from *A. aeolicus* is of particular interest because it was, as mentioned above, the first crystallisable protein from the TyrA family, and to date is the only protein for which a product-bound complex has been reported. The recombinantly expressed full-length PD consists of 311 amino acids and possesses a monomer molecular weight of ~35 kDa. The only form that crystallized, however, lacked the first 19 amino acids. Both enzymes were extensively studied using biophysical and biochemical analysis (30). Both forms are active as dimers and exhibited the highest activity around 95 ºC which is near the physiologically optimal growth temperature. The enzyme requires NAD^+ as a cofactor and greatly prefers prephenate as a substrate over L-arogenate. There were small but significant differences between the full length and the Δ19PD (30). Both were resistant to temperature unfolding, although the half-life at 95 °C of full-length PD was about twice that of the truncated form. A comparison of k_{cat}/K_m ratio with prephenate as the variable substrate showed that both PD forms were equally effective catalysts; however, values of the kinetic parameters for Δ19PD were twice that of PD. Both forms were sensitive to feedback inhibition by L-Tyr and displayed kinetic indicative of cooperative interactions between subunits promoted by L-Tyr, although L-Tyr plus NAD^+ did not accompany the formation of tetramers as reported for *E. coli* CM-PD (28, 48, 42). Interestingly, low concentrations of guanidine-HCl (Gdn-HCl) doubled enzyme activity as recorded at 30 °C, but at higher concentrations of Gdn-HCl, activity was lost and could be correlated with a complex denaturation process that involved oligomerization prior to forming unfolded monomers (30). *A. aeolicus* Δ19PD contains two tryptophan residues per monomer. Measurements of steady-state fluorescence intensity and its quenching by acrylamide in the presence and absence of substrates were in agreement with the crystal structure which shows that W190 is completely buried within the hydrophobic core of the Rossman fold of the NAD^+ binding domain, while W259 is partially buried within the prephenate binding pocket. Additionally, it has been determined through mutagenesis experiments that W190 is the major contributor to the Δ19PD protein fluorescence emission (30,60 61).

Further mutagenesis experiments are now being employed in the Turnbull lab, guided by crystallographic data, to probe the role of residues in the catalytic mechanism of Δ19PD. Some of the findings are outlined below. As mentioned above, H147 has been identified as the catalytic H-bond acceptor in the reaction; Turnbull, Christendat and colleagues (63) reported that the H147N variant is essentially inactive but binds prephenate with apparent affinity similar to native 19Δ PD. Additional mutagenesis studies identified S126 to be important for catalysis and prephenate binding. The findings of these studies are consistent with the structural data which show S126 as part of an H-bonding network including, H147, the N1 atom of NAD^+ and C4-hydroxyl group of prephenate, which may bring together these groups in a catalytically competent conformation. An additional H-bonding network has been identified, including a water molecule, H217, S254 and the oxygen atoms of HPP's propionyl side chain (Figure 7 A) and will be probed further in this thesis. Kinetic analyses of H217A and H217N showed that the apparent binding affinity for prephenate was increased by 40-fold and 30-fold respectively but also the turnover number decreased 10 to 20 fold. Additionally, both variants are insensitive to feedback inhibition by L-Tyr. Christendat, Turnbull and colleagues (63) proposed that H217 is important for positioning prephenate in a catalytically important conformation and/or in maintaining the integrity of the active site (61, 63). Interestingly, Christendat and colleagues have further proposed that H217 might be protonated in the ternary complex of Δ19PD bound with NAD^+ and either HPP or L-Tyr and that this histidine group is a key determinant in L-Tyr binding. As shown in Figure 7 B the amine of L-Tyr is pointing away from H217 in contrast to the carbonyl group of the side chain of HPP (Figure 7A). Work in the Turnbull lab has shown that R250 is important but not critical for prephenate binding since R250Q displayed only a 10-fold increase in the K_m for prephenate without a significant change in the enzyme's apparent affinity for NAD^+ or in its turnover rate. It is likely that additional residues may work in concert to assist in the binding of prephenate (61). Analysis of the crystal structure solved at pH 3.2 (Figure 6) bound with NAD^+ but with prephenate modeled in the active site revealed that K246' from the adjacent monomer points towards prephenate's ring carboxyl group and, therefore, this electrostatic interaction might also be important for substrate binding. The biochemical analyses of K246Q and K246A concurred with this finding, showing that the different substitutions had a selective effect on the K_m for prephenate, increasing it 5 and 20-fold, respectively, without altering catalytic activity and K_m for NAD^+. Given that neither R250 nor K246' on their own appear critical for prephenate binding it has to be established if or how these two residues are working together. Additionally it has been proposed that access of substrate into the active site is regulated via a gated mechanism involving an ionic network consisting of residues E153, R250 and D247' from the adjacent monomer (Figure 7) (32, 63). These and other important interactions predicted from crystallographic data are probed through mutagenesis analysis in this thesis.

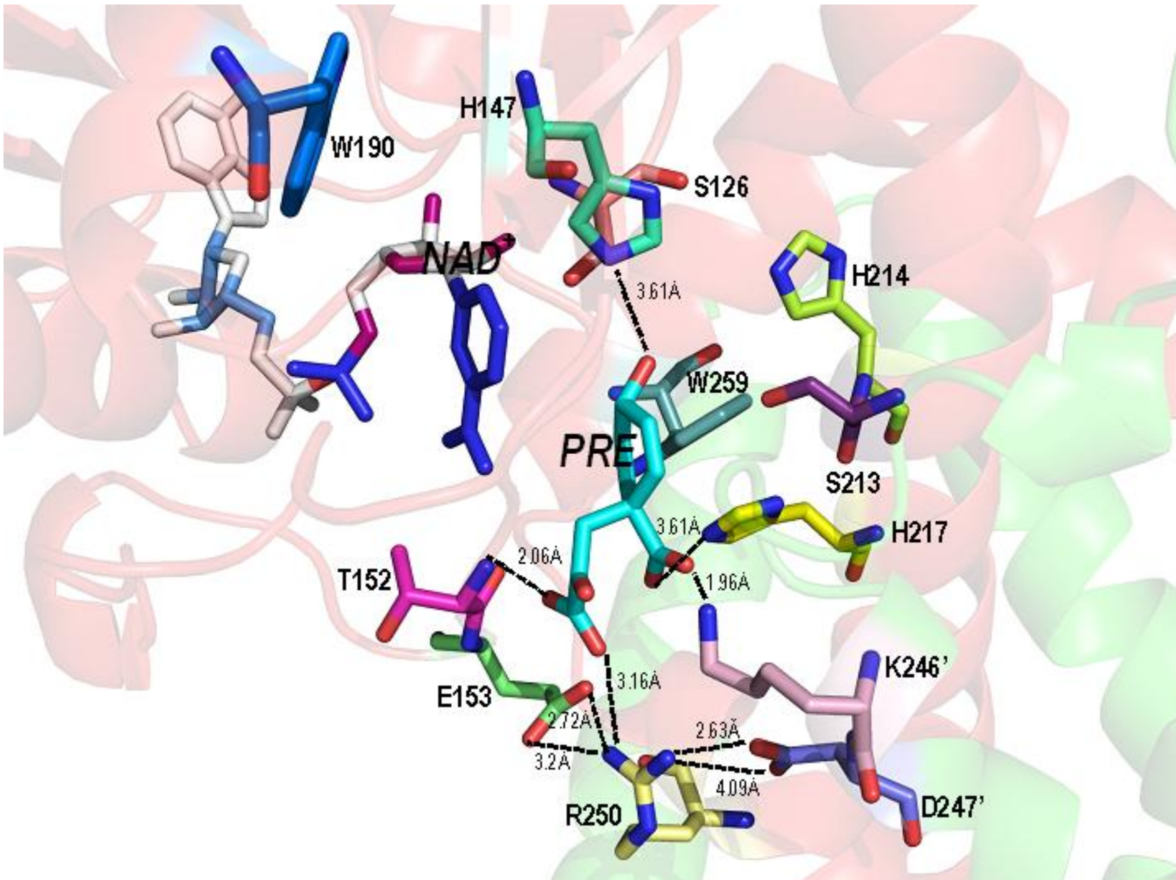

Figure 6: Selected active site residues of A. aeolicus Δ19PD complexed with NAD+ at pH 3.2 with prephenate modeled in the active site. The primed residues denoted those groups associated with the adjacent monomer (61).

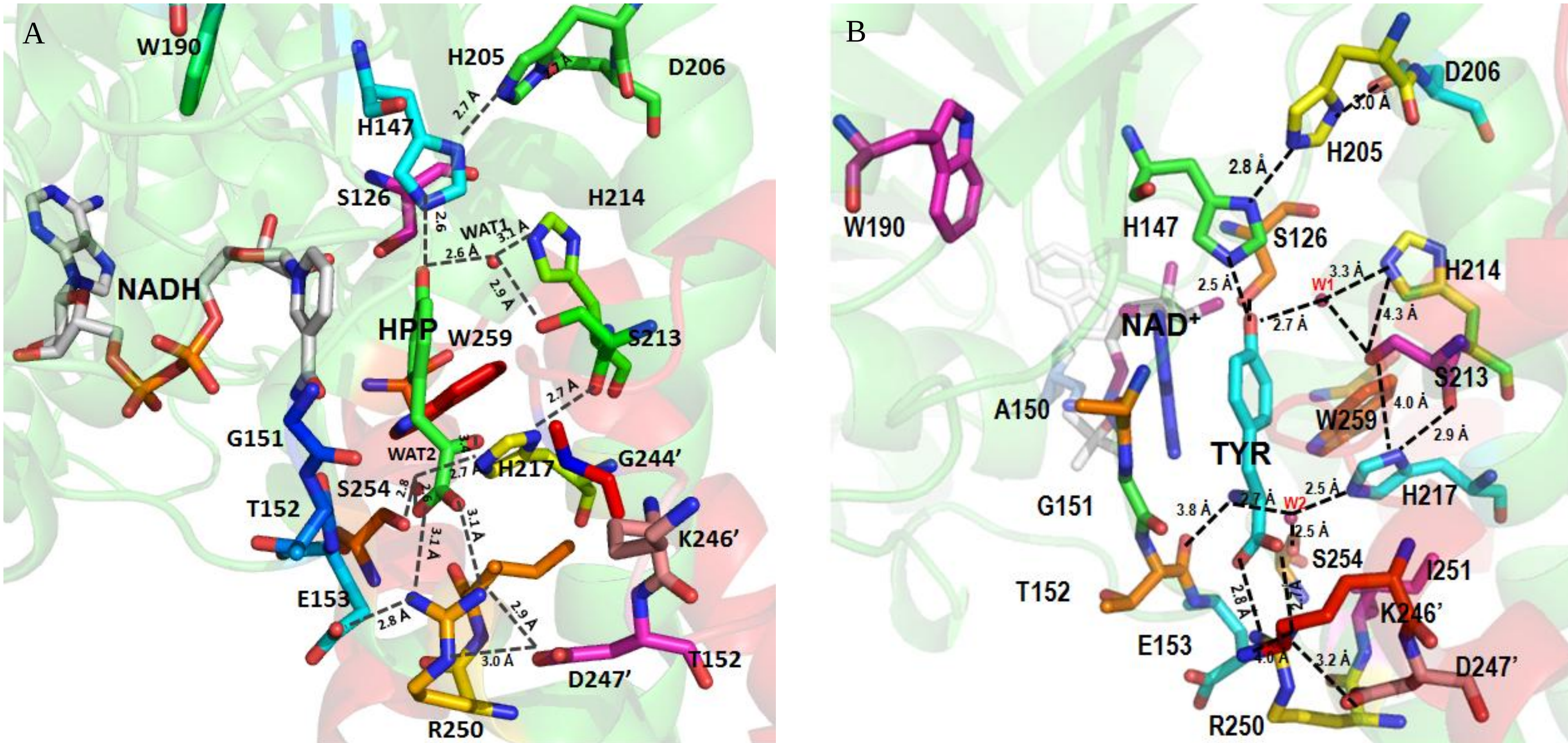

Figure 7: Selected active site residues of A. aeolicus Δ19PD complexed with NAD+ and (A) HPP or (B) L-Tyr at pH 7.8. Pictures created using PyMOL (62) using the coordinates derived from reference (63). The primed residues denote those groups associated with the adjacent monomer.

1.8 Research Objective

The overall goals of this study were two-fold: first, to identify the roles of several amino acids in substrate binding, catalysis and feedback inhibition; and second, to determine binding affinities of NAD^+, L-Tyr and prephenate or HPP to Δ19PD through non-kinetic approaches, along with some information concerning the stoichiometry, in solution, for the interaction of some of these ligands with the enzyme.

Residues have been selected for site-directed mutagenesis studies for various reasons. As mentioned above, neither R250 nor K246' alone appear critical for prephenate binding. Thus, in this study the effects of a double substitution at these positions have been examined. Additionally, it has been proposed through crystallography data that the passage of substrates into the active site is regulated via a gated mechanism involving an ionic network consisting of E153, R250 and D247' (57, 63). Accordingly, E153 and D247' have been substituted both individually and together in order to probe this hypothesis through solution studies. H205 and D206, two highly conserved residues within all TyrA proteins have been chosen for site-directed mutagenesis. As proposed in the mechanism of *H. influenzae* CM-PD (58), it may be that these two residues participate in an H-bonding network along with the catalytic H147 to maintain the critical H-bond acceptor in a deprotonated state. Two other residues, S213 and H214 are located in the polar region of the active site of *A. aeolicus* Δ19 PD (along with S126 and H147), and are part of a H-bonding network which includes a highly conserved water molecule, suggesting that these residues might be important for catalysis and/or substrate binding. Primary sequence alignment comparisons (Figure 4) revealed that the S213-H214 pair, common in monofunctional TyrA proteins is replaced by Gln and Ala in bifunctional enzymes, suggesting that these two residues define two classes of TyrA proteins. S254 contributes to an H-bonding network consisting of H217, the oxygen groups within the pyruvyl side chain of HPP or the amine group of L-Tyr, and a water molecule. It has been suggested that H217 is critical for positioning prephenate in a catalytically important conformation. Therefore, it may be that S254 plays similar or perhaps additional roles as part of its contribution to this H-bonding network. Lastly, the crystal structure (Figure 7 B) demonstrated that the main chain carbonyl of T152 is interacting directly with the amine group of L-Tyr. This contact is absent in the enzyme-NAD^+-HPP/HPPropionate complex and therefore it may be important for feedback inhibition by L-Tyr (63). Amino acid substitutions at position 152 attempt to probe this interaction.

In our second goal, the crystal structures of Δ19PD bound with nucleotide cofactor plus either HPP, 4-hydroxyphenylpropionate or L-Tyr at pH 7.8 revealed that only one molecule of the product or product analogue is bound per dimer, whereas both subunits in the dimer contain a molecule of NAD^+ or NADH (see Figure 5). This finding has prompted Christendat and colleagues to suggest that substrate binding and product release are ordered; NAD^+ binds first to the enzyme followed by prephenate while HPP needs to be released before NADH from the active site (63). Thus, we attempted to examine the binding affinity for NAD^+, L-Tyr and prephenate or HPP with Δ19PD and to ascertain the stoichiometry of ligand association in solution.

To achieve our goals seventeen *A. aeolicus* Δ19PD variants were generated by site-directed mutagenesis, expressed in *E. coli* cells and purified to near homogeneity using Ni-NTA affinity chromatography. Circular dichroism (CD) was used to confirm that secondary structure was not disrupted by the amino acid conversions and to assess the thermal stabilities of selected enzymes. Additionally, the effects of the amino acid substitutions on the tertiary structure of Δ19PD were determined using fluorescence emission spectroscopy. Kinetic parameters of the reactions catalyzed by all Δ19PD proteins studied in this thesis were determined spectrophotometrically. Additionally, the degree of feedback inhibition by L-Tyr was examined for each protein as well as the pH dependence of the inhibition by L-Tyr of the native enzyme. Fluorescence spectroscopy, equilibrium dialysis and isothermal titration calorimetry were used as complementary techniques to determine the binding affinities for NAD^+, L-Tyr and prephenate or HPP, and to help shed light on the solution stoichiometry for the interaction of some of these ligands with the enzyme. Our results are interpreted in light of the available crystal structures of *A. aeolicus* Δ19PD plus modelling studies we have conducted placing prephenate in the active site of selected structures determined at neutral pH.

Chapter 2: Materials and Methods

2.1. Materials

Chorismate (free acid form) was isolated and purified from *Klebsiella pneumonias* (64). Prephenate (barium salt) was prepared enzymatically from chorismate as previously described (65). NAD^+ (grade I) was obtained from Roche. Stock solutions of substrates were prepared in the appropriate buffers and stored at –20ºC in small aliquots. Their concentrations were determined using extinction coefficients (NAD^+) or enzymatic end-point analysis (prephenate and chorismate) (66, 67). L-Tyr and L-Phe were purchased from ICN Biochemicals Inc., while radiolabeled L-Tyr (L-[ring3,5-^{3}H] tyrosine) with a specific activity of 40.0 Ci/mmol was obtained from Perkin Elmer Inc. Hydroxyphenylpyruvate (HPP) was purchased from Sigma and was purified according to the method of Bonvin (55). Ampicillin (sodium salt), kanamycin sulphate and chloramphenicol, IPTG and Phenyl-methyl-sulfonyl fluoride (PMSF, prepared to 0.5M stock solutions in methanol and stored at –20ºC) were obtained from BioShop. Oligonucleotides of standard purity were ordered from BioCorp (Montréal, QC). Restriction enzymes *Dpn*I, *Nde*I, *Bam*HI (all at 10 U/μL), recombinant *PfuTurbo*® DNA polymerase (2.5 U/μL) and the deoxy-NTP (dNTP) mixture (5 mM of each dNTP, stored at -20ºC in small aliquots) were purchased from MBI Fermentas. *Phusion*® *High-Fidelity* DNA Polymerase (2.0 U/μL) was purchased from New England Biolabs Inc. Benzonase Nuclease was obtained from Novagen. Complete™, Mini, EDTA-free protease inhibitor cocktail tablets were purchased from Roche. Amersham Biosciences supplied thrombin protease (purified from bovine plasma, 500 U resuspended in 500 μL of phosphate buffered saline) and NAP™-5 size exclusion buffer exchange columns pre-packed with

DNA grade Sephadex™ G-25, while Ni-NTA Superflow™ chromatography resin was supplied by Qiagen. Dialysis membrane (MW cut-off 12-14 kDa) from Spectrapor was washed according to manufacturer's instructions. All other chemical reagents and solvents were purchased commercially and were of the highest quality available.

2.2. Strains and Plasmids

The *E. coli* strain XL10-Gold ultracompetent (Stratagene) $Tet^r\Delta$ (*mcrA*)*183* *Δ*(*marCB-hsdSMR-mrr*)*173 endA1 supE44 thi-1 recA1 gyrA96 relA1 lac* Hte [F'*proAB lacI*^{q}*ZΔM15* Tn10 (Tet^r) Amy Cam^r] was used for plasmid production while BL21(DE3) (Stratagene) [F^- dcm^+ Hte ompT hsdS(r_B^- m_B^-) gal λ (DE3) endA Tet^r] was used for protein expression. The cells were either purchased commercially ready to use or rendered competent using calcium chloride (56). The helper plasmid pMagik which encodes three rare tRNAs (AGG and AGA for Arg and ATA for Ile) was kindly donated by Dr. A. Edwards, Ontario Cancer Institute, University of Toronto. Recombinant wild-type Δ19PD plasmid was previously constructed by Dr. D. Christendat by cloning *A. aeolicus tyrA* encoding amino acid residues 20-311 of PD into *E. coli* expression vector pET15b (Novagen) which carries a cleavable N-terminal hexahistidine tag (30).

2.3. Bacterial Growth Media

LB medium was prepared with 1% tryptone, 0.5% yeast extract and 1% NaCl in distilled H_2O (pH was adjusted to 7.5) while LB agar was prepared with 1.5% agar in LB medium. Both media were sterilized by autoclaving at 121ºC. Stock solutions of ampicillin (100 mg/mL) and kanamycin (10 mg/mL) were prepared in MilliQ-H_2O, filter sterilized by passage through a 0.45 μm syringe (VWR) and stored at -20°C.

2.4. Site-Directed Mutagenesis

Oligonucleotides used for the mutagenesis reactions (see Table 1) were resuspended in MilliQ-H_2O and their concentrations were determined by measuring OD_{260} of 100-fold dilutions. The plasmid pRA-Δ19PD-3, encoding Δ19PD with a removable N-terminal hexahistidine-tag (57) and was used as template plasmid for site-directed mutagenesis. The plasmid was isolated from a 15 mL culture of *E. coli* XL-10-Gold ultracompetent cells harbouring the plasmid using the GeneJET™ Plasmid Miniprep Kit (Fermentas Life Sciences) and its concentration was determined spectrophotometrically at 260 nm.

Site-directed mutagenesis was conducted according to the instructions supplied in the QuickChange™ XL Site-Directed Mutagenesis Kit. Depending upon the source of the DNA polymerase, the PCR-based mutagenesis reactions were set up slightly differently (see Table 2 and 3). When using *PfuTurbo*® DNA polymerase, the reaction mixtures were prepared with 15 ng of double stranded (ds) DNA template, 150 ng of each oligonucleotide primer (forward and reverse), 1 µL of *PfuTurbo*® DNA polymerase (2.5 U/µL), 5 µL of 10x *Pfu* buffer containing Mg_2SO_4 and 2 µL of a 5 mM dNTP solution in a final volume of 50 µL. When using *Phusion*® High-Fidelity DNA polymerase, the reaction mixtures were prepared with 15 ng of double stranded (ds) DNA template, 150 ng of each oligonucleotide primer (forward and reverse), 0.5 µL of *Phusion*® High-Fidelity DNA polymerase (2 U/µL), 10 µL of 5x *Phusion*® HF buffer, 3 µL of a 5 mM dNTP solution and 1.5 µL DMSO in a final volume of 50 µL. In both sets of reactions, DNA polymerase was added just prior to the first denaturation cycle. PCR amplification was carried out using a GeneAmp PCR system 9700 (Applied Biosystems). The temperature cycle parameters are listed in Tables 2 and 3. Briefly, double stranded plasmid DNA was denatured at 95˚C or 98˚C then oligonucleotide primers were annealed to the plasmid at 50 to 55 ºC. Synthesis and extension of the new DNA strand was catalyzed by the DNA polymerase at 72˚C. Reaction mixtures were stored at 4 ˚C in the apparatus until processed further.

Table 1: Primer sequences for site-directed mutagenesis of *A. aeolicus* Δ19PD

Δ19PD Variants	Oligonucleotide Primer Sequence
T152G	5’ CACCCGATAGCAGGA**GGC**GAGAAATCTGGG 3’
T152P	5’ CACCCGATAGCAGGA**CCG**GAGAAATCTGGG 3’
E153A	5’ CCCGATAGCAGGAACG**GCG**AAATCTGGGG 3’
H205L	5’ GAGTACATGAGTCCTGAACTT**CTC**GACTACGTGTTTGG 3’
H205Q	5’ GAGTACATGAGTCCTGAACTT**CAG**GACTACGTGTTTGG 3’
D206A	5’ GAACTTCAC**GCG**TACGTGTTTGGTGTTGTTTCTCACCTTCCC 3’
D206E	5’ GAACTTCAC**GAA**TACGTGTTTGGTGTTGTTTCTCACCTTCCC 3’
D206N	5’ GGATTGCAAAGAGC**AAC**CCCATTATGTGG 3’
S213A	5’ CGTGTTTGGTGTTGTT**GCG**CACCTTCCCCATGC 3’
H214L	5’ GGTGTTGTTTCT**CTG**CTTCCCCATGCCGTTGCC 3’
H214Q	5’ GGTGTTGTTTCT**CAA**CTTCCCCATGCCGTTGCC 3’
H217V	5’ CACCTTCCC**GTG**GCCGTTGCCTTTGCACTC 3’
D247A	5’ CCGGAGGAGGTTTTAAG**GCG**TTCACGAGGATTGC 3’
R250A/K246A	5’ AGGAGGTTTT**GCG**GACTTCACG**GCG**ATTGCAAAGAGCG 3’
S254A	5’ CGAGGATTGCAAAG**GCG**GACCCCATTATGTGG 3’
W259Y	5’ GCGACCCCATTATG**TAT**AGAGACATATTTCTGG 3’

Primers were designed considering length, GC content and location, and melting temperature using Primer3 Output program (http://frodo.wi.mit.edu/primer3/input.htm (68)). Bold and underlined letters represent the bases that differed from the wild-type sequence. Complementary primers are not shown.

Table 2: Temperature cycling parameters for PCR using *PfuTurbo* DNA polymerase

Number of Cycles	Temperature (ºC)		Time
1	Denaturation	95	3 min
18	Denaturation	95	1 min
	Annealing	55	1 min
	Extension	72	25 min
1	Extension	72	17.5 min
	Cooling	4	overnight

Table 3: Temperature cycling parameters for PCR using *Phusion*® *HF* DNA polymerase

Number of Cycles	Temperature (ºC)		Time
1	Denaturation	98	45 s
20	Denaturation	98	30 s
	Annealing	50	45 s
	Extension	72	5 min
1	Extension	72	10 min
	Cooling	4	overnight

Upon completion of the temperature cycling, methylated and hemi-methylated parental DNA were digested by incubation of the reaction mixtures with *Dpn*I restriction endonuclease (10U) at 37°C for 2h. The presence of amplified DNA was confirmed by electrophoresis on a 0.5 % agarose gel (see section 2.6). Digested PCR products were purified using the *Illustra* GFX™ PCR DNA and Gel Band Purification Kit (GE Healthcare) and transformed into *E. coli* stain XL10-Gold ultracompetent cells (see section 0). All cells were then plated on LB/agar containing ampicillin (100 µg/mL). After overnight incubation at 37ºC, single colonies were selected and inoculated separately into 10 mL of liquid LB medium containing ampicillin (100 µg/mL) and grown overnight at 37ºC with shaking at 250 rpm. The plasmid DNA was extracted and purified using the GeneJET^{TM} Plasmid Miniprep Kit (Qiagen). The protocol was modified by eluting the DNA using MilliQ-H_2O instead of the buffer provided in the kit. The concentration and purity of the plasmid DNA were determined by recording the OD_{260} and the ratio of OD_{260}/OD_{280}, respectively.

Aliquots of purified plasmid DNA were sent for sequencing of the *tyrA* gene (McGill University and Génome Québec Innovation Centre). The resulting sequences were aligned with that of WT *tyrA*, using the BLAST tool on NCBI (http://www.ncbi.nlm.nih.gov/blast) to ensure that the desired mutation was achieved and that no other mutations had been introduced.

2.5. Transformation

*Dpn*I-treated PCR products were transformed using a rapid transformation protocol described by Sambrook and Russell (71) modified previously by Dr. J. Manioudakis in the Turnbull lab (56). Briefly, purified *Dpn*I- treated PCR products (10 μL) were added to 50 μL of XL10-Gold ultracompetent cells, mixed and incubated on ice for 5 min. The cells were then incubated at 42ºC for 45 s (heat-shock) and subsequently kept on ice for 2 min. The transformed cells were then plated on LB/agar containing 100 μg/mL ampicillin and grown overnight at 37ºC.

Transformation for Δ19PD protein expression was performed using the same method as described above. Briefly, plasmid DNAs (Δ19PD plasmids and pMagik helper plasmid, ~100 ng of each) were mixed with 50 μL of BL21(DE3) competent cells, placed on ice for 5 min followed by heat-shock for 45 s at 42ºC and then incubated on ice for 2 min. The entire mixture was plated on LB/agar containing 100 μg/mL ampicillin and 5 μg/mL kanamycin and incubated overnight at 37ºC.

2.6. Agarose Gel Electrophoresis

Agarose gel electrophoresis (0.5% agarose) was used to verify the amplification of plasmid DNA. Agarose (0.5 g) was dissolved in 50 mL TBE buffer (45 mM Tris-borate/1 mM EDTA, pH ~ 8.3) and heated for 2 min in a microwave. After the agarose solution had cooled to 55ºC, ethidium bromide (0.5 μg/mL) was added. DNA samples and molecular weight markers (Gene Ruler 1kbp DNA ladder, Fermentas) were mixed with 6 x loading dye (Fermentas). Electrophoresis was performed at 100V until the loading dye migrated to the middle of the gel. DNA was visualized using a FluoroChem FC2 Imaging Illuminator.

2.7. Expression and Purification of Δ19PD Proteins

Plasmid containing native or mutant *tyrA* (50-100 ng) was co-transformed with helper plasmid pMagik into *E. coli* BL21(DE3) cells (see section 2.5). A single colony selected from LB/agar plates containing 100 μg/mL ampicillin and 5 μg/mL kanamycin were then used to inoculate 50 mL of antibiotic-supplemented LB medium. After incubating overnight at 250 rpm and 37ºC, the culture was then diluted into 1.5 L of the same medium. The 1.5 L culture was propagated at 37ºC with shaking at 250 rpm until an OD_{600} of 0.6-0.8 was reached. Protein expression was then induced by adding 0.4 mM isopropyl-β-D-thiogalactopyranoside (IPTG). The culture was further incubated for 3 h at

37ºC. Cells were harvested by centrifugation at 10000 x g at 4ºC for 15 min and the cell pellet was stored at -20ºC until further processed.

Purification of Δ19PD proteins was carried out with cold buffer and all chromatography steps were performed in the cold room. The cell pellet was thawed and then resuspended in buffer A (50 mM Tris, 500 mM NaCl, 5% glycerol, pH 7.5) using ~ 5 mL/g of wet cell pellet. Buffer A was supplemented with 5 mM imidazole, Complete^{TM} protease inhibitor cocktail tablet (one tablet per 50 mL of resuspension), 0.5 mM phenyl-methyl-sulfonyl fluoride (PMSF) and benzonase nuclease (Amersham Biosciences, 6 μL/gram of wet cell pellet). The mixture was homogenized using a Dounce Homogenizer (at least 5 up-and-down strokes), and then the suspended cells were further lysed by two passages through a French pressure cell with a setting of 1000 psi. The cell lysate was then centrifuged using a Beckman centrifuge for 45 min at 40 000 x g and 4ºC to remove insoluble cellular debris.

The cell-free extract was applied to a 15 ml Ni-NTA Superflow column (binding capacity: 5-10 mg of His-tagged protein per mL resin), previously equilibrated with ice-cold buffer A containing 5 mM imidazole using a flow-rate of 1 mL/min. After the flow-through was collected, the column was washed at a flow-rate of 3 mL/min with 300 mL of buffer A supplemented with 30 mM imidazole. Bound His-tagged protein was eluted with buffer A containing 300 mM imidazole and 1.5 mL fractions supplemented with 1 mM EDTA were collected during elution. Protein elution was monitored quantitatively by adding 10 µL of every third fraction collected to 990 µL Bio-Rad Bradford dye and recording the absorbance at 595 nm. Additionally, fractions were assayed for prephenate dehydrogenase activity by adding 20 µL aliquots from selected fractions to a reaction mixture containing 100 mM Tris-HCl, (pH 7.5), 150 mM NaCl, 2 mM NAD^+ and 0.5 mM prephenate. Those fractions with the highest protein content and dehydrogenase activity were pooled and thrombin was added at a ratio of 1000:1 (w/w) of protein-to-thrombin. The solution was dialyzed (Spectrapore, 12kDa cut-off) overnight at 4ºC against buffer A containing 2.5 mM $CaCl_2$. Thrombin-treated Δ19PD protein was concentrated, if necessary, to 2-10 mg/mL (Amicon Ultra-15, MW cut-off 10kDa) and stored at -20ºC in buffer A supplemented with 20% glycerol. Each step of the purification procedure was monitored by SDS-PAGE (12% acrylamide). Protein concentration was determined by Bio-Rad Protein assay kit using BSA as a standard (see section 2.8).

2.8. Determination of Protein Concentration

Protein concentration was calculated using the Bio-Rad protein assay kit (Bio-Rad Laboratory) with bovine serum albumin (BSA, Sigma) as a standard (69). BSA was dissolved in 10 mM Tris-HCl, pH 7.4, filtered using a 0.2 μm syringe and its concentration was determined by OD_{280} readings using an extinction coefficient of 0.667 mL/mg/cm (70).

2.9. Polyacrylamide Gel Electrophoresis

Sodium dodecyl sulfate polyacrylamide gel electrophoresis (SDS-PAGE) was used to assess the purity and estimate the molecular weights of proteins under denaturing conditions. SDS-PAGE was performed using a 4% acrylamide stacking gel (pH 6.8) and 12% acrylamide resolving gel (pH 8.3) as reported by Sambrook *et al.* (71). The 30% acrylamide stock solution was prepared by mixing 29% (w/v) acrylamide and 1% (w/v) N, N'-methylene-bis-acrylamide in distilled H_2O. Resolving gel buffer (1.5 M Tris-HCl, pH 8.3) and stacking gel buffer (0.5 M Tris-HCl, pH 6.8) were prepared in distilled water and the pH was adjusted using HCl. The acrylamide and Tris buffer solutions were stored at 4ºC. Ten percent SDS (w/v) in distilled water was stored at room temperature while 10% (w/v) ammonium persulfate prepared in distilled water was stored at -20ºC. Electrophoresis buffer was composed of 25 mM Tris-base, 250 mM glycine and 0.1% SDS, pH 8.3. Protein samples and protein molecular weight marker (Fermentas) were diluted 1:1 (v/v) into 2 x SDS gel-loading buffer (1.5 M Tris-HCl, 4% SDS, 20% glycerol (v/v), 0.002% Bromophenol Blue, pH 6.8) and denatured in boiling water for 5 min before loading onto the gel. Electrophoresis was conducted at 120 V and terminated when the Bromophenol Blue tracking dye migrated off the resolving gel. Proteins were visualized by first washing the gel in warm distilled water three times for 2 min, followed by staining in a solution of 0.1% (w/v) Brilliant Blue-G250 (BioShop) and 35 mM HCl in distilled water, until bands appeared (72). Contrast could be enhanced by placing the gel in distilled water to remove excess staining solution.

2.10. ESI-ToF Mass Spectrometry

The molecular weight of native and variant Δ19PD proteins was confirmed using ESI-ToF-MS. Samples were prepared by mixing 100 μg of protein with 300 μL methanol, 100 μL chloroform and 200 μL MilliQ water. The mixture was vortexed for 5 s after each solvent addition. Next, the sample was centrifuged (Eppendorf Centrifuge 5415 C) at 16 000 x g for 3 min. The two visible liquid phases were now separated by a thin layer of precipitate containing the protein. After carefully removing all of the liquid, 300 μL methanol was added to the precipitated protein, and the sample was vortexed for

5 s and then centrifuged (16 000 x g) for 2 min. This wash step repeated once more. After the second wash step the methanol was decanted and the protein pellet was dried at room temperature in the fume hood. The dried pellet was resuspended in 300 μL of 30% methanol/0.2% formic acid (v/v) and then the sample was centrifuged for 5 min to remove all insoluble material (73). The samples were applied to a Waters Micromass Q-ToF 2 triple-quadrupole mass spectrometer by direct injection at a flow rate of 1 μL/min. Samples were analyzed in the positive-ion mode within an m/z range of 700-2000 using Mass Lynx 4.0 software (Waters Micromass). Instrument parameters were as follows: source block temperature: 80 °C; capillary voltage: 3.5 kV; cone voltage: 35 V; ToF: 9.1 kV; MC: 1.8 kV; resolution: 8000. Calibration of the instrument was performed with myoglobin (Sigma).

2.11. Determination of Enzyme Activities and Kinetic Parameters

The oxidative decarboxylation of prephenate in the presence of NAD^+ was monitored at 340 nm as described previously (50). The reactions (total volume 1 mL) were monitored continuously by using a Varian Cary 50 spectrophotometer equipped with a thermostated cuvette holder.

Standard activity assays for Δ19PD proteins were measured at 55ºC in a reaction buffer containing 50 mM HEPES, 150 mM NaCl, pH 7.5. Buffer was incubated in a quartz cuvette of 1 cm path length at 55ºC for 2 min, while NAD^+ and prephenate in appropriate concentrations were added. Then the reaction was initiated by the addition of enzyme. Components were mixed by inversion of the cuvette. All substrates and enzyme were kept on ice prior to their addition (55).

OD_{340} was recorded continuously for 1.5 min and reaction rates were calculated from the linear portion of the progress curves using the software supplied with the spectrophotometer. Exact concentrations of substrates are listed in figure legends in the results section. Values of steady-state kinetic parameters k_{cat} and K_m were obtained by fitting initial velocity data to the Michaelis-Menten equation*:* $v_0 = (V_{max}[S])/ ([S] + K_m)$ rate equations using nonlinear least-squares analysis provided by Grafit Software version 5.0 (Erathicus Software).

The turnover number k_{cat} was calculated using the relationship: $k_{cat} = V_{max}/$ [active site]$_{total}$ where V_{max} represents the specific activity recorded at saturating concentrations of substrates. A unit of activity is defined as the amount of enzyme required to produce 1 μmol of product/ min at desired temperature. Calculations of units of activity, specific activity and k_{cat} are shown below:

$$\textbf{Units (μmol/min/mL)} = \frac{\Delta OD_{340}/\text{min}}{1\text{ cm} \times 6400\text{ M}^{-1}\text{ cm}^{-1}} \times \frac{10^6\ \mu\text{mol}}{\text{mol}} \times \frac{1\text{L}}{10^3\text{ mL}} \times \text{dilution factor}$$

$$\textbf{Specific activity (μmol/min/mg)} = \frac{\text{Units}}{\text{mg/mL protein}}$$

$$\boldsymbol{k_{cat}}\ \mathbf{(s^{-1})} = V_{max}\ (\mu\text{mol/s/mg}) \times \frac{33196\text{ mg*}}{\text{mmol active site}} \times \frac{\text{mmol}}{10^3\ \mu\text{mol}}$$

* Exact mass of Δ19PD proteins were determined from ESI-ToF-MS

The pH dependence of the kinetic parameters k_{cat} and k_{cat}/K_m for prephenate were also determined for the reaction catalyzed by native Δ19PD. The activity of the enzyme was recorded at 55ºC, over the pH range from 5.5 to 9.0 in a buffer containing 25 mM HEPES, 25 mM 3-(N-morpholino)propanesulfonic acid (MES), 25 mM Tris-HCl with

150 mM NaCl. Saturating concentrations of 2 mM for NAD^+ were used and the prephenate concentrations varied between 75 - 997 µM. The pH of the assay mixture was determined at room temperature using a Fisher Scientific Accumet® 15 pH meter standardized with appropriate reference standard buffers and at 55 °C before the reaction using pH indicator paper. The variation of the values of k_{cat}/K_m as a function of pH was fit best to the non-linear fit to the pK_a, double equation in Grafit Software version 5.0 (Erathicus Software) which fits data where the observed variation depends upon two ionizing groups. The equation is:

temp1 = antilog(pH-pK_a1)

temp2 = antilog(pH-pK_a2)

y = ((Lim1 + Lim2 * temp1)/ (temp1+1) - (((Lim2 -Lim3)

where Lim1, 2 and 3 denotes lower, middle and upper limit, respectively.

2.12. Determination of the Effect of L-Tyr on Δ19PD Activity

The effect of L-Tyr on the activity of native and variants of Δ19PD were determined using the activity assay described in 2.11 in the presence of different L-Tyr concentrations. L-Tyr was prepared fresh in reaction buffer, as a stock solution at a concentration of 10 mM. The stock solution was heated while dissolving L-Tyr and the pH adjusted to pH 7.5 with NaOH. Assays (1 mL reaction volume) were conducted in the presence of 0 – 7 mM L-Tyr by combining reaction buffer and tyrosine stock solution in the appropriate ratios to obtain the desired concentrations of L-Tyr. The resulting reaction mixture was incubated at 55°C for 2 min, followed by the consecutive addition of NAD^+ and prephenate and the reaction was initiated by the addition of enzyme. Unless otherwise stated in the text, substrate concentrations used were 2 mM (saturating) NAD^+ and prephenate at approximately 4 x K_m. Reaction rates were calculated as described in section 2.11

The effect of L-Tyr on the velocity of the reaction obtained by varying prephenate at a fixed concentration of NAD^+ (2mM) were determined for native Δ19PD and select variant proteins. Assays were conducted at 55 °C and pH 7.5 as described above using concentrations of NAD^+, prephenate and L-Tyr listed in the Results. Data were plotted in double reciprocal form to identify any deviations from linearity and then fitted to equations describing either linear competitive inhibition, hyperbolic competitive inhibition or hyperbolic mixed inhibition (74).

Linear competitive inhibition:

$$\boldsymbol{v = \frac{V_{max} * [S]}{K_m\left(1 + \frac{[I]}{K_i}\right) + [S]}}$$

Hyperbolic competitive inhibition:

$$\boldsymbol{v = \frac{V_{max} * [S]}{K_m\left(\frac{1 + \frac{[I]}{K_i}}{1 + \frac{[I]}{\alpha * K_i}}\right) + [S]}}$$

Hyperbolic mixed inhibition:

$$\boldsymbol{v = \frac{V_{max} * [S]}{K_m\left(\frac{1 + \frac{[I]}{K_i}}{1 + \frac{\beta * [I]}{\alpha * K_i}}\right) + [S]\left(\frac{1 + \frac{[I]}{\alpha * K_i}}{1 + \frac{\beta * [I]}{\alpha * K_i}}\right)}}$$

Where v is the initial velocity of the reaction, Vmax is the maximum velocity, [S] represents the concentration of prephenate, K_m is the Michaelis constant for prephenate, [I] equals the inhibitor concentration, K_i is the inhibitor constant for L-Tyr, α is the factor by which K_s changes when I occupies the enzyme, β describes the factor by which K_p changes when going from an enzyme-substrate-inhibitor complex to product formation.

The pH dependence of the inhibition of native Δ19PD by L-Tyr was determined by obtaining substrate saturation curves at 55°C using prephenate as variable substrate (75 – 1200 µM) and fixed NAD^+ concentration (2 mM) in the presence of 0 and 100 µM L-Tyr in a buffer containing 25 mM HEPES, 25 mM 3-(N-morpholino)propanesulfonic acid (MES), 25 mM Tris-HCl with 150 mM NaCl at nine different pH values within pH range from 5.5 to 9.5. Assuming that L-Tyr acts as a competitive inhibitor for native Δ19 PD from *A. aeolicus*, the K_i was obtained using the following relationship (74):

$$K_i = {}^{[I]}\Big/\left(\frac{K_{m,100\ \mu M\ L-Tyr}}{K_{m,0\ \mu M\ L-Tyr}} - 1\right)$$

where K_i is the inhibition constant, [I] represents the concentration of L-Tyr, Km,0 and 100 µM L-Tyr are the Michaelis constants for prephenate in the presence of 0 µM and 100µM L-Tyr respectively. The variation of pK_i = -log (K_i) as a function of pH was analyzed using Grafit Software version 5.0 (Erathicus Software) as described in section 2.11.

2.13. Far-UV Circular Dichroism Spectroscopy

Far-UV CD spectra of native Δ19PD and variants were obtained using a Jasco-815 spectropolarimeter equipped with a Peltier heating/cooling temperature control system.

Spectra were recorded at 25°C in a 0.2 cm path-length rectangular cell (600 µL) from 260 to 200 nm with the following parameters: 20 nm/min scan rate, 0.2 nm resolution, 0.25 sec response time, 1 nm bandwidth and a sensitivity of 100 mdeg. For each spectrum, five accumulations were averaged and the absorbance contribution of the buffer was subtracted. Protein samples were prepared fresh from a -20°C stock solution of enzyme stored in 50 mM Tris-HCl, 0.5 M NaCl, 25% glycerol (v/v). Proteins were first exchanged into a buffer containing 50 mM KH_2PO_4 / K_2HPO_4, 75 mM NaCl, pH 7.5 (PPS) using pre-equilibrated NAP-5 column (Amersham Biosciences) or concentrating tubes (PALL). Protein concentrations were then adjusted to ~ 7 µM monomer in the same buffer. Buffers were filtered (Millipore, 0.22µm) and their pH corrected at room temperature.

For variable temperature experiments, changes in ellipticity at 222 nm (1 nm band width) were recorded from 25°C to 95°C by using instrument's software controlled temperature ramping program. The following parameters were used: ΔT of 40°C/h, a 0.2°C step resolution, and a 0.25 s response time. The protein samples were prepared according as described above. Spectral scans from 200-260 nm were recorded for each sample at the beginning and the end of each the variable temperature experiments.

2.14. Fluorescence Spectroscopy

Fluorescence spectra for native Δ19PD and each protein variant were recorded at 30°C using a Varian Cary Eclipse spectrofluorimeter equipped with Scan Software version 1.1. Protein samples were prepared as described in 2.13 using a monomer concentration of 2 µM. Excitation wavelengths of 280 for tryptophan and tyrosine emission and 295 nm for tryptophan emission were used. Fluorescence emission was scanned from 300 to 400 nm in 2 nm increments at a fast scan speed (1200 nm/min) with the PMT voltage set at 700 V. Both excitation and emission slit widths were set at 5 nm. The average of 10 scans was used to obtain the final spectrum which was then processed by Savitzky-Golay smoothing with a filter size of 5. A Varian 400 µL fluorescence micro cell (1 cm x 1cm) was used throughout all experiments. Data were exported in ASCII (.csv) format and spectra were constructed in Windows Word Excel 2010. All spectra were corrected for buffer contributions.

The pH dependence of fluorescence emission was also determined for native Δ19PD over a pH range of 4-9 and upon excitation at 280 nm. The PPS buffer described above was used and the desired pH values were obtained by titrating with HCl or NaOH appropriately. The protein was buffer exchanged into the buffers at the desired pH values using pre-equilibrated NAP-5 columns (Amersham Biosciences). The protein concentration was subsequently adjusted to 2 µM. The same instrument settings as described above were used for the scans.

2.15. Determination of Dissociation Constants for Substrates and Substrate Analogs by Intrinsic Fluorescence Emission

Values for the dissociation constants of NAD^+, prephenate and HPP from the complex with Δ19PD were determined at 30°C by monitoring the quenching of intrinsic protein fluorescence. The excitation wavelength was set at 295 nm and fluorescence emission was scanned from 300 to 400 nm using the same settings as described in 2.14. Protein samples were prepared as described in 2.13. NAD^+, prephenate and HPP were diluted in PPS buffer to appropriate concentrations.

Samples were prepared by titrating Δ19PD (final concentration of 6 μM monomer) with increasing amounts of NAD^+ (0.25 μM – 100 μM), prephenate (11 – 250 μM) or HPP (0.25 – 100 μM). After each addition, samples were mixed by gentle inversion and the reaction was allowed to equilibrate for 1 min prior to recording measurements. The fluorescence data were corrected for concentration effects, inner filter effects, if necessary, as well as for background fluorescence.

If required, corrections of the fluorescence emission for the inner filter effect (75) utilized the following relationship: $F_{corr}=F_{obs}$ x antilog$[(A_{ex}+A_{em})/2]$, where F_{obs} and F_{corr} represent the observed fluorescence intensities and those corrected for the inner filter effect respectively. Absorbance readings (A), (cell plus sample blanked with air), were determined at both the excitation (ex) and emission (em) wavelengths. It should be noted that absorbance readings were recorded using an alternate cuvette (4 x 10 mm inner dimension) since the mask of the Varian fluorescence micro cell prevented accurate absorbance readings.

The dissociation constants were determined by different methods. Data describing the change in fluorescence emission (ΔF) intensity at a selected wavelength (shown in "Results") as a function of ligand concentration were fitted to the quadratic equation using Grafit 5.0 (76). The quadratic equation is given by:

$$\Delta F = \Delta F_{m}(([L_{t}]+[E_{t}]+K_{d})-(([L]_{t}+[E_{t}]+K_{d})^{2}-4[L_{t}][E_{t}])^{0.5})/(2[E_{t}]),$$

where ΔF describes the difference in fluorescence intensities in presence and absence of the titrant, ΔF_{m} is the maximum change in fluorescence intensity, $[L_{t}]$ is the total concentration of titrant, $[E_{t}]$ is the total enzyme concentration and K_{d} is the dissociation constant. An alternate method, described by Pawelek, (77) facilitated a

Scatchard Plot analysis and yielded values for the dissociation constant if assumed that at least one molecule NAD^+ binds per monomer PD.

The maximal change in fluorescence (ΔF_{max}) was obtained from plotting the observed fluorescence change (ΔF) as a function of total ligand concentration ($[L]_{total}$) and fitting the data to the equation that describes single site ligand binding (1) or to the equation describing cooperative binding (2);

$$\Delta F = \frac{[L]_{total} * \Delta F_{max}}{K_d * [L]_{total}} \quad (1)$$

$$\Delta F = \frac{{[L]_{total}}^n * \Delta F_{max}}{{K_d}^n * {[L]_{total}}^n} \quad (2)$$

Since the decrease of florescence intensity is due to the binding of ligand to the enzyme, the ratio of ΔF / ΔF_{max} (Q) at a selected wavelength can be directly related to the amount of PD complexed with the ligand as shown below:

$$[PD]_{bound} = Q * [PD]_{total}$$

In order to calculate the amount of ligand that is bound, the assumption that at least one ligand molecule combines with one monomer PD. Therefore:

$$[PD]_{bound} = [Ligand]_{bound}$$

Since the total ligand concentration upon each titration step is known, the fraction of free ligand can be calculated as follows;

$$[Ligand]_{free} = [[Ligand]_{total} - [Ligand]_{bound}$$

The calculated concentrations of free and bound ligand were analyzed using the standard ligand binding template in Grafit Software version 5.0 (Erathicus Software) which fits the data to a single site saturation curve, where the amount of ligand bound ($[L]_{bound}$) is plotted as a function of the amount of free ligand ($[L]_{free}$) using the following equation:

$$[\boldsymbol{L}]_{\boldsymbol{bound}} = \frac{\boldsymbol{Capacity} * [\boldsymbol{L}]_{\boldsymbol{free}}}{\boldsymbol{K_d} + [\boldsymbol{L}]_{\boldsymbol{free}}}$$

K_d is the dissociation constant and Capacity describes the maximum amount of ligand bound and is equal to n * $[PD]_{total}$ where n is the number of binding sites per monomer.

In order to confirm that only one ligand is bound per monomer, Hill plots were constructed. Therefore, the factional binding (Θ) is defined as $\Theta = \Delta F / \Delta F_{max}$ and the Hill equation is as follows:

$$\text{Log}\ (\Theta / (1- \Theta) = n * \log [L]_{free} - \log (K_d')$$

where n is the Hill coefficient and K_d' is the apparent dissociation constant of the interaction between ligand and PD. The Hill coefficient was determined from the slope of a straight line fit to midpoint data in the Hill plot (using values between 10 – 90% of ΔF_{max}).

2.16. Equilibrium Dialysis

The binding of L-Tyr to the NAD^+ - enzyme complex was determined using a 12 cell equilibrium dialysis unit designed by John Manioudakis and manufactured by Concordia's SP Technical Center. Each cell, which held a total volume of 280 μL, could be divided into two chambers by the placement of a dialysis membrane; each chamber contains a stoppered sampling port. Dialysis membranes (Fisherbrand, MWCO 12 000 – 14 000) were prepared according to manufacturer's instructions to remove trace amounts of sulphur or heavy metals and separate membrane patches were used to separate each chamber into two segments. Protein stocks were prepared in 50 mM HEPES, 150 mM NaCl, pH 7.5 and the concentration was adjusted to ~ 19 µM monomer. Stock solutions of NAD^+ and L-Tyr were prepared in the same buffer at concentrations of 50 mM and 2.4 mM respectively. NAD^+ was added to the protein solution to yield a final ligand concentration of 2 mM. Final L-Tyr concentrations used for the dialysis experiments ranged between 0.01 and 50 µM. Initial controls confirmed that pipetting errors could be minimized if each L-Tyr sample was prepared in a test tube by combining the appropriate volume of unlabeled L-Tyr stock solution, 1µCi L-[ring3,5-^{3}H] tyrosine and buffer to yield a final volume of 140 µL and then the L-Tyr solution mixtures of labeled and unlabeled L-Tyr were introduced at once into one chamber of each cell. The protein samples containing NAD^+ (140 µL) were introduced into the other chambers.

The concentration of labelled tyrosine in the reaction solution, at 8.9×10^{-14} µM/µCi, was considered negligible. Equilibrium was established by placing the device on a rocking shaker overnight at room temperature or in an incubator, set at 55°C and 50 rpm. Aliquots (50 µL) from each chamber were pipetted into scintillation vials and 4 ml scintillation fluid (EcoLite (+), MP Biomedicals) was added. Radioactivity was quantified (1 min per sample) using a 1217 RackBeta liquid scintillation counter (LKB Wallac). The data were analyzed using the following relationship (78):

$$[L_F]= A_2/ (A_1+A_2)*[L_T] \text{ and } [L_T] = [L_i]_1 + [L_i]_2$$

$$[L_B]= (A_1- A_2) / (A_1+A_2)*[L_T] \text{ and } [L_T] = [L_i]_1 + [L_i]_2$$

Where $[L_F]$ is the concentration of free ligand, $[L_B]$ is the concentration of bound ligand, $[L_i]_1$ and $[L_i]_2$ are the initial ligand concentrations introduced into chambers one and two, A1 and A_2 are the measured radioactivities in chamber one and two. Chamber one is the chamber containing protein, chamber two does not contain protein. The calculated concentrations of free and bound L-Tyr were then analyzed using the standard ligand binding template in Grafit Software version 5.0 (Erathicus Software) which fits the data to a single site saturation curve (see section 2.15) to obtain values for K_d and number of binding sites.

2.17. Isothermal Titration Calorimetry

Isothermal Titration Calorimetry (ITC) was used to determine thermodynamic parameters associated with the interaction of ligands with Δ19PD, such as ligand dissociation constants, number of binding sites, and changes in enthalpy and entropy upon ligand binding. The protein sample was first buffer exchanged using pre-equilibrated NAP-5 columns (Amersham Biosciences) into 50 mM phosphate, 150 mM NaCl, pH 7.5 or 50 mM phosphate, 150 mM NaCl, 1 mM NAD^+, pH 7.5 and subsequently the sample (approximately 20 µM) was dialyzed overnight against 4 L of 50 mM phosphate, 150 mM NaCl (pH 7.5) or 0.5 L 50 mM phosphate, 150 mM NaCl, 1 mM NAD^+ (pH 7.5). Ligands were prepared by dissolving the appropriate amounts of the free acid of NAD^+, Ba-salt of prephenate or the free base of L-Tyr at a concentration of about 2 mM in the dialysate (buffer remaining after protein dialysis was complete) and the pH of the ligand solution was adjusted to match the pH of the dialysate using HCl or NaOH. The ligand was further diluted in the dialysate to obtain a final concentration about 5 to 10-fold higher than protein concentration used, or as described in the text. A VP-ITC

Micro Calorimeter (MicroCal Inc.) was used throughout all experiments and was set up according manufacturer's instruction. The following parameters were used: 40 injections (1 injection of 1 µL, 39 injections of 7.4 µL), cell temperature: 20 °C, reference power: 10 µCal/s, initial delay: 60 s, stirring speed: 300 rpm, spacing: 240 s, filter period: 2 s. The Δ19 PD protein (1.4 mL) was used as cell reactant whereas ligand was inserted into the syringe and injected into the cell reactant. Protein samples and ligand preparations were degassed immediately before the experiment using a ThermoVac sample degassing and thermostat (MicroCal Inc.). Identical parameters were used when the experiment was performed at 55°C, except, the cell temperature was adjusted to the higher temperature. After integration of each injection, the heats were converted to enthalpies by using the Microcal Origin software, and the heat of dilution, as estimated from postsaturation heats was subtracted by subtracting a straight line. Thermodynamic parameters were obtained by fitting the values to a single site binding model in the Microcal Origin software, whereat ΔH (reaction enthalpy) and K_a (binding constant; $K_a = 1/K_d$) were determined from the curve fit. The changes in free energy (ΔG) and in entropy (ΔS) were calculated from the values of K_a and ΔH using the following equation: $\Delta G = - RT\ln(K_a) = \Delta H - T\Delta S$, where R is the universal molar gas constant and T is the absolute temperature.

2.18. Molecular Modelling

Molecular modelling was used to dock the substrate prephenate into an existing crystal structure for *A. aeolicus* Δ19 PD. First, the pdb file "3ggp" was prepared by removing all atoms and heteroatoms attributed to chains A and C using WordPad. Therefore only chain B and C were used for computing the model but additionally all heteroatoms forming HPPropionate and all water molecules in chain B were removed.

Next, a PDBQT file was prepared by uploading the prepared pdb file into AutoDock Tools (Molecular Graphics Laboratory), removing all non-polar hydrogen atoms and saving the file as PDBQT. Next the search space was defined in AutoDockTools. The search space restricts where the movable atoms, including those in the flexible side chains, should lie. The spacing of the grid points was set to 1.000 Å and 20 grid points in all three directions were used. Therefore the search space was cubic with a volume of in which each site measured 20 Å. Using important residues as a guideline, the center for x was chosen to be at 22.981, for y at 9.286 and for z at -6.875. The pdb file "prephenic acid" (http://ligand-expo.rcsb.org/ld-search.html) was then converted into a PDBQT file by loading the pdb file into AutoDockTools, defining all bonds as rotable bonds and saving the file as PDBQT file. Docking was performed using AutoDock Vina, the defined centers for x, y, and z and an exhaustiveness of 12. (Molecular Graphics Laboratory) and the resulting structures were visualized using PyMol (Schroedinger) (79).

Chapter 3: Results

3.1 Site-Directed Mutagenesis

The truncated tyrA gene from *A. aeolicus* had been cloned previously into the *E. coli* expression vector pET15b between *Nde*I and *Bam*HI restriction sites to construct the plasmid pΔ19PD harboring a cleavable N-terminal hexahistidine tag (57). The recombinant plasmid is approximately 6.6 kbp including a 5708 bp pET15b vector and an 886 bp insert. The variant proteins were obtained using site-directed mutagenesis according to Stratagene's QuickChange^{TM} protocol. Mutants were selected by incubation with *Dpn*I which digests only the methylated or hemi-methylated parental DNA. PCR products were then transformed into XL-10 Gold *E. coli* cells that are able to repair the nicked mutagenic strand and plasmid preparations were performed on selected colonies. DNA sequencing of the inserts confirmed that the mutant plasmids carried only the base change(s) desired.

The variants H217A, W190F and W259F were previously constructed, expressed and purified by Hou and Sitaras (60, 61).

3.2 Expression and Purification of *A. aeolicus* Δ19PD Variant Proteins

The following eighteen Δ19PD proteins were expressed and purified: native enzyme and the variants T152P/G, E153A, D247A, E153A/D247A (double substitution), H205Q/L, D206E/N/A, S213A, H214Q/L, H217V, S254A, W259Y, and R250A/K246A (double substitution).

The purification procedure adopted was based on the protocol originally developed for native Δ19PD as outlined by Bonvin *et al*. (30) and Sun *et al*. (57). Briefly, WT or mutant Δ19PD plasmids and the helper plasmid pMagik were co-transformed into

BL21(DE3) cells which were then grown in LB medium supplemented with antibiotics, and protein expression was induced by the addition of IPTG. Cells were disrupted by high pressure in the presence of protease inhibitors and the recombinant proteins were purified using Ni-NTA affinity chromatography at 4 °C. The N-terminal hexa-His tag was cleaved by dialyzing the purified protein overnight in the presence of thrombin and $CaCl_2$ at 4 °C. The previously reported heat treatment of the cell-free extract was omitted.

Protein purification was monitored by activity assays and denaturing gel electrophoresis. Figure 8 shows a representative SDS-PAGE analysis of the purification of native Δ19PD. Over-expression of the recombinant protein can be observed in the cell lysate and the cell-free extract (lanes 1 and 2). After applying the cell-free extract only once to the Ni-NTA column, no relevant band at the size corresponding to native Δ19PD can be observed in the flow-through (lane 3), leading to the conclusion that all tagged protein bound to the column. After an extensive washing step of more than 20 column volumes (lane 4), the protein was eluted with a buffer containing a high concentration of imidazole. The purification appears to yield homogeneous protein before and after thrombin-treatment (lanes 5 and 6) as judged by Coomassie blue staining. The molecular mass of His-tagged Δ19PD WT is about 35 kDa, whereas the thrombin-treated protein shows a mobility shift which is consistent with the removal of the 14 residue tag. Table 4 shows a purification table of Δ19PD WT.

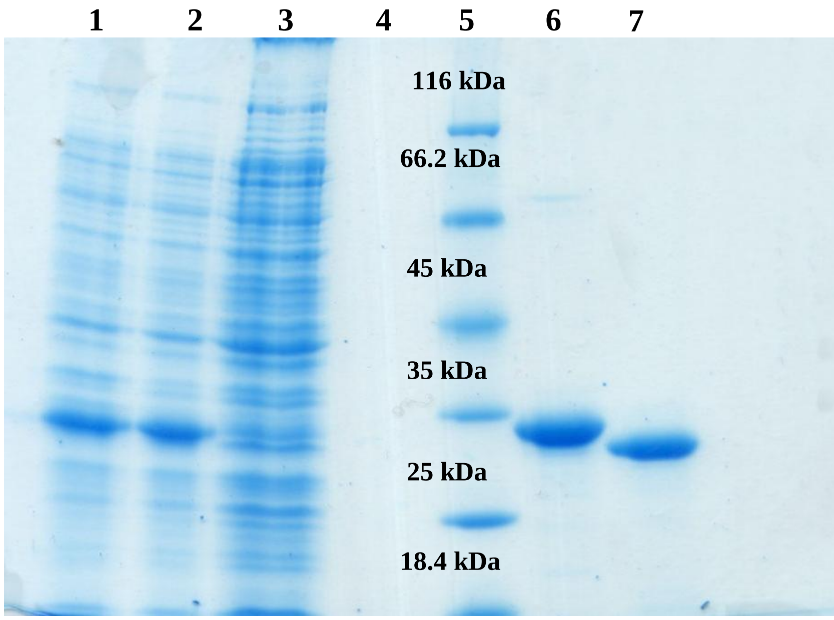

Figure 8: SDS-PAGE analysis of a native Δ19PD purification. Lane 1: Cell lysate (1/10 dilution), Lane 2: Cell-free extract (1/10 dilution), Lane 3: Ni-NTA flow-through, Lane 4: 30 mM imidazole last wash, Lane 5: Protein Molecular Weight Marker, Lane 6: 300 mM imidazole wash (pooled protein), Lane 7: Thrombin-treated pooled protein

Table 4: Representative purification table for native Δ19PD

	Total protein (mg)	Total activity (Units)	Specific activity (Units/mg)	Activity yield (%)	Purification fold
Cell-free extract	2341	1865	0.80	100	1.00
Ni-NTA flow-through	1230	116	0.09	6.2	0.1
Ni-NTA pooled	301	1605	5.3	86	6.6
Thrombin-treated	273	1363	5.0	73	6.3

Activity assays performed at 55°C at 2 mM NAD^+ (> 10 x K_m) and 138 µM prephenate (~ 4 K_m).

Almost all Δ19PD proteins were purified to approximately 90% homogeneity or greater (Figure 9) and behaved similarly during the purification process, exhibiting typical yields of purified protein of ~ 60-100 mg/L of cell culture. The exception was

E206A (Figure 10) which yielded 13 mg of protein in the final preparation per L of culture.

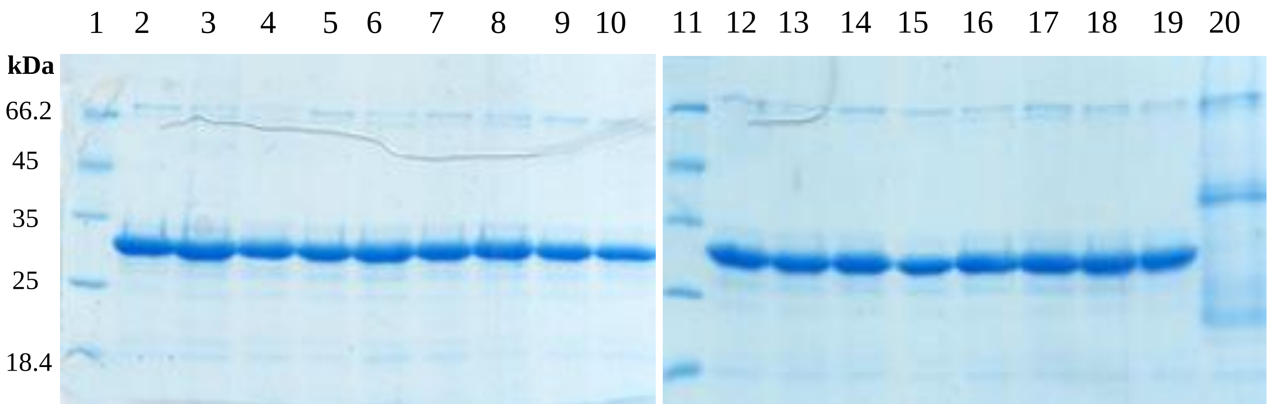

Figure 9: SDS-PAGE analysis of purified Δ19PD proteins. Lane 1: Protein Molecular Weight Marker, Lane 2: native enzyme, Lane 3: H217V, Lane 4: W259Y, Lane 5: T152P, Lane 6: T152G, Lane 7: D247A, Lane 8: E153A, Lane 9: E153A/D247A, Lane 10: S254A, Lane 11: Protein Molecular Weight Marker, Lane 12: S213A, Lane 13: H214Q, Lane 14: H214L, Lane 15: R250A/K246A, Lane 16: H205Q, Lane 17: H205L, Lane 18: D206E, Lane 19: D206N, Lane 20: D206A. Proteins samples after Ni-NTA affinity chromatography and treatment with thrombin were analyzed on 12% acrylamide gels. Approximately 10 μg of protein were applied in lanes 2-10 and 12-20.

The cell lysate and the cell-free extract (lanes 1 and 2 in Figure 10) show that there is poor over-expression of protein in the mass range of 32-35 kDa protein relative to the total protein in those fractions. Additionally, protein that was eluted in the 300 mM imidazole wash (lane 6) shows evidence of protein degradation which was further magnified after treatment with thrombin (lane 7).

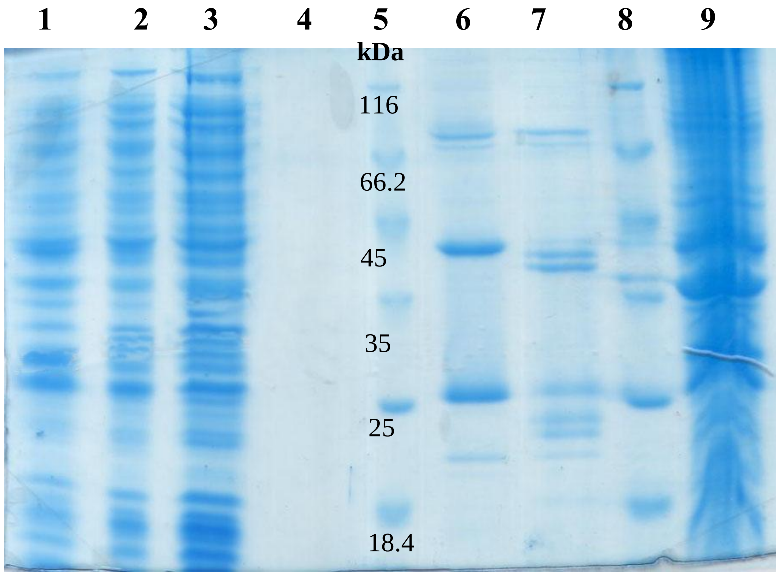

Figure 10: SDS-PAGE analysis of Δ19 PD D206A purification. Lane 1: Cell lysate (1/10 dilution), Lane 2: Cell-free extract (1/10 dilution), Lane 3: Ni-NTA flow-through, Lane 4: 30 mM imidazole last wash, Lane 5: Protein Molecular Weight Marker, Lane 6: 300 mM imidazole wash (pooled protein), Lane 7: Thrombin-treated pooled protein, Lane 8: Molecular Weight Marker, Lane 9: Pellet of insoluble cellular debris solubilized in 10% SDS.

3.3 Electrospray Ionization Mass Spectrometry

Purified Δ19PD proteins were analyzed by ESI-Q-ToF MS to confirm that the correct amino acid conversions occurred. Figure 11 shows a representative spectrum.

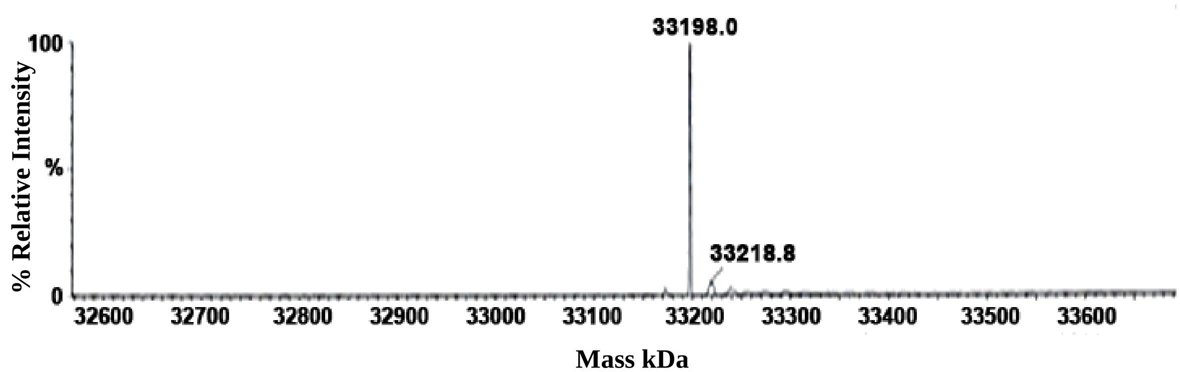

Figure 11: Deconvoluted ESI-MS spectra of the native Δ19 PD thrombin-treated protein. The peak shows the molecular weight of the monomeric form of the protein.

The theoretical and experimental mass values of each thrombin-treated protein (Table 5) were, for the most part, in excellent agreement. The sole exception was D206A whose major peak on the mass spectrum (data not shown) was about 10 kDa less than expected based on the protein's predicted amino acid sequence. These results are in agreement with the SDS-PAGE analysis which indicated that this variant protein is likely not stable. The mass values of H205Q/L could not be determined since these variants did not resuspend sufficiently in the solution (30% methanol/0.2% formic acid (v/v)) routinely used for direct injection into the mass spectrometer.

Table 5: Summary of molecular weights of native and variant Δ19PD proteins.

Δ19PD variants	**Expected Mass[a] (Da)**	**Observed Mass (Da)**	**Difference (Da)**	**Δ19PD variants**	**Expected Mass[a] (Da)**	**Observed Mass (Da)**	**Difference (Da)**
Native	33196.5	33198	1.5	**W190F**	33157.5	33157.2	0.3
H217A	33130.4	33129.6	0.8	**H217V**	33158	33160.6	3.6
W259F	33157.5	33158.3	0.8	**W259Y**	33173.5	33171.5	2
T152P	33192.5	33193.9	1.4	**T152G**	33152.5	33150.5	2
H214Q	33187.5	33188.6	1.1	**H214L**	33172.5	33176.5	4
S213A	33180.5	33168.5	12	**S254A**	33180.5	33180.1	0.4
D247A	33152.5	33153.3	0.8	**E153A**	33138.5	33140.3	1.8
E153A/D247A	33094.5	33096	1.5	**R250A/K246A**	33053.8	33057.2	3.4
H205Q	33187.5	n/a	n/a	**H205L**	33172.5	n/a	n/a
D206N	33195.5	33198.6	3.1	**D206E**	33210.5	33213.4	2.9
D206A	33187.5	22204.8	10982.7	**H147A**	33129.9	33134.7	4.8

[a] Expected mass based on the predicted amino acid sequence was calculated using EXPASY-PeptideMass program which gives the average molecular weight of the deprotonated side chain. Mass differences of +/-5 Da were considered to be sufficient to accurately identify the enzyme in question. Values differ from sample to sample based on the particular instrument conditions and ambient temperature fluctuations on the day of spectral analysis.

3.4 Far-UV Circular Dichroism Spectra of Δ19PD Proteins

Far-UV circular dichroism (CD) spectroscopy was used to determine if the amino acid conversions within Δ19PD perturbed the global secondary structure of the protein. In CD spectroscopy the protein sample is subjected to both left-handed and right-handed components of circular polarized light. At wavelengths in the far-UV, this light is absorbed by amide and carbonyl groups in the protein's peptide backbone and the degree of absorption of the right versus left components depends on the conformation of the protein backbone (80). CD spectra were acquired between 200 – 260 nm at 25 °C. All proteins showed pronounced absorption minima at 208 and 222 nm (Figure 12) which are characteristic of proteins with considerable α-helical content. The spectra of the different variants, except for D206A, are nearly superimposable which indicates that the global secondary structure has not been affected by the amino acid substitutions.

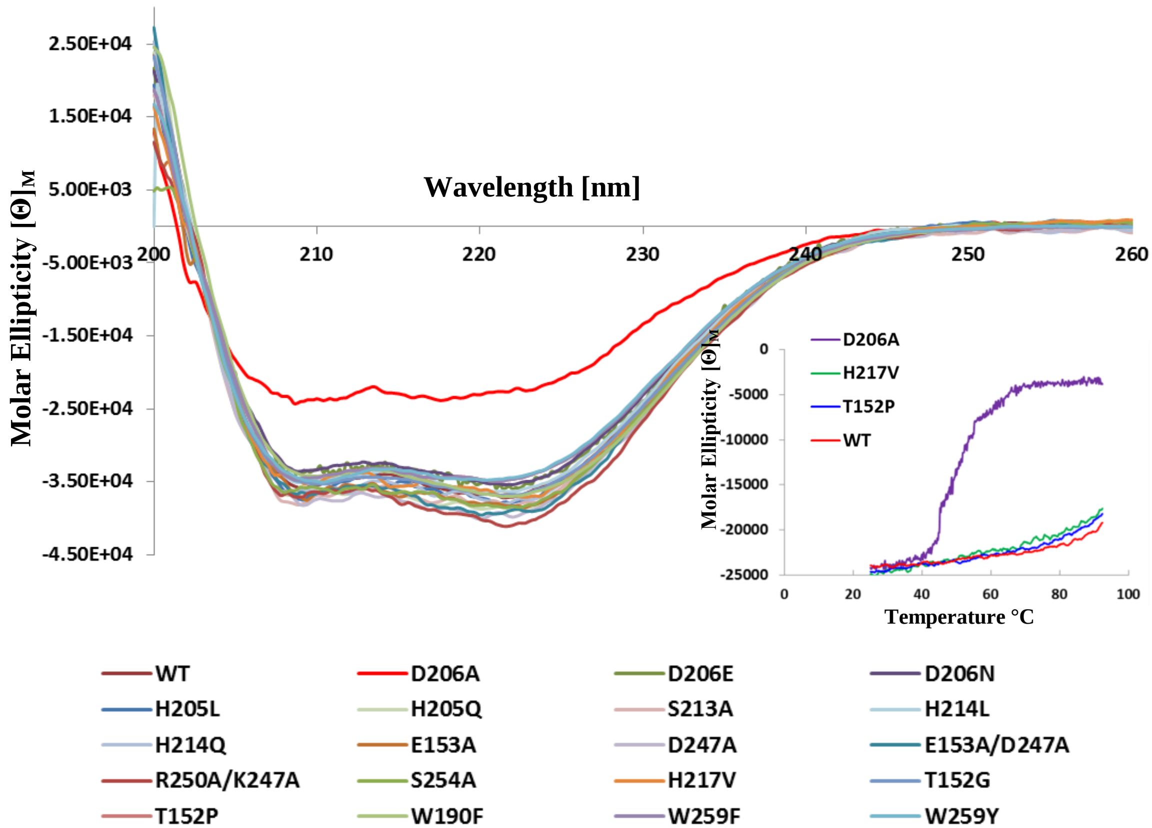

Figure 12: Far-UV CD spectra of native and variant Δ19PDs. Variant proteins (~ 7 µM monomer) were buffer exchanged into 50 mM potassium phosphate, 75 mM NaCl, pH 7.5. Spectra were recorded at 25ºC in a 0.2 cm path-length rectangular cell with a scan rate of 100 nm/min. Each curve presents the average of 5 accumulations. Inset: **Variable temperature far-UV CD spectra of native and selected variant Δ19PD enzymes (**5 µM monomer), prepared in the above. Spectra were recorded at 222 nm in a 0.2 cm path-length rectangular cell from 25ºC to 95ºC, using a ramping speed of 40 ºC/h.

Thermal stability studies were performed on Δ19PD proteins by monitoring the change in ellipticity at 222 nm with increasing temperature under the conditions listed in section 2.13 and in the legend of Figure 12. Most proteins were very resistant to thermal unfolding, even those variants with significantly altered kinetic parameters (H217V, T152P shown in the inset in Figure 12); their T_m values could not be determined. In contrast, D206A exhibited the most dramatic change, yielding a T_m value of ~ 45 °C, providing further evidence that this variant was very unstable or that protein isolated during the purification of D206A belonged mainly to the mesophilic *E. coli* host strain.

3.5 Kinetic Studies of Native Δ19PD and Variants

3.5.1. Determination of Steady-State Kinetic Parameters

In order to probe the importance of selected active site residues of Δ19PD for catalysis, substrate binding and feedback inhibition, steady-state kinetic assays were performed on the variant proteins. Substrate saturation curves were obtained from initial rates with either prephenate or NAD^+ as variable substrate (data not shown). The kinetic parameters obtained from the analysis of the saturation curves are summarized in Table 6. The Michaelis constant (K_m) loosely reflects the affinity that the enzyme has for substrates, while the turnover number k_{cat} describes the rate at which substrate is converted to product per unit per active site when the enzyme is fully saturated with the appropriate substrates. The ratio of k_{cat}/K_m describes the overall efficiency of the catalyst.

Table 6: Kinetics parameters for the reactions catalyzed by Δ19PD proteins

Variable Substrate	**Prephenate**			**NAD^+**		
Protein	**K_m [μM]**	**k_{cat} [s^{-1}]**	**k_{cat}/K_m [$M^{-1}s^{-1}$]**	**K_m [μM]**	**k_{cat} [s^{-1}]**	**k_{cat}/K_m [$M^{-1}s^{-1}$]**
Native Δ19PD	**89.5 ± 9.7**	**7.6 ± 0.2**	**8.5×10^4**	**58.5 ± 4.9**	**6.9 ± 0.3**	**1.2×10^5**
H217A[a]	**3507 ± 194**	**0.20 ± 0.01**	**5.7×10^1**	**29.0 ± 1.1**	**0.40 ± 0.002**	**1.4×10^4**
H217V	**2577 ± 336**	**0.95 ± 0.06**	**8.6×10^2**	**18.7 ± 2.0**	**0.72 ± 0.02**	**3.9×10^4**
W190F[a]	**54.2 ± 3.9**	**5.9 ± 0.3**	**1.1×10^5**	**32.3 ± 2.8**	**5.5 ± 0.2**	**1.7×10^5**
W259F[a]	**820 ± 89**	**2.5 ± 0.1**	**3.1×10^3**	**56.6 ± 9.0**	**2.5 ± 0.1**	**4.4×10^4**
W259Y	**145 ± 14**	**7.2 ± 0.2**	**4.9×10^4**	**65.6 ± 8.7**	**5.0 ± 0.3**	**7.6×10^4**
T152P	**864 ± 87**	**0.74 ± 0.02**	**3.7×10^2**	**82.2 ± 10.8**	**0.70 ± 0.02**	**8.2×10^3**
T152G	**16.0 ± 1.6**	**1.74 ± 0.04**	**1.1×10^5**	**16.5 ± 2.7**	**1.38 ± 0.04**	**8.4×10^4**
D247A	**168 ± 23**	**3.5 ± 0.1**	**2.1×10^4**	**25.6 ± 4.2**	**2.7 ± 0.07**	**1.1×10^5**
E153A	**242 ± 41**	**2.9 ± 0.1**	**1.2×10^4**	**24.1 ± 4.9**	**2.1 ± 0.07**	**8.9×10^4**
D247A/E153A	**161 ± 21**	**0.75 ± 0.022**	**4.7×10^3**	**8.44 ± 1.03**	**0.55 ± 0.01**	**6.5×10^4**
H205Q	**75.6 ± 14.5**	**1.9 ± 0.08**	**2.7×10^4**	**15.4 ± 1.7**	**1.5 ± 0.02**	**9.7×10^4**

Variable Substrate	Prephenate			NAD^+		
Protein	**K_m [μM]**	**k_{cat} [s^{-1}]**	**k_{cat}/K_m [$M^{-1}s^{-1}$]**	**K_m [μM]**	**k_{cat} [s^{-1}]**	**k_{cat}/K_m [$M^{-1}s^{-1}$]**
H205L	**510 ± 79**	**0.06 ± 0.003**	**1.1×10^2**	**28.1 ± 5.3**	**0.06 ± 0.002**	**2.1×10^3**
H214Q	**64.7 ± 10.5**	**1.0 ± 0.03**	**1.6×10^4**	**11.5 ± 1.9**	**0.80 ± 0.02**	**6.9×10^4**
H214L	**832 ± 188**	**2.6 ± 0.2**	**3.1×10^3**	**16.2 ± 4.7**	**2.0 ± 0.3**	**1.3×10^5**
S213A	**1930 ± 292**	**1.3 ± 0.09**	**6.7×10^2**	**25.6 ± 4.1**	**0.80 ± 0.02**	**3.1×10^4**
S254A	**200 ± 35**	**4.3 ± 0.2**	**2.2×10^4**	**45.6 ± 7.0**	**2.8 ± 0.09**	**6.2×10^4**
R250A/K246A	**19708 ± 4908**	**4.9 ± 0.8**	**2.5×10^2**		**Not determined[b]**	
D206E	**404 ± 53**	**5.2 ± 0.2**	**1.3×10^4**	**21.9 ± 6.0**	**3.9 ± 0.2**	**1.8×10^5**
D206N	**25.3 ± 3.0**	**2.3 ± 0.05**	**9.2×10^4**	**12.7 ± 3.2**	**1.5 ± 0.05**	**1.2×10^5**
D206A		**n. a.[c]**			**n. a.[c]**	
H147A		**n. a.[c]**			**n. a.[c]**	

Reactions were performed at pH 7.5 and 55ºC. Values were calculated from initial rates using a minimum of five different concentrations ranging from ½ - K_m up to 15 x K_m for the variable substrate. When prephenate was the variable substrate NAD^+ was fixed at 2 mM, while when NAD^+ was the variable substrate, prephenate was fixed at 4 x K_m for all variants except for H217V (2x K_m = 5.9 mM), H217A (5 x K_m = 18 mM), S213A (2x K_m = 3.8 mM).[a] Variants were constructed, expressed and purified by Hou and Sitaras (60, 61). Values of k_{cat} were normalized with respect to k_{cat} obtained for native Δ19PD in this study. [b] No saturation of enzyme with prephenate possible. [c] No activity detectable when adding 90 μg to reaction mixture containing 0.5 mM prephenate, 2 mM NAD^+.

Variant proteins exhibited a range of values for the K_m for prephenate as well as the turnover number for the enzyme. Interestingly, in most cases the conversion decreased the enzyme's K_m for NAD^+. Such an effect has been reported for several variants of *A. aeolicus* Δ19PD (30, 63) as well as for the native enzyme in the presence of low concentrations of Gdn-HCl where it has been shown that small perturbations in the active site can promote the binding of the hydrophobic cofactor (30).

The most common substitution used in this battery of variants was alanine, a small non-polar residue, which eliminates H-bonds or ionic interactions. In some instances, such as for His, replacements of Gln, Leu or Val were used. Gln with an amide group best preserves electrostatic interactions associated with the imidazole ring, while the larger, non-polar side chains of Leu or Val eliminate H-bonding capacities while providing "bulk". For Trp groups, the aromatic non-polar residue Phe was used, or its polar analog Tyr. Backbone flexibility was probed by introducing a Pro or a Gly. Lastly, the importance of side chain length could be defined by converting Asp to Glu while replacing Asp with Asn was used to examine polar versus charge effects.

Those variants that resulted in the largest increases in K_m for prephenate (8 to 220 fold) were W259F, H214L, T152P, S213A, H217V/A and R250A/K246A. Of these, H217V/A, T152P and H205L also showed significant decrease in k_{cat} (8 to 127 fold). Others showed only moderate increases in K_m for prephenate (usually 2 to 4 fold) with accompanying decreases in k_{cat} (2 to 7 fold). None of the substitutions for which activity could be detected, selectively affected k_{cat}.

Interestingly, the K_m values for NAD^+ for the variants were either unchanged compared to the native enzyme or a lower value (1.5 to 7-fold).

The kinetic parameters for the variant proteins will be described further in the "Discussion", placing the effects of the amino acid substitutions in context of the available crystal structures.

3.5.2. Effects of L-Tyr on PD activity of Native and Variant *A. aeolicus* Δ19PD proteins

To determine the effects of the amino acid replacements on the sensitivity of PD activity to L-Tyr, initial rates were recorded at 55ºC in the presence of 0 to 7000 µM L-Tyr keeping the substrate concentrations fixed at 2 mM for NAD^+ and ~4 x K_m (or unless stated otherwise) for prephenate. The percent residual activity was then plotted as a function of L-Tyr concentration (Figure 13). Some variants were more sensitive to feedback inhibition by L-Tyr (D247A, H205Q, H214L/Q), while others (W190F, W259F, E153A, and D206N/E) exhibited a response similar to the native enzyme. The remaining variants were less inhibited by L-Tyr than native Δ19PD and could be grouped as follows: 1) those that appeared almost completely resistant to feedback inhibition (W259Y, S213A, S254A, H217A and H217V), 2) those that are less resistant (R250A/K246A, T152G and H205L) and 3) those that exhibited a mixed and unusual pattern of inhibition. For example, the activity of T152P and E153A/D247'A decreases rapidly at low inhibitor concentrations, similar to WT, but at higher L-Tyr concentrations retain ~50% and 70% activity, respectively.

Table 7 shows approximate IC_{50} values (concentration of L-Tyr required to reduce activity by 50%) that were obtained by fitting the effects of L-Tyr on PD activity to sigmoidal dose-response curves using non-linear regression analysis in Grafit Software version 5.0 (data not shown). The IC_{50} values were used to derive apparent inhibition constants for L-Tyr (K_i) (Table 7) from the relationship described in the table legend.

Table 7: Summary of IC_{50} and K_i values for the interactions of Δ19PD proteins with L-Tyr. Initial rates were obtained at 55°C, in the presence of at least 5 different concentrations of L-Tyr between 0-7000 µM under the assay conditions listed in Figure 13. IC_{50} values were calculated using the Grafit IC50 four parameter fit software while K_i values were derived using the relationship $K_i = IC_{50} / (1 + [S] / Km)$ where IC_{50} refers to the concentration of inhibitor to reduce PD activity by 50%, [S] represents the concentration of prephenate used in the assay and K_m is the Michaelis constant for prephenate. L-Tyr is assumed to act as a competitive inhibitor with respect to prephenate in the PD reaction. [a] Data could not be fitted to the equation.

Enzyme	Approximate IC_{50} (µM)	K_i (µM)	Enzyme	Approximate IC_{50} (µM)	K_i (µM)
Native Δ19PD	213 ± 16	43 ± 6.3	**W190F**	378 ± 29	67.5 ± 5.2
H205Q	139 ± 20	34.8 ± 6.9	**H205L**	1030 ± 257	240 ± 60
D206N	314 ± 22	54.6 ± 3.8	**D206E**	536 ± 29	107 ± 6
W259F	462 ± 20	156 ± 6.7	**W259Y**	n/d[a]	n/d[a]
H214Q	52.2 ± 7.8	10 ± 1.5	**H214L**	55.6 ± 5.9	14.3 ± 1.4
T152P	n/d[a]	n/a	**T152G**	7610 ± 4458	1545 ± 896
D247A	54.3 ± 3	9.6 ± 0.53	**E153A**	218 ± 87	44 ± 17.6
E153A/D247A	n/d[a]	n/d[a]	**R250A/K246A**	n/d[a]	n/d[a]
H217A	n/d[a]	n/d[a]	**H217V**	n/d[a]	n/d[a]
S254A	n/d[a]	n/d[a]	**S213A**	n/d[a]	n/d[a]

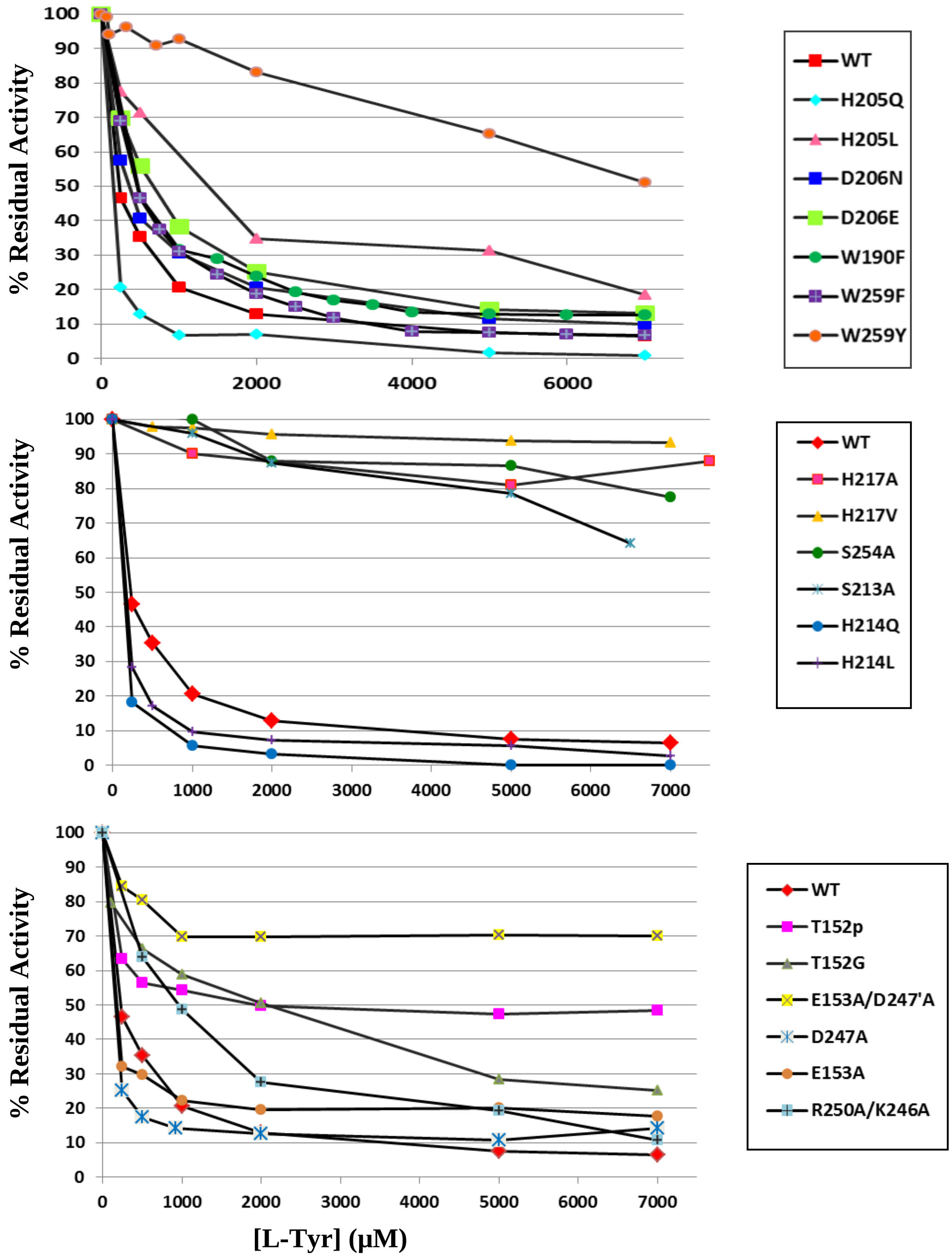

Figure 13: Effect of L-Tyr on PD activity of Δ19PD proteins. Assays were carried out at 55ºC in reaction buffer containing 50 mM HEPES, 150 mM NaCl, pH 7.5, in the presence of L-Tyr (0-7000 µM), 2 mM NAD^+ and ~ 4 x K_m for prephenate (except ~ 0.1 x K_m for R250A/K246'A).

3.5.3. Pattern of Inhibition by L-Tyr of Native Δ19PD and T152P

Crystal structure analysis of Δ19PD in complex with NAD^+ and HPP or L-Tyr (Figure 7) showed that L-Tyr combines to the same site as does HPP and presumably prephenate. In order to confirm that L-Tyr acts as a competitive inhibitor with respect to prephenate in the PD reaction, activity was recorded at different concentrations of prephenate at fixed concentrations of L-Tyr. The family of lines appeared to intersect on the y-axis and the lowest standard errors in the kinetic parameters were obtained by fitting the data to the equation describing linear competitive inhibition. A K_i of 83.3 ± 16.6 µM was obtained (Figure 14 A). The Michaelis constant derived from this plot (185 ± 33 µM) and the turnover number (8.4 ± 0.5 s^{-1}) are comparable with the values given in Table 6 and 7. It is worth noting, that at the lowest concentrations of prephenate and the highest concentrations of L-Tyr, the double reciprocal plots were concave upwards. This is in agreement with data reported previously (55) and has been attributed to the fact that L-Tyr promotes positive cooperativity in the binding of prephenate to the two subunits. Surprisingly, the K_i value of 15.9 ± 1.3 µL previously reported was approximately 3-fold lower than the value calculated during this study even though the experimental conditions appeared to be identical (63).

The effect of L-Tyr on PD activity of T152P yielded a best fit to the equation for hyperbolic competitive inhibition. Thus, with increasing concentrations of L-Tyr the enzyme becomes progressively less inhibited by L-Tyr than predicted for simple, linear competitive inhibition. Also worth noting, L-Tyr did not appear to promote cooperative interactions in binding as evidenced by the straight lines in the double reciprocal plots even at 500 µM L-Tyr and prephenate concentrations of one half K_m.

The fit yielded a K_m for prephenate of 800 ± 183 µM which is in good agreement with the value obtained by kinetic analysis (864 ± 87 µM), a K_i of 4.1 ± 2.8 µM and a value for α of 2.9 ± 0.5 µM.

.

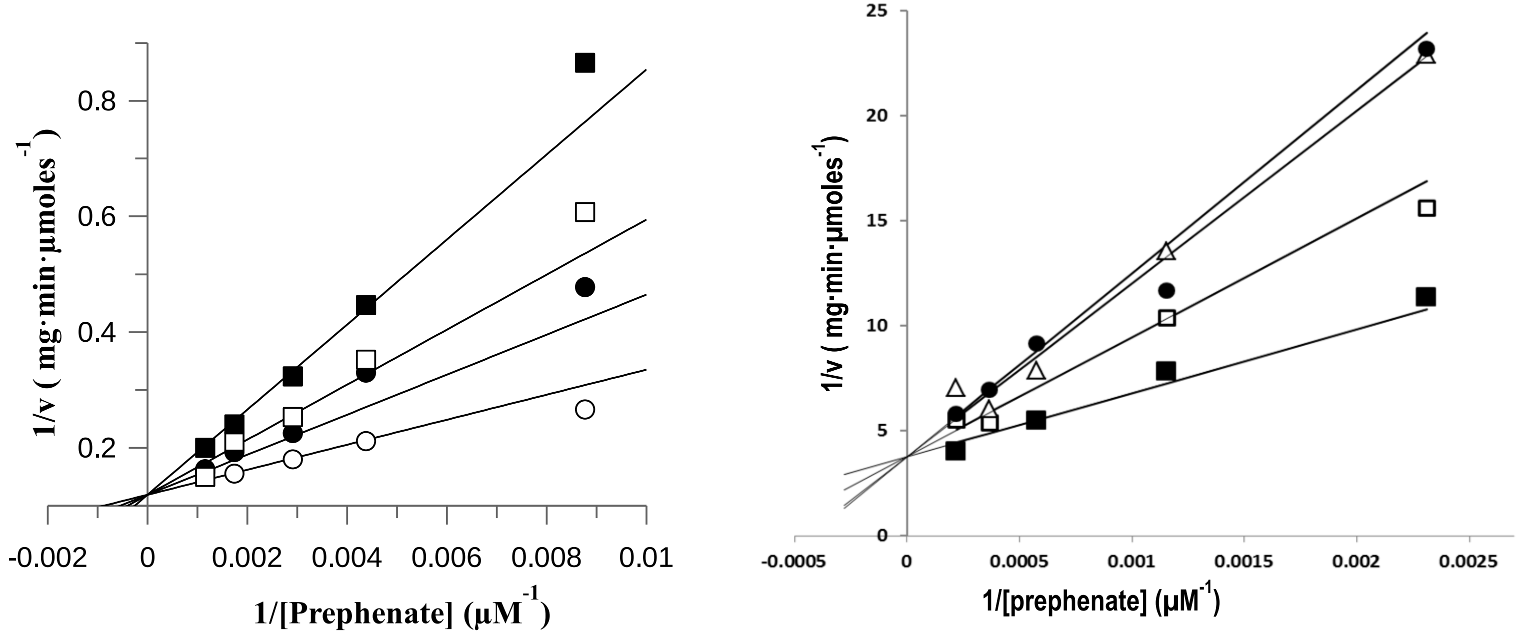

Figure 14: Double reciprocal plot of the inhibition of *A. aeolicus* Δ19PD by L-Tyr at 55ºC. (A) PD activity of native Δ19PD was recorded by varying prephenate concentrations from 1 x K_m to 10x K_m (113 – 853 µM), keeping NAD^+ fixed at 2 mM and in the presence of L-Tyr concentrations from 0 (○), 50 (●), 100 (□) and 200 µM (■). The linear data were fit to the equation describing linear competitive inhibition using the non-linear regression analysis by Grafit 5.0 as described in section 2.12. A K_i of 83.3 ± 16.6 µM, a Michaelis constant of 185 ± 33 µM and a V_{max} of 8.4 ± 0.5 s^{-1} was obtained. (B) PD activity of the T152P variant was recorded by varying prephenate concentrations from 1/2 K_m to 3.5 x K_m (433 – 2737 µM), keeping NAD^+ fixed at 2 mM and in the presence of L-Tyr concentrations from 0 (■), 10 (□), 100 (Δ), 500 (●) µM. The data were fit to the equation describing hyperbolic competitive inhibition and the kinetic parameters determined, yielding a K_i of 4.1 ± 2.8 µM, a Michaelis constant for prephenate of 800 ± 183 µM and a V_{max} of 0.26 ± 0.02 s^{-1}. The value for α was 2.9 ± 0.5 µM.

3.6 Dependence of pH on the Ionization of Active Site Residues

Fluorescence emission spectroscopy was used to determine if the amino acid substitutions had altered the environment of the aromatic chromophores Trp and Tyr in Δ19PD. The fluorescence emission spectra of most variants were comparable to the native protein with the exceptions of W190F, W259F, H217A/V, H214Q/L and S213. Figure 15A shows the fluorescence emission spectra of native Δ19 PD and these variants upon excitation at 280 nm. As expected, W190F and W259F showed reduced fluorescence intensities at 280 nm reflecting the absence of one of the two Trp per monomer. The W259Y conversion restored most of the fluorescence intensity. In contrast, the spectra of H217A/V variants as well as H214L/Q and S213A were significantly higher than that of the native enzyme. This might be caused by the relief of the quenching of fluorescence emission by the removal of ionizable residues. In order to determine the pK_a values of ionizable groups that could quench tryptophan fluorescence emission of the native Δ19PD (75), the fluorescence spectra of the WT enzyme were collected at several different pH values. Surprisingly, the fluorescence intensity of native Δ19PD did not change with increasing pH values as shown in Figure 15B. This indicated that there is no ionisable group near a Trp that could quench fluorescence emission.

.

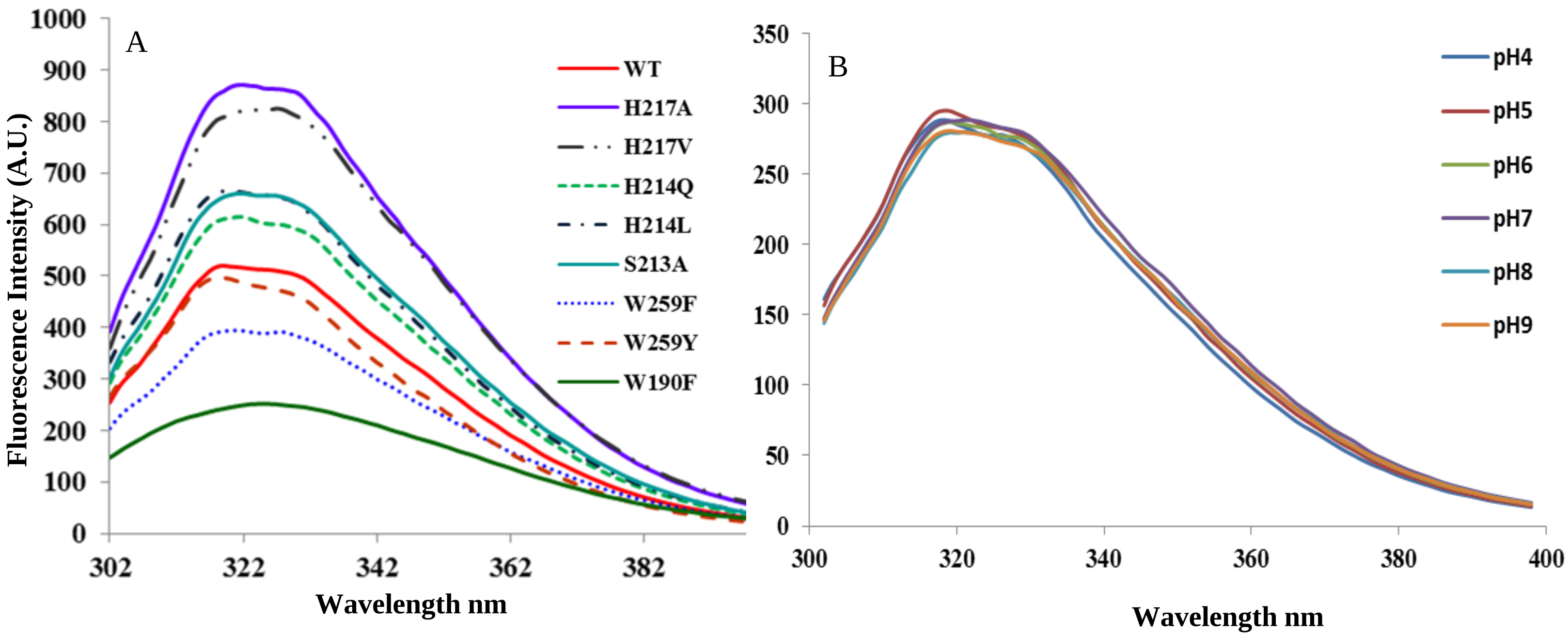

Figure 15: Fluorescence emission spectra for selected Δ19PD proteins. (A) Fluorescence emission spectra for variants at pH 7.5. Proteins (5µM monomer) were buffer exchanged into 50 mM KH_2PO_4, 75 mM NaCl buffer (pH 7.5) and placed in Varian 400 µL fluorescence micro cell (1.0 cm path-length). Excitation wavelength was fixed at 280 nm. The fluorescence emission was scanned at 30°C from 300 to 400 nm using excitation and emission slit widths set at 5 nm. Spectra were corrected for buffer contribution. (B) Fluorescence emission spectra for native Δ19PD at different pH values. Protein was buffer exchanged to a final concentration of 2 µM into 50 mM KH_2PO_4, 75 mM NaCl buffer pH varied from 4 to 8. Spectra were recorded as explained for panel A.

Additionally, it has been proposed that the ionization state of H217 within the ternary complex may play an important role in feedback inhibition by L-Tyr (63). Thus the pH dependence of the dissociation of L-Tyr from the enzyme-NAD^+-complex was determined from pH rate profiles. Substrate saturation curves were obtained using prephenate as variable substrate and fixed NAD^+ concentration (2 mM) in the presence of 0 and 100 µM L-Tyr at nine different pH values ranging from 5.5 to 9.5. Assuming that L-Tyr acts as a competitive inhibitor for native Δ19PD, the K_i was obtained using the relationship described in section 2.12. The plot of pK_i vs. pH shows that the inhibition of Δ19PD by L-Tyr is pH independent over this range and as determined in this kinetic experiment. This is in contrast to the pH dependence of the kinetic parameters for Δ19PD. When the kinetic parameters, k_{cat} and K_m for prephenate, were determined from pH 5.5 to 9.0 a bell-shaped profile of log $(V/E_t)/K_{m,pre}$ vs. pH was obtained, indicating that there were two ionisable groups (one protonated, one deprotonated) involved in catalysis and/or prephenate binding to the enzyme-NAD^+-complex. Their pK_a values were calculated to be 5.9 ± 0.1 and 10.0 ± 0.6 as described in section 2.11. Bonvin *et. al.* (55) previously assigned the group on the acidic limb to the catalytic H-bond acceptor H147 while the other titrating residue was not identified. It is worth noting, that the V/E_t profile appears to be independent of pH presumably due to the shift in pK_a to higher or lower values as a result of the formation of the enzyme-NAD^+-prephenate complex.

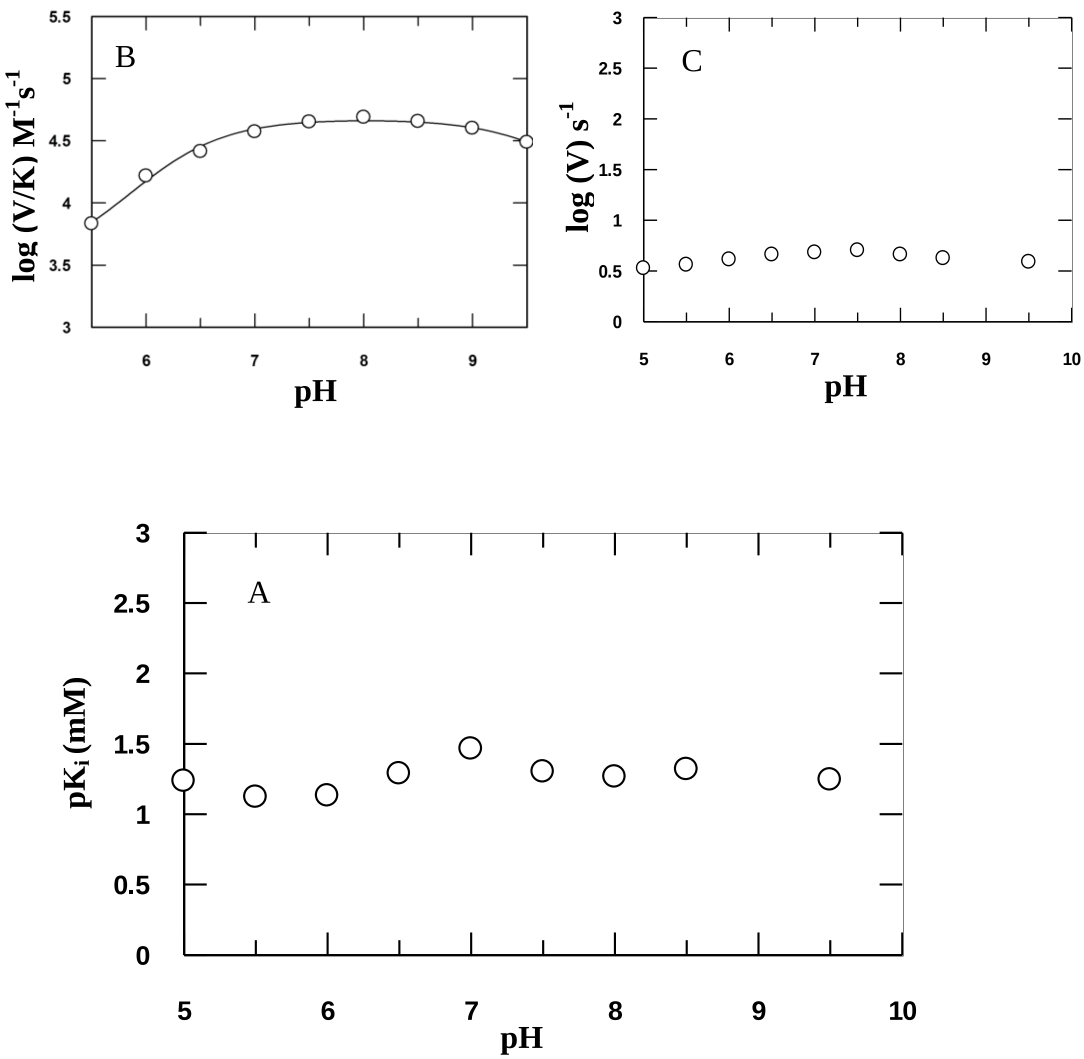

Figure 16: pH dependence of kinetic parameters and L-Tyr inhibition of the PD activity of Δ19 PD from *A. aeolicus*. Dehydrogenase activity was recorded at 55ºC over the pH range from 5.5 to 9.5 in 3-component buffer containing 25 mM HEPES, 25 mM Tris/HCl, 25 mM 3-(N-morpholino)propanesulfonic acid (MES), 150 mM NaCl. NAD^+ concentration was kept fixed at 2 mM while prephenate was varied from 75 - 997 µM. Values for k_{cat} (denoted V) and K_m (denoted K) were obtained. The values for the K_i were obtained as described in the text (section 2.11and 2.12). **(A) pH vs. pK_i, (B) pH vs. log (V/K), (C) pH vs. log(V),** the curves represent the best non-linear, least square fit of the data to the pK_a, double equation in Grafit 5.0 (section 2.11). Fit of log(V/K) yielded pKa values of 5.9 ± 0.1 and 10.0 ± 0.6. The data obtained for pK_i and log(V) could not be fitted adequately to the equation.

3.7 Determination of Dissociation Constants for Substrates and Inhibitor

3.7.1. Isothermal Titration Calorimetry (ITC)

Isothermal Titration Calorimetry (ITC) is a very sensitive biophysical tool that can measure the amount of heat released or absorbed upon the interaction of two biomolecules. From the analysis of one experiment, parameters such as binding affinity, number of binding sites, enthalpy (ΔH) and entropy (ΔS) can be obtained (81).

Representative data (Figure 17) show the enthalpy changes from the addition of L-Tyr to the T152P-NAD^+-complex (A) and from the addition of L-Phe to the native Δ19PD-NAD^+-complex at 20 °C. The two figures clearly highlight the differences of a titration in which the ligand binds (A) and does not bind (B) to the enzyme-NAD^+-complex. All other spectra are shown in Appendix 1A, B, C and D. Table 8 summarizes the thermodynamic parameters for the interaction of substrates or inhibitor with native and selected variants of Δ19PD.

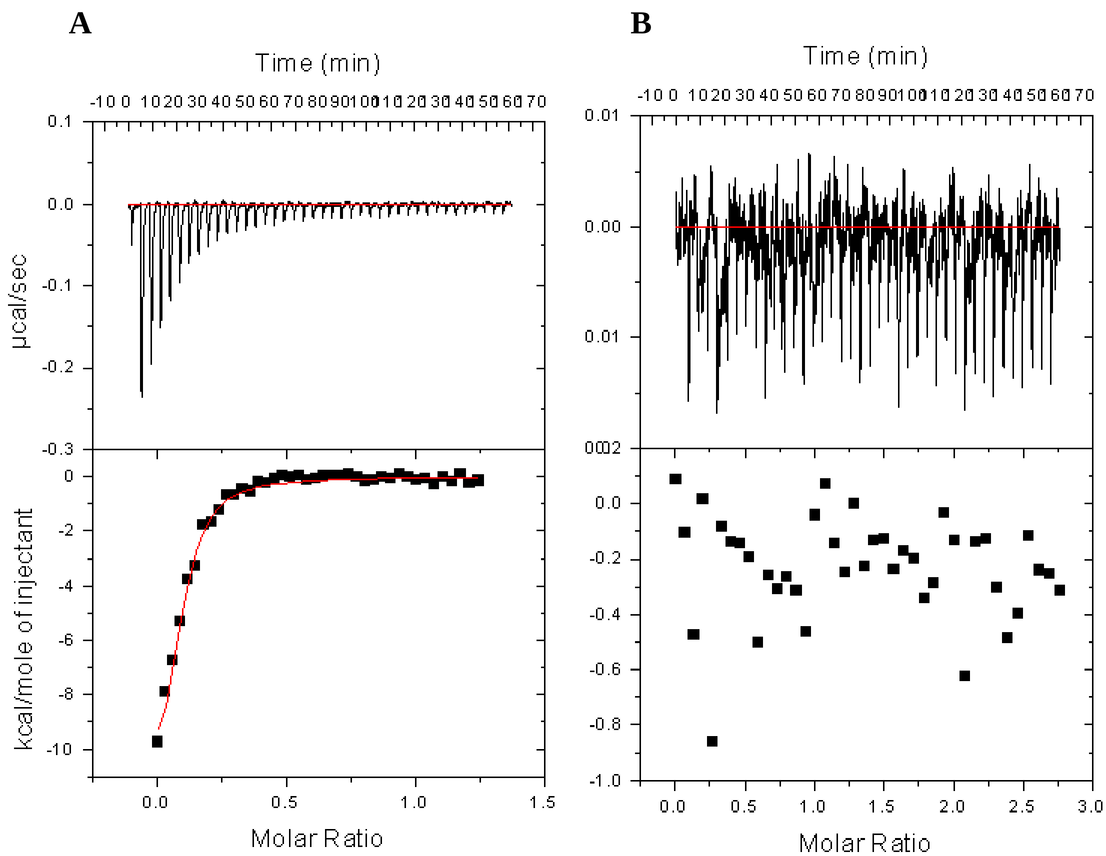

Figure 17: Isothermal titration calorimetry analysis of select Δ19PD proteins. The interaction of (A) the T152P Δ19PD-NAD^+ -complex with L-Tyr and (B) the native Δ19PD-NAD^+-complex with L-Phe were studied in 50 mM KH_2PO_4 / K_2HPO_4, 75 mM NaCl, pH 7.5 at 20 °C. The initial concentrations of T152P and native enzyme in the cell were 36 µM and 20µM, respectively, while the initial ligand concentration in the syringe was 350 µM L-Tyr and 500 µM L-Phe. The upper panels are raw data of enthalpy changes, each peak corresponding to the injection of L-Tyr (first injection 1 µL, subsequent 39 injections 7 µL) into the enzyme-NAD^+-complex. The lower panels show the integrated enthalpy plot. The areas under each peak were integrated and plotted against the molar ratio ([Ligand] to [Enzyme]). The red solid line is the best fit of the data to the one-binding-site model of the Origin® plotting software from MicroCal.

Table 8: Binding parameters for native Δ19PD and selected variants obtained by ITC. n, ΔH and TΔS were determined by analyzing ITC raw data obtained at 20°C with Origin® plotting software; ΔG was calculated by the following relationship: $\Delta G = -RT*\ln(K_a)$, all data are corrected for heat of dilution. [a] Average of two experiments. [b] at 55°C

Enzyme-NAD$^+$ complex titrated with L-Tyr					
	n **(mole ligand/ mole enz)**	**K_d** **(μM)**	**ΔH** **(kcal/mole)**	**TΔS** **(kcal/mole)**	**ΔG** **(kcal/mole)**
WT[a]	0.100 ± 0.004	0.50 ± 0.02	-12.7 ± 0.6	-4.17	-8.6
S254A[a]	0.23 ± 0.01	1.20 ± 0.14	-7.5 ± 0.5	0.5	-8.0
T152P	0.090 ± 0.004	1.40 ± 0.18	-13.4 ± 0.8	-5.36	-8.0
WT[b]	0.04 ± 0.02	2.40 ± 0.58	-24.3 ± 16.3	-14.9	-9.4
Free Enzyme titrated with NAD$^+$					
WT[a]	0.15 ± 0.07	4.9 ± 1.5	-8.84 ± 5.3	-1.7	-7.73

The binding parameters for the titration of the unligated native enzyme with NAD$^+$ yielded a dissociation constant of 4.9 ± 1.5 μM (data shown in Appendix 1A) whereas the titration of the enzyme-NAD$^+$-complex with L-Tyr resulted in a K_d of 0.5 ± 0.02 μM. Increasing the temperature to 55 °C from 20 °C caused a decrease in binding affinity of the native enzyme for L-Tyr (Appendix 1B). The number of ligand binding sites of ~0.1 per monomer determined for the ligands was unexpectedly low and it could be interpreted that only 1 in 10 enzyme molecules is in a conformation that permits binding. Binding of NAD$^+$ and L-Tyr is enthalpically favourable (negative ΔH value) but not entropically favourable (negative TΔS value, randomness decreases). The calculated free energy changes (ΔG) at 20 °C were -8.6 kcal/mole and -7.7 kcal/mole for L-Tyr and NAD$^+$, respectively.

The analysis of the variants T152P and S254A (Appendix 1A) revealed K_d values for L-Tyr only about 2-fold higher than for native enzyme. In addition, ΔG of - 8.0

kcal/mole is only slightly lower. All other parameters determined for T152P were comparable to the native enzyme, whereas the S254A variant showed a significantly less favourable enthalpy contribution. These findings are surprising given that both variants are significantly less inhibited by L-Tyr (Figure 13). Interestingly, ITC experiments confirmed that the H217A and the R250A/K246A variant did not bind L-Tyr and resulted in only small changes in heat capacity (Appendix 1C, D). Furthermore, the titration of the native enzyme-NAD^+-complex with phenylalanine did not yield a binding isotherm as shown in Figure 17 indicating that the C4-hydroxyl group of prephenate or L-Tyr is important for binding to the enzyme.

3.7.2. Fluorescence Quenching Assays

Stepwise changes in fluorescence emission intensity induced by the binding of a ligand to a protein can be used to determine an apparent dissociation constant (K_d) for the ligand from the enzyme complex. In the case of Δ19PD the ligands were NAD^+ and prephenate. As previously shown, the two tryptophan residues are nearby or in the active site of the Δ19PD enzyme (63). Therefore, emission spectra with λ_{ex} set at 295 nm were recorded of the free enzyme and each time following the sequential addition of ligand (Figure 18). Spectra were corrected for changes in enzyme concentration, buffer contribution and inner filter effect.

Representative spectra for titration with NAD^+ and HPP are shown in Figure 18 A and Figure 18 B, respectively. Apparent binding constants (K_d) were calculated as described in section 2.16 and Figure 19 shows a representative analysis of the binding of NAD^+ to Δ19PD. Analysis of the Scatchard Plots for NAD^+ yielded a K_d value of 2.4 ± 0.2 μM. Additionally, the deviation from linearity in the Scatchard Plot at low NAD^+

concentrations (1/5 to ½ of K_d) indicates that NAD^+ binds in a cooperative manner to the free enzyme. The dissociation constant for NAD^+ of 2.4 ± 0.2 μM for WT Δ19PD is comparable to the K_d of 4.9 ± 1.5 μM obtained by ITC experiments. The non-linear least square analysis for HPP and prephenate (data not shown) yielded dissociation constants of 38.2 ± 12.1 μM and 13.6 ± 5.1 μM, respectively.

It is worth noting, that significantly smaller fluorescence changes were observed upon addition of HPP or prephenate compared to the addition of NAD^+ resulting in a more error-prone experiment. Accordingly, the Scatchard Plot analysis of the experimental data obtained from HPP or prephenate could not provide explicit information concerning any cooperative interactions in the binding of these ligands to the enzyme. Also worth noting, similar experiments by Bonvin (55) also yielded comparable values of K_d but no cooperativity was observed presumably as NAD^+ concentrations greater than ½ K_d were used.

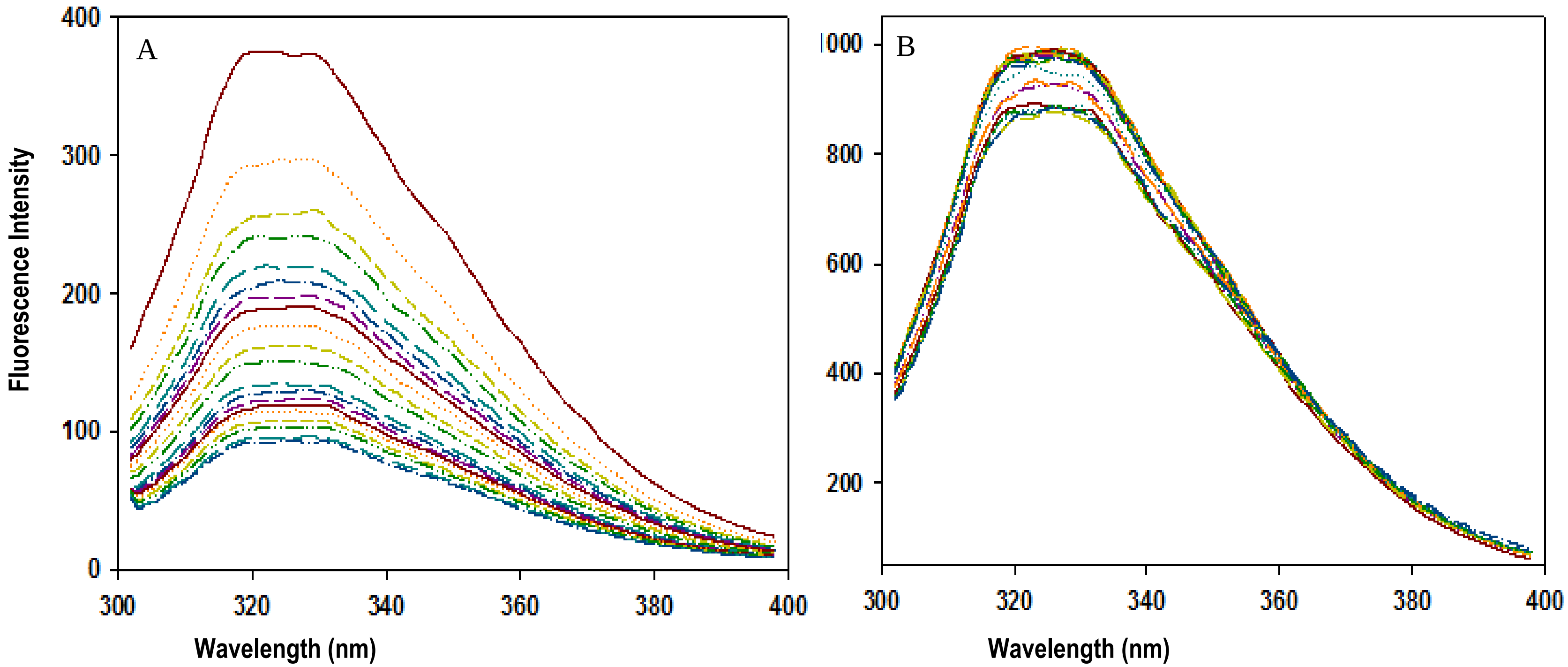

Figure 18: Changes in fluorescence intensity of Δ19PD upon binding of (A) NAD^+ and (B) HPP. The change in intrinsic Trp fluorescence of native Δ19PD (6 µM) was observed by excitation at 295 nm and measuring the emission from 300 to 400 nm in 50 mM KH_2PO_4 / K_2HPO_4, 75 mM NaCl, pH 7.5. NAD^+ was varied from 0 to 79 µM and HPP from 0 to 90 µM. All spectra are corrected for buffer contribution, dilution effects upon titration and when applicable inner filter effects.

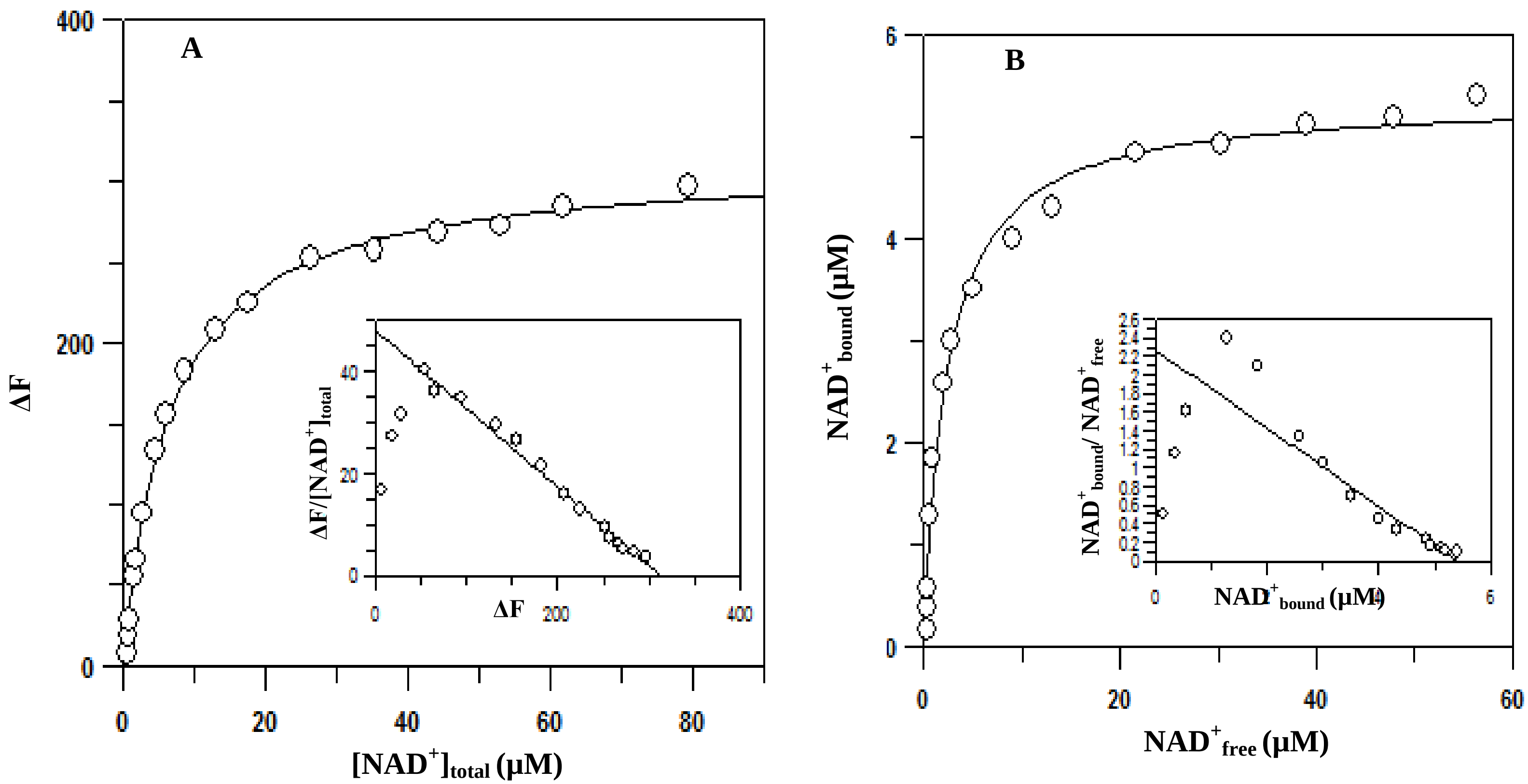

Figure 19: Determination of K_d using intrinsic fluorescence quenching. (A) Maximum fluorescence quenching is determined by plotting fluorescence change shown in Figure 18 as a function of total [NAD^+]. (B) The concentrations of free and bound NAD^+ in each titration were determined as described in section 2.15. The data were fitted to the equation that describes single site ligand binding using non-linear least square analysis (Grafit 5.0) to determine a dissociation constant of 2.4 ± 0.2 µM for NAD^+. Data for HPP and prephenate are not shown although K_d values of 38.2 ± 12.1 µM and 13.6 ± 5.1 µM, respectively, were obtained from the analyses. The changes in fluorescence intensity (ΔF) were also fitted to the quadratic equation (data not shown) yielding comparable dissociation constants of 3.2 ± 0.4 µM for NAD^+, 43.7 ± 15.8 µM for HPP and 21.1 ± 19.5 µM for prephenate.

Unfortunately, the decrease of intrinsic fluorescence intensity upon ligand binding could not be used to determine the dissociation constant for L-Tyr because of its intrinsic fluorescence properties. Additional attempts to use a displacement assay and the fluorescence dye 1-anilinonaphthalene-8-sulfonic acid previously reported for the *E. coli* CM-PD (56) were not successful with Δ19PD from *A. aeolicus.*

3.7.3. Equilibrium Dialysis

Equilibrium dialysis is another direct and simple solution technique to study protein-ligand interactions under physiological conditions. The basic principle involves the separation of the free ligand from the protein-bound ligand by allowing the free ligand to dialyze through a semi-permeable membrane placed between two chambers of a cell in an equilibrium dialysis apparatus. Equilibrium dialysis allows the determination of not only the ligand dissociation constant, but also the number of binding sites for the ligand that are present on the protein (81). This method was used to determine the dissociation constant of L-Tyr from the Δ19PD-NAD^+-complex. Tritiated L-tyrosine was used as a labeled "tracer" in order to obtain the concentrations of free and bound ligand in the chambers. The enzyme, Δ19 PD, was placed in one chamber of each of the cells of the equilibrium dialysis device along with NAD^+. It was dialyzed against fixed, increasing concentrations of unlabeled L-Tyr (a higher concentration for each cell) and a constant concentration of radiolabeled L-Tyr (1 µCi). After equilibrium was established over night at room temperature, equal volumes from each chamber within each cell were collected and the radioactivity was analyzed by scintillation counting. Control experiments measuring protein concentration and activity before and after equilibrium was established, confirmed that the protein did not precipitate or attach to the dialysis membrane or the wall of the dialysis cells during the experiment. Analysis of the Scatchard-Plot yielded a dissociation constant of 0.81 ± 0.21 μM and 0.1 binding sites per monomer for L-Tyr for the native Δ19PD. These data are in excellent agreement with the number of binding sites as well as the dissociation constant for L-Tyr obtained by ITC (0.100 ± 0.004 and 0.50 ± 0.02 μM, respectively).

Analysis of the equilibrium dialysis experiments proved difficult as there are several sources for errors associated with the methodology: 1) small volumes had to be pipetted into and removed from the chamber for analysis; 2) at concentrations of ligand which approached saturation of the available sites, the amount of radioactivity in each chamber within the cell is almost equal and the slightest pipetting errors result in data that cannot be used for the fitting. The data presented for the native Δ19PD can be considered reliable since they represent the average of 6 results that were chosen from 14 experiments. Regrettably, there are no reliable data for any of the variant proteins.

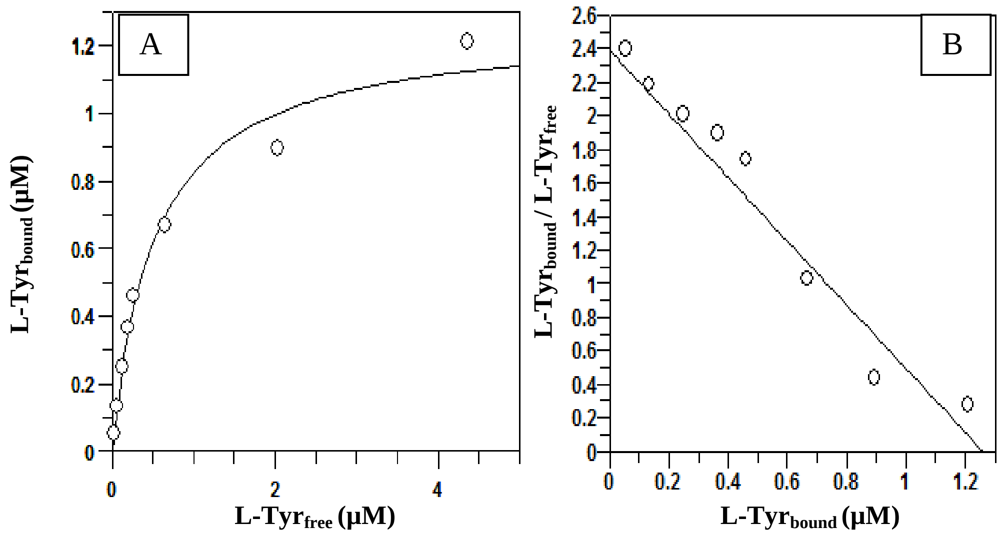

Figure 20: Equilibrium dialysis analysis for dissociation constant and solution stoichiometry for native Δ19PD. (A) Non-linear fit of L-Tyr concentration when equilibrium was established to the equation describing a single site saturation curve. Free and bound L-Tyr concentrations were obtained by dialyzing increasing concentrations of L-Tyr (0.1 – 50 µM) in the presence of 1µCi L-[ring3,5-^{3}H] tyrosine, 2 mM NAD^+ and a fixed concentration of WT Δ19PD. After equilibrium of the reaction was established, the amount of radioactivity on both sites of the chamber was analyzed. (B) Representative Scatchard- Plot analysis of an equilibrium dialysis experiment. Linear transformation of the data represented in (A) yielded a dissociation constant of 0.81 ± 0.21 µM and 0.1 binding sites for L-Tyr. Data was fitted using Grafit 5.0 (shown in section 2.15).

3.8 Molecular Docking of Prephenate in the Active Site of Δ19PD from *A. aeolicus*

Recent crystal structures solved at pH 7.8 are available of *A. aeolicus* Δ19PD in complex with the products NADH and HPP (pdb file 3GGO), with NAD^+ and the product analog HPPropionate (pdb file 3GGP), and NAD^+ and L-Tyr (pdb file 3GGG). Unfortunately, the co-crystallization did not result in a crystal structure which harboured prephenate in the active site since the presence of NAD^+ is essential for the protein to adopt a crystallisable conformation (55, 57, 63). However, prephenate had previously been modeled into the active site of the enzyme-NAD^+-complex at pH 3.2 (57). Comparisons of the crystal structures obtained at pH 3.2 and 7.8 showed that there are structural differences. In order to gain further insight into the interactions of prephenate with

A. aeolicus Δ19PD at pH 7.8, prephenate was modeled into the putative active site of the crystal structure 3GGP using AutoDock Vina (Figure 21). These coordinates were chosen because the active site is bound with NAD^+ and not with NADH. For simplification, this structure is denoted **3GGP-A**. Previous site-directed mutagenesis studies suggested that R250 from one subunit and K246 from the adjacent subunit are both important for binding (61). However, in all crystal structures obtained at pH 7. 8 the side chain of K246 points away from the active site and towards the protein surface (Figure 7). Therefore we allowed this residue to be flexible and to adopt different positions upon the docking procedure (**3GGP-B**). Additionally, we created a pdb file (denoted **3GGP-C**), that was missing the side chain of R250 and allowed K246 to be flexible, therefore imitating the R250A variant protein. It was prepared by deleting the appropriate atoms from the original 3GGP pdb file. The crystallized water molecules were also deleted to exclude docking positions that result from the created pattern rather than from interactions with the enzyme.

Prephenate could be docked in nine possible orientations in each of the prepared files. All orientations harboured binding affinities between -4.7 kcal/mole and -2.6 kcal/mole. These differences between the best and the worst proposed position are very small and can hardly be used to exclude a certain position. Thus, these results suggest that prephenate can adopt more than one of the proposed positions or oscillates between several positions in solution. In a control experiment the product, HPP, was re-docked into the pdb file 3GGO. Accordingly, the heteroatoms forming HPP were deleted from the original file and the coordinates were used to create a new pdb file describing HPP. The preparation of the pdbqt files and the docking was performed as described in section

2.18. A binding affinity of -4.0 kcal/mole was obtained for the position corresponding best with the original position of HPP in the crystal structure which agrees well with the binding affinities obtained for the docking of prephenate into the active site.

Results of previous site-directed mutagenesis studies were considered when choosing the best orientations. Figure 21 panel A shows prephenate docked at the active site of 3GGP-A (K246 is pointing away from the active site). Of the nine possible orientations of prephenate, this docked position yielded an affinity of -4.3 kcal/mole. The C4-hydroxyl group is positioned within 3.3 Å to the Nε2 of H147 (the catalytic H-bond acceptor) and R250 is involved in ionic interactions with the side chain carboxyl group. Additionally, H217 and W259 are H-bonding to the side chain carboxyl group of prephenate, and the C4-hydroxyl group of prephenate is close to the C4 of the nicotinamide moiety of NAD^+ where the hydride transfer occurs (~3.6 Å). In Figure 21 panels B and C prephenate is docked into 3GGP-B which allows the side chain of K246’ to adopt different orientations upon substrate binding; two of these are shown in panel B and C. Docking of prephenate as shown in panel B rendered the highest binding affinity (-4.7 kcal/mole). The side chain amino group of K246’ shifted ~ 4 Å away from its original position (see K246’ and * K246’) and in its new position it now only 3.5 Å away from the side chain carboxyl group of prephenate and ideally poised to form electrostatic interactions. R250 can form ionic interactions with the side chain keto group of prephenate. The C4-hydroxyl group of prephenate is positioned ~ 3.4 Å from the C4 of the nicotinamide moiety of NAD^+. The distance of the C4-hydroxyl group of prephenate from the Nε2 of H147, which has been shown to be critical for catalysis, is 4.0 Å. Interactions of the ring carboxyl group with H217, W259 and the side chain amino group of the nicotinamide moiety of NAD^+ can be observed. Figure 21 panel C shows another orientation which prephenate could adopt in the active site, yielding a binding affinity of -3.7 kcal/mole. Prephenate adopts an orientation similar to that in which HPP crystallized during co-crystallization studies. The major differences between Figure 21 panels B and C are that in panel C, both amine groups of R250's side chain could maintain electrostatic interactions with the side chain carboxyl group of prephenate as opposed to the single interaction with the side chain keto group R250 is making as shown in panel B. Additionally, in panel C, the C4-hydroxyl group of prephenate is positioned closer to H147 (2.9 Å) than in panel B. Therefore, panel C might reflect best the orientation prephenate adopts in the active site. The interactions between H217, W259 and the amine group of the nicotinamide moiety of NAD^+ seen in Figure 21 A, B and C are comparable. The major differences between the three positions are seen in the positioning of the side chain propionyl group, whereas the overall position of the ring carboxyl group and the C4-hydroxyl group of prephenate are similar in these positions. Interestingly, prephenate adopts almost identical orientations displaying the same interactions and distances from key residues, regardless of the flexibility of the side chain of K246' (orientation A and C).

Docking of prephenate into 3GGP-C, a pdb file that simulates the R250A variant, yielded only one possible orientation for prephenate with a binding affinity of -4.0 kcal/mole (Figure 21 panel D). In this orientation, K246' maintains ionic interactions with the side chain keto group of prephenate. The interactions and the positioning of the ring carboxyl group and the C4-hydroxyl group resemble closely the ones shown in panel C.

Interestingly, it has been proposed that H217 positions prephenate in a catalytically competent orientation through an interaction with the side chain keto group (63). In both orientations a direct interaction between the side chain carboxyl group of prephenate and H217 can be observed as well as a close proximity to W259 (~3.8 Å) and T152 (~3.3 Å). The ring carboxyl group of prephenate is, therefore, placed in close proximity to the hydrophobic region of the active site of PD from *A. aeolicus* composed of residues I149, A150, G151, T152, H217, F221, M258, and W259 as described by Sun *et. al.* (63).

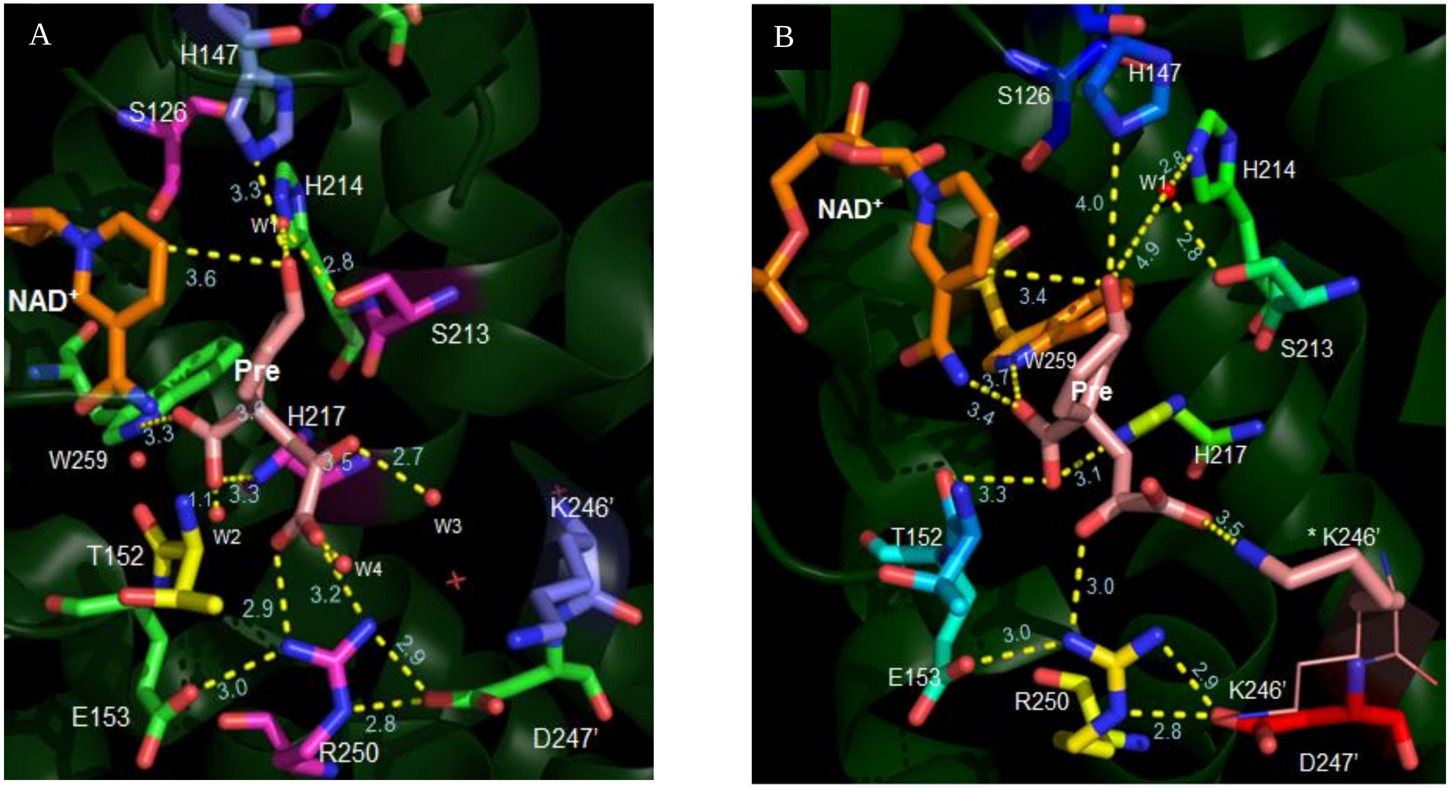

Figure 21: Active site of *A. aeolicus* Δ19PD with docked prephenate showing possible complexes. (Panel A) Prephenate docked into the active site without allowing flexibility in the side chain of K246'. AutoDock Vina rendered an affinity of -4.3 kcal/mole for prephenate docked in this orientation. Shown are possible interactions with key residues of the active site. (Panel B) Flexibility in the side chain of K246' was introduced into the crystal structure while docking of prephenate into the active site. AutoDock Vina rendered the highest affinity for prephenate binding in this orientation (-4.6 kcal/mole). *K246' describes the orientation the residue adopts when prephenate is docked in this orientation into the active site. K246' (lines) shows the orientation K246' adopted in the original crystal structure. Images are generated by PyMOL (62), docking files were prepared using AutoDock tools and AutoDock Vina (82) as described in Materials and Methods.

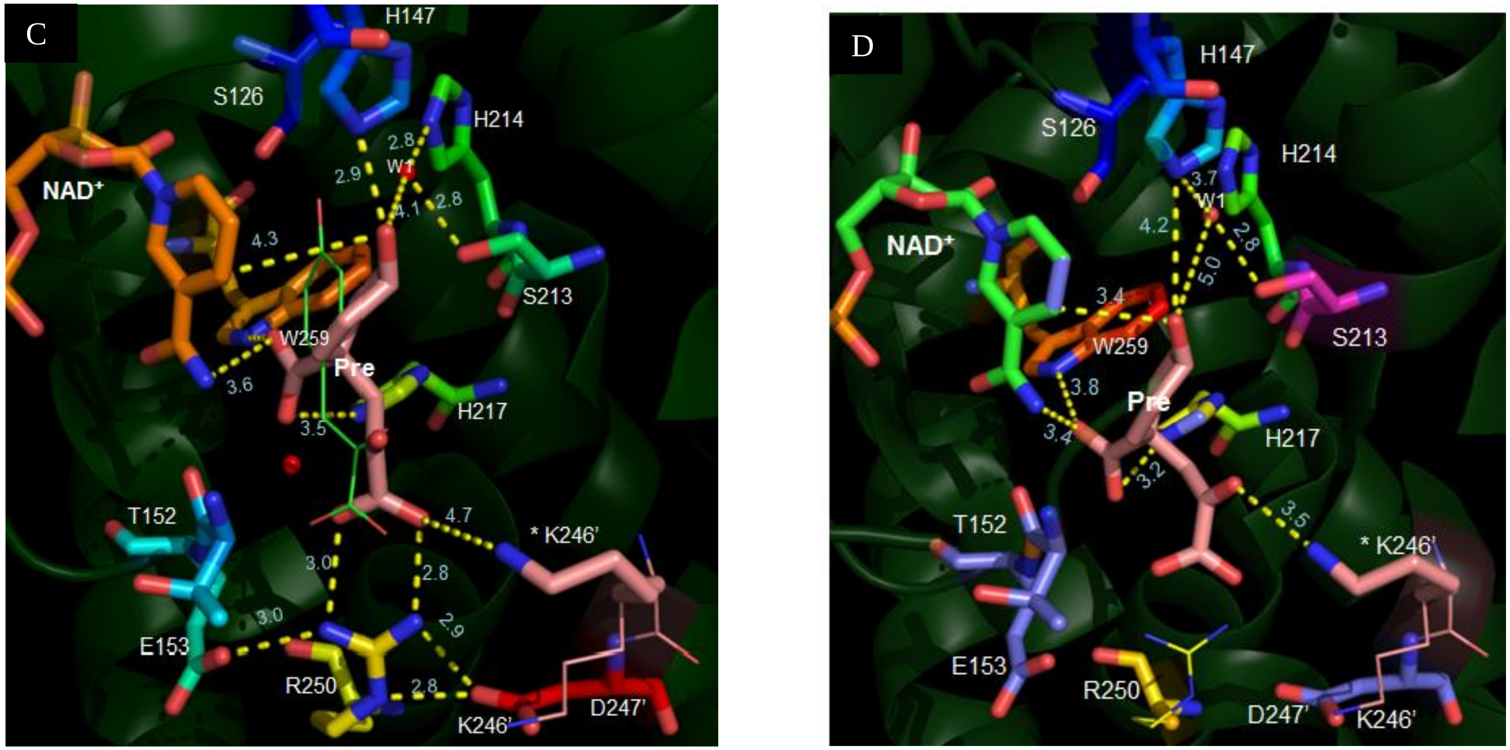

Figure 21: Active site of A. aeolicus Δ19PD with docked prephenate showing possible complexes (cont.). (Panel C) Prephenate is docked in the active site in an orientation similar to the orientation the product HPP crystalized during co-crystallization studies (-3.7 kcal/mole). The hydroxyl group is in close proximity to H147 and the side chain carboxyl group is directly interacting with R250 and K246. Prephenate was docked into 3GGP-B which is complexed with HPPropionate, but shown in the crystal structure of the prephenate-NADH-HPP complex. The two structures align with R.M.S.D of 0.23. (Panel D) Prephenate docked into a file simulating the R250A variant protein. R250 (sticks) is the residue as it is left in the file whereas R250 (lines) show the original residue. K246' interacts with the side chain keto group of prephenate. Overall positioning of the ring carboxyl group and the hydroxyl group of prephenate are comparable to positioning shown in Figure 21 A. *K246' describes the orientation the residue adopts when prephenate is docked in this orientation into the active site. K246' (lines) shows the orientation K246' adopted in the original crystal structure. Images are generated by PyMOL (62), docking files were prepared using AutoDock tools and AutoDock Vina (82) as described in Materials and Methods.

Chapter 4: Discussion

The purpose of this study was to identify the importance of selected amino acid residues in substrate binding, catalysis and feedback regulation of the monofunctional prephenate dehydrogenase from the thermophilic bacterium *Aquifex aeolicus*. Additionally, we attempted to provide insights into the binding of prephenate, NAD^+ and L-Tyr to the enzyme through biophysical and computational methods. Many interactions were probed for the first time in this study. When applicable, the results have been correlated with the crystal structure of other TyrA proteins and mutagenesis studies. Sequence alignment of *A. aeolicus* PD with other bacterial and yeast TyrA proteins (Figure 4) showed that many of the key residues appear well conserved, including the catalytic H-Bond acceptor H147 and R250, H217, H205 and D206. A battery of variant proteins was expressed and purified; in some cases a single replacement was made (S254A, S213A, D247A, E153A) while in other cases multiple substitutions at the same position (H205Q/L, D206E/N/A, T152P/G, H214L/Q, W259F/Y, H217A/V) or two replacements within one variant (R250A/K246A, E153A/D247A) were studied.

All variants were routinely obtained in excellent yield (except for D206A) by Ni-NTA affinity chromatography. The kinetic parameters of the native enzyme and some variants that were previously studied were in reasonable agreement with the parameters given in this study.

Histidine 217 maintains active site integrity and coordinates catalysis

The results from kinetic studies show striking differences in the kinetic parameters for the reaction catalyzed by H217V compared to the native enzyme. The efficiency constant of the variant is reduced by two orders of magnitude; the K_m of 2.6 mM increased 30-fold relative to the native enzyme, while k_{cat} was reduced 8 fold (Table 6). This closely resembles the perturbations for H217A reported by Sun *et. al.* (63 and presented in Table 6) who showed a decrease in k_{cat}/K_m of 2.5 to 3 orders of magnitude relative to the native enzyme. The crystal structure of the enzyme in complex with HPP (Figure 7) showed the Nε2-group of His's imidazole ring coordinated to bound water (WAT2), which in turn coordinates to the side chains of S254 and R250 and the pyruvyl side chain of the ligand. Thus, a conversion of H217 to valine would affect binding. Additionally, the H217 Nδ1-group also H-bonds to the main chain carbonyl group of S213. S213 is linked to an important H-bonding network involving the catalytic H-bond acceptor, H147, and so H217V could indeed affect catalysis. H217 is also ~ 3.3 Å from W259 and involved in π-stacking with the aromatic residue and thus its absence in this structure could readily perturb the structural geometry of the active site. The marginal improvements in k_{cat}/K_m of H217V compared to H217A might reflect that some of these hydrophobic interactions are restored by the valine conversion. Interestingly, in the structure with prephenate modeled in the active site (Figure 21C), H217 has retained its hydrophobic stacking with W259. However, the imidazole is coordinated towards the ring carboxyl group of the substrate. As previously mentioned in section 3.8, H217 appears to be part of a hydrophobic region consisting of 6 residues (63) that surround the ring carboxyl group. This is also in good agreement with the hypothesis of Hermes *et. al.*

(52) who proposed for the *E. coli* CM-PD that the ring carboxyl group might reside in a hydrophobic pocket within the enzyme to promote rapid decarboxylation.

Also in agreement with the studies on H217A by Sun *et. al.*, the valine replacement rendered PD activity insensitive to inhibition by L-Tyr even up to concentrations of 7 mM (Figure 13). In accordance with the crystal structure which shows HPP and L-Tyr combining at the same pocket (Figure 7 A and B) and since H217V cannot bind prephenate well, it follows that it would no longer retain its interactions with L-Tyr. Additionally, preliminary studies using ITC indicated that the H217A variant does not bind L-Tyr (Table 8).

Both of H217's imidazole nitrogen groups appear coordinated to oxygen atoms from WAT2 and the backbone carbonyl of S213. Thus, it has been proposed that at pH 7.5 the imidazole ring is protonated in the ternary complex of enzyme-NAD^+-L-Tyr or HPP, and provides the steric repulsion required to direct the amine group of L-Tyr away from H217 towards the main chain carbonyl group of T152 and WAT2 (Figure 7). If this is the case, the binding of L-Tyr to the enzyme should be pH dependent. The results from the solution studies in this thesis do not support this hypothesis (Figure 16). Our kinetic results show that the inhibition constant (K_i) describing the interaction of the enzyme-NAD^+-complex with L-Tyr does not vary over a broad pH range (pH 4 to 9) (Figure 16) indicating that in this structure H217's ionization state in not critical for feedback inhibition by L-Tyr. If it is protonated then its pK_a is outside the experimental accessible pH range.

Interestingly, the fluorescence emission intensity of H217A/V is considerably elevated compared to the native enzyme (Figure 15). As previously indicated, H217 is closely stacked to W259 in the active site of Δ19PD and, therefore, in its protonated state, the imidazole group would be an excellent quencher of Trp fluorescence emission (75). This prompted us to consider H217's ionization state in the unliganded Δ19PD. However, the fluorescence emission intensity of Δ19PD is not affected by changes in pH (Figure 15 B) indicating that in the unliganded structure H217 is not ionisable in the pH range of 4 to 9. Likely complex structural perturbations in the active site are involved in the increase in fluorescence emission intensities of the H217A/V variants.

<u>Serine 254 appears critical for tyrosine inhibition but not tyrosine binding</u>

Crystal structure analysis identified that S254 contributes to an H-bonding network which includes H217, the keto and the carboxyl groups of HPP's propionyl side chain, or the amine group of L-Tyr, and most importantly WAT2 (Figure 7 B) (63). Since H217 has been shown to be critical for positioning prephenate in a catalytically important conformation, a similar role was proposed for S254. We would predict that a conversion of Ala at position 254 should reduce the apparent binding of prephenate as well as inhibition by L-Tyr. The equivalent residue in *E. coli* CM-PD (Q298) has been deemed important for binding prephenate and L-Tyr inhibition; the Q298A variant exhibited over a 10-fold increase in K_m for prephenate and displayed considerable resistance to feedback inhibition by L-Tyr (56). By comparison, in the present study we showed that the S254 to Ala conversion has only modest effects on the K_m for prephenate (2-fold increase) and k_{cat} compared to the native enzyme (Table 6). This observation is more in keeping with the model of prephenate in the active site, which shows no interaction between S254 and prephenate.

Most strikingly was the considerable feedback resistance of S254A. The variant retained 90% of its residual activity at 5 mM L-Tyr; at this concentration of L-Tyr the native enzyme was completely inhibited (Figure 13). Given the results from the kinetic inhibition studies, the results from ITC experiments titrating S254A with L-Tyr, were most unexpected. The isotherm reveals that L-Tyr does indeed interact with the S254A-NAD^+-complex. A K_d value was obtained that was only 2-fold higher than for native enzyme; this corresponds to a difference of ΔG of 0.6 kcal/mole, which is less than would be expected for the loss of a strong H-bonding interaction. Additionally, the $\Delta\Delta H$ of 5.2 kcal/mole and a positive $T\Delta S$ of 0.5 kcal/mole were observed. This indicates that the reaction of L-Tyr with the S254A-NAD^+-complex is largely entropy driven, whereas enthalpic interactions are more important for the same reaction of native enzyme. While this might be in keeping with the loss of water (WAT2) by the S254 to Ala conversion, our data for this variant tend to support the idea that L-Tyr likely binds at an allosteric site and that Ser to Ala conversion prevents the enzyme from undergoing a conformational change which is required for inhibition of activity. This is the first report of a TyrA protein that binds the end product inhibitor but is not inhibited.

Tryptophan 259 – a hydrogen bond matters

A. aeolicus Δ19PD possesses only two tryptophan residues per monomer. The results from fluorescence quenching experiments, in accordance with all available crystal structures for Δ19PD, confirmed that the side chain of W190 is fully buried and in close proximity to the NAD^+ binding site, whereas W259 resides in a partially buried environment within the prephenate binding site (30, 60, 61). Additionally, a comparison of the fluorescence emission of the W259 and W190 variants (Figure 15) confirms previous fluorescence data (60) showing that W190 contributes more significantly to the overall fluorescence intensity but does not markedly alter the kinetic parameters of the PD reaction. Interestingly, the W259 to Phe replacement increased the K_m for prephenate ~9 fold and decreased the k_{cat} approximately 2-fold while the conversion of W259 to Tyr restored catalytic activity and apparent binding affinity to levels comparable with the native enzyme (Table 6). This finding illustrates that prephenate binding and activity are linked to this residue's capability to form H-bonds. Our results are in line with the structure with prephenate modeled in the active site; it shows W259 is interacting with the ring carboxyl group of prephenate (Figure 21C). In contrast, no direct electrostatic interaction involving W259 were observed in the structure with HPP (Figure 7A).

It is noteworthy that both W190F and W259F variants were highly sensitive to inhibition by L-Tyr similar to the native enzyme. In contrast, the W259Y variant appears strikingly L-Tyr resistant (Figure 13). By 5 mM L-Tyr, where the native enzyme has less than 10%, W259Y retains ~ 70% of its activity. At this time we have no thermodynamic data to establish whether or not W259Y binds L-Tyr (like S254A).

The results for the variant can be interpreted in light of the structure of Δ19PD bound with L-Tyr, however, as previously discussed, a H-bonding network including the amine of L-Tyr, the –OH of S254, the Nε2 of H217 and WAT2 (see Figure 7) has been shown to be important for L-Tyr inhibition but not prephenate binding. Additionally, the indole ring of W259 does not participate in this network as it is too far away from WAT2. When Trp is replaced by a tyrosine residue however, the –OH group of this tyrosine is positioned close to WAT2 (~1.8 Å) and can participate in the H-bonding network (Figure 22). Additionally a tyrosine residue in this position can form direct polar interactions with

H217 and S254, two residues that have been shown to be important for feedback inhibition. Thus, any perturbations in L-Tyr's electrostatic interactions with WAT2, H217 and/or S254 by the amino acid replacement could explain the relative insensitivity of W259Y to L-Tyr feedback inhibition. Our findings can be compared to the report by Hassounah (56) who showed that conversion of Tyr303 to Phe in *E. coli* CM-PD (equivalent to W259) eliminates L-Tyr inhibition without affecting prephenate binding. Here the Tyr303 is proposed to interact electrostatically with the amine of L-Tyr (56). It is worth noting that the crystal structure of *H. influenza*e PD, whose amino acid sequence is highly homologues to *E. coli* PD, also shows L-Tyr bound at the active site of the PD domain (58).

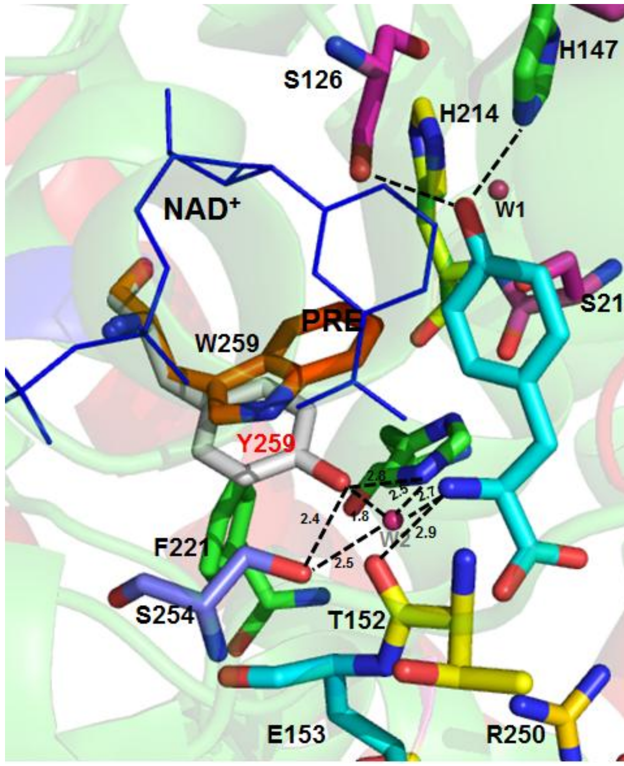

Figure 22: Active site of *A. aeolicus* Δ19PD W259Y complexed with NAD$^+$ and L-Tyr at pH 7.8. The picture shows the relative position of W259 (orange sticks) to L-Tyr and also possible interactions of Y259 (white sticks). The indole ring of W259 is not participating in the H-bonding network including S254, the side chain amine of L-Tyr, H217 and W2. The replacement of W259 with Tyr results in a perturbation of this H-bonding network. W259 has been replaced with Tyr using the mutagenesis wizard in PyMOL. Pictures created using PyMOL (62) using the coordinates derived from reference 63. The primed residues denoted those groups associated with the adjacent monomer.

Threonine 152: The story of backbone interactions

The crystal structure of Δ19PD in complex with NAD$^+$ plus L-Tyr at pH 7.5 shows that the amine group of L-Tyr is directed towards T152's backbone carbonyl group. In addition, the residue is positioned in a very flexible loop within the active site (residues 149 to 156) which shifts T152 closer to the active site upon substrate binding (63). One of our goals was to determine if sensitivity to L-Tyr could be selectively targeted. To disrupt this backbone interaction, T152 was converted to the cyclic imino acid Pro to impart rigidity into the loop region, or to Gly (smallest side chain) which could induce additional flexibility; this loop already carries two Gly residues. The efficiency constant for the reaction catalyzed by T152P was reduced by a factor of 100, with equal but opposite effects on k_{cat} and K_m for prephenate. In contrast, k_{cat}/K_m for T152G did not change since a 4-fold reduction in k_{cat} is accompanied by a 5-fold increase in K_m for prephenate (Table 6). Additionally, the enzymes appeared to interact more tightly with NAD^+ as the K_m for the cofactor was also 5-fold lower. Previously, it had been reported that the K_m for NAD^+ decreased in the presence of low concentrations of guanidine-HCl which was attributed to the increased mobility of active site residues in the thermophilic PD (30). Introducing a glycine into an already flexible region of the active site might promote similar effects. In support of this idea, the introduction of Pro which increases local rigidity in the backbone could result in an increase in K_m for prephenate.

Remarkably, the two amino acid substitutions produced strikingly different effects on feedback inhibition by L-Tyr. The plot of % residual activity as a function of L-Tyr (Figure 13) showed that while T152G is less sensitive but steadily loses activity with increasing concentrations of inhibitor, the T152P variant was rapidly inhibited but to a finite level leaving 50% residual activity. Such behaviour is not consistent with L-Tyr acting as a simple competitive inhibitor with respect to prephenate in the PD reaction. Double reciprocal plots of velocity versus prephenate concentration at fixed, increasing concentrations of inhibitor yielded a family of lines whose slopes were hyperbolic with increasing ligand concentrations (Figure 14 B). In this model of hyperbolic competitive inhibition (Figure 23) it is assumed that: 1) prephenate (S) and L-Tyr (I) bind to the enzyme (E) at different sites to yield enzyme-substrate complexes (ES), enzyme-inhibitor complexes (EI) and enzyme-substrate-inhibitor complexes (ESI); 2) the substrate binds to the free enzyme with greater affinity than to the EI complex; and 3) that the ES as well as ESI complex yield product with equal facility (74). α describes the extent to what K_s changes when I occupies the enzyme. Fit of the data to the equation describing this model (see section 2.12) yielded an α of 3.

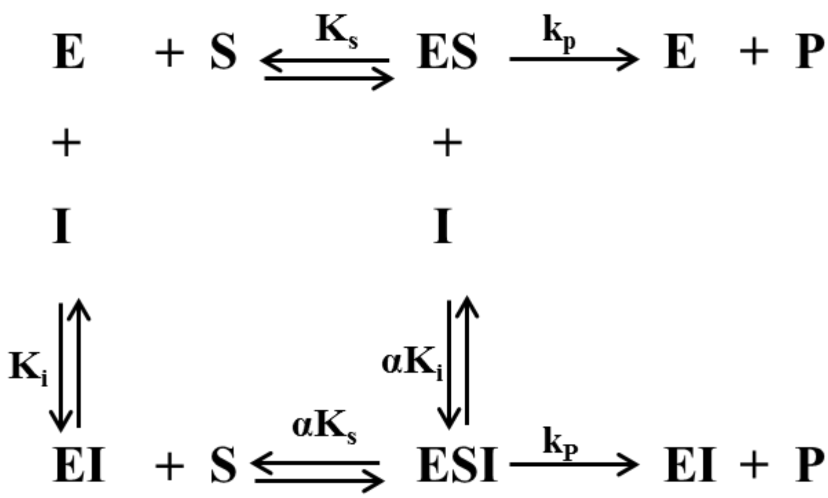

Figure 23: Mechanism for partial competitive inhibition observed for inhibition of T152P by L-Tyr. α describes the extent to what K_s changes when I occupies the enzyme.

This low value obtained for α indicates that a significant proportion of enzyme forms ESI. Kinetic data for this variant also support the idea that L-Tyr binds to an allosteric site and the Thr to Pro conversion perturbs the extent to which the binding of prephenate to the active site and L-Tyr to the allosteric site are mutually exclusive. The data do not necessarily eliminate more complex models where L-Tyr can combine with the same site as prephenate as well as an allosteric site. This point is important to consider since binding of L-Tyr to T152P as determined by ITC experiments yields a K_d value, enthalpy and entropy changes similar to native enzyme when concentrations of L-Tyr up to 70 µM are used (Table 8). The agreement in these parameters between native and variant enzyme suggests that L-Tyr combines at the same site in both proteins. Interestingly, the K_i value obtained from the fit to the hyperbolic competitive inhibition model (4.1 ± 2.8 µM) agrees well with the K_d obtained by ITC (1.4 ± 0.18 µM). Double inhibition studies in the presence of HPP and L-Tyr could help decipher which of the two (or more) models is most plausible.

Ser 213 is more important than Histidine 214 in positioning WAT1

S213 and H214 are located in the polar region of the active site of Δ19 PD from *A. aeolicus*. Both residues form a hydrogen bonding network including S126 and H147 and a highly conserved water molecule suggesting that they might be important for catalysis and/or substrate binding (Figure 7) (63). Sequence alignment comparisons revealed that S213 and H214 are replaced by Q253 and A254 in *E. coli* CM-PD (Figure 4). Conversion of Q253 to Ala in *E. coli* CM-PD (equivalent to S213 in *A. aeolicus* PD) indicated that the Gln residue might be coordinating key catalytic groups since a decrease in k_{cat} is observed without a significant change in K_m for prephenate. Additionally, the variant protein was significantly less susceptible to feedback inhibition by L-Tyr than the native enzyme (83). Crystal structure analysis of a model generated for *E. coli*'s PD domain derived from the structure of the *H. influenzae* enzyme revealed that the side chain is in close proximity (3 Å) to the C4-hydroxyl group of L- Tyr (56, 58). In Δ19PD, the –OH group of S213 is approximately 4.6 Å away from the hydroxyl group of L-Tyr but this direct interaction is bridged by an important water molecule, WAT1 (Figure 7). Of S213 and H214, S213 is the more important residue in positioning WAT1 with the C4-hydroxyl group of the ligand. The Ser to Ala conversion increased K_m for prephenate 20-fold and eliminated L-Tyr sensitivity. In contrast, the conversions of H214 to Leu or Gln did not perturb L-Tyr sensitivity. H214L showed a 10-fold increase in K_m for prephenate. Moreover, the conversion to Gln restored the H-bond with WAT1 and therefore restored the enzyme's affinity for prephenate. These results confirm that the conserved WAT1 included in this H-bonding network plays a role in both substrate binding and L-Tyr inhibition, mainly through S213.

<u>H147-H205-D206: Perhaps charge does not matter</u>

Sequence alignment analysis revealed that H147, H205 and D206 are highly conserved in TyrA enzymes from all organisms. H147 is proposed to be deprotonated to help polarize the 4-hydroxyl group of prephenate and assist in hydride transfer and decarboxylation of the PD reaction. Given their positions in the available structures of Δ19PD (Figure 7), it has been proposed that H205 (protonated) and D206 (ionized) may be involved in an H-bonding network with H147 to keep this key catalytic residue deprotonated for catalysis. In this network of residues, the Nδ1 of H147 H-bonds to Nε2 of H205 and H205 Nδ1 H-bonds to Oδ1 of D206 (36, 58). The pH rate profiles of $\log(V/E_t)$ and $\log(V/E_t)/K$ pre) for Δ19PD activity (Figure 16) performed during this study, showed that an ionisable group (likely H147) titrates in the E-NAD^+-complex with a pK_a of ~6 ($V/E_t/K_{m\ pre}$ profile) while in the ternary complex of enzyme-NAD^+-prephenate (V/E_t profile) its pK_a is shifted lower outside of the experimentally accessible pH range. Thus, H147 should be mainly deprotonated at neutral pH. Interestingly, although H147 is pointed towards the C4-hydroxyl group of L-Tyr or HPP or prephenate, our ITC data show that H147A does not bind L-Tyr. Previous data (63) indicate that H147N appears to have a K_m for prephenate similar to the native enzyme. It remains to be established if the Ala variant also binds prephenate like the native enzyme.

The results presented represent the first site-directed mutagenesis study of H205 and D206 variants. The conversion of H205 to a non-polar Leu yields a poor catalyst with k_{cat} values reduced by over 100-fold compared to the native enzyme with a moderate (5-fold) increase in K_m for prephenate. Interestingly, electrostatic interactions afforded by a Gln replacement restored much of the catalytic activity and most of the apparent prephenate binding. These results support the idea that polar interactions between H147 and H205, rather than a protonated imidazole group are important for catalytic efficiency. H205 likely positions H147 in the correct orientation.

Amino acid conversions of D206 indicate that the negative charge is not critical for catalytic efficiency (k_{cat}/K_m) as the D206N variant is as effective a catalyst as the native enzyme (Table 6). Additionally, an increase in chain length by one methylene group (conversion of Asp to Glu) has only minimal effects on k_{cat} and modest effects on the K_m for prephenate (5-fold increase). The most pronounced effect however, is on the Asp to Ala conversion which yields a variant that is: 1) easily degraded as observed by SDS-PAGE analysis (Figure 10); 2) more poorly expressed than other variants; and 3) possesses a significantly lower T_m (45 °C) as determined by variable temperature circular dichroism experiments (Figure 12). Taken together, the data suggest that the loss of electrostatic interactions at position 206 is critical for the structural integrity of the enzyme. Crystal structure analysis showed that the side chain of D206 is interacting with the backbone amine group of K128 which in turn sustains a H-bonding network with residues near S126 and H147 and which also include mainly backbone interactions with G146, V127, G125, D123. Eliminating the interaction between D206 and K128 might result in the loss of this H-bonding network which in turn could destabilize the enzyme.

Unfolding studies on D206E/N using variable temperature CD or chemical denaturation could be informative.

Bob & Carol & Ted & Alice

Bob & Carol (Arginine 250 & Lysine 246')

The crystal structure of Δ19PD in complex with NAD^+ and HPP at pH7.5 (63) shows that R250's guanidinium group forms two ion pairs (< 3 Å) with the side chain carboxyl groups of the product (Figure 7A). Moreover, R250 appears to be locked in place aided by the negatively charged side chain oxygens of E153 and D247'. In contrast, K246' is oriented away from the active site in the crystal structure and does not directly interact with HPP or with any other acidic groups such as E153 or D247'. Given the number of interactions which are dependent on R250 but not on K246', it is surprising that the R250A conversion caused only a 13-fold reduction in apparent binding affinity for prephenate while the K246A variant exhibited a 20-fold reduction (61). From these studies by Hou (61), it would appear that both residues play important but not critical roles in binding prephenate. We showed in the present study, that the variant carrying two conversions (R250A/K246A) resulted in an increase in K_m for prephenate greater than 200-fold thus showing that the effects on the apparent binding of prephenate are additive. As with the single mutations, the double replacement did not affect k_{cat} or the enzymes affinity to bind NAD^+ (Table 6).

Molecular docking experiments presented here suggest that Lys246's side chain is very flexible and can adopt several orientations to facilitate the binding of prephenate through direct interactions. In model C (Figure C) both, R250 and K246' are pointing towards the side chain carboxyl group of prephenate. In model D (Figure D) which mimics the R250A variant, Lys246’ maintains electrostatic interactions with the side chain keto group of prephenate and, therefore, partially asumes the function of R250. In both models the catalytic histidine (H147) is poised to effectively participate in catalysis. Our molecular docking studies parallel the findings of the crystal structure of Δ19PD-NAD^+ at pH 3.2 with prephenate modeled in the active site. Here, K246’ is placed in close proximity to the ring carboxylate and the pyruvyl side chain of the substrate to help support prephenate binding along with Arg250.

The active site geometry of *E. coli* CM-PD might be somewhat different than in *A. aeolicus* PD. In *E. coli* CM-PD a substitution of R294 (the equivalent residue of R250 in *A. aeolicus*) resulted in a 120 fold decrease in apparent binding affinity for prephenate (47, 63) whereas the R286A variant (equivalent to K246 in *A. aeolicus*) yielded less than a 2-fold increase in K_m for prephenate (47). In addition, Q286 is on the same sub-unit as R294 rather than on the adjacent monomer as for K246’ in *A. aeolicus*.

Finally, direct ionic interactions with the substrate might not be the only explanation for the importance of these residues in prephenate binding. Figure 24 shows K246’ and R250 as well as K169 and K239’ enclosing the active site cleft of Δ19 PD suggesting that these residues may help guide the negatively charged prephenate into the active site. A similar mechanism has been proposed for AD of *Synechocystis* sp. In the structure of AD, a cluster of basic residues that could guide prephenate into the active site involves the residues R213, R217, R274’, K202 and K276’ (R213 and R217 are the equivalent residues to K246’ and R250 in *A. aeolicus* Δ19PD).

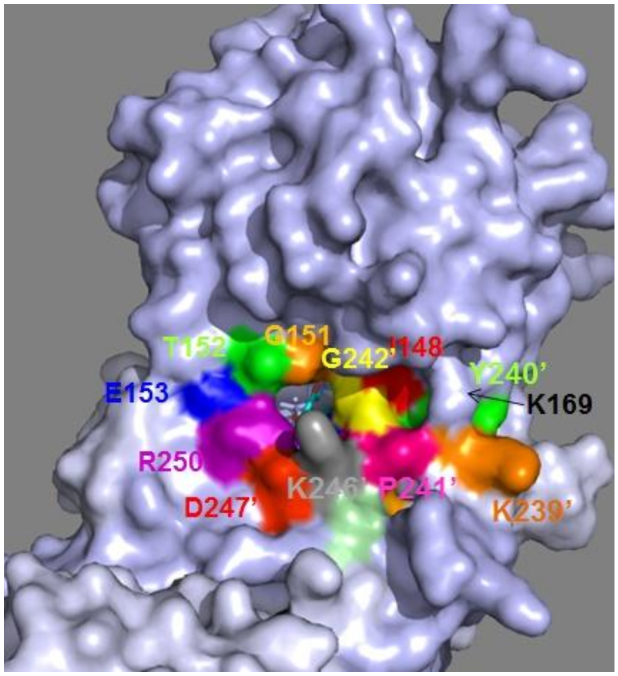

Figure 24: Surface view of *A. aeolicus* Δ19PD-NAD$^+$ complex with prephenate modeled into the active site, pH 7.5. R250 and K246' are lining the surface of the active site and attracting prephenate. Picture created using PyMOL (62) using the coordinates derived from reference 63. The primed residues denote those groups associated with the adjacent monomer.

Ted & Alice (Aspartate 247 & Glutamate 153)

It has been proposed that E153 from one subunit and D247 from the adjacent monomer act, together with R250, in a gated mechanism to modulate substrate access to the active site. Crystal structure analysis showed that a loop, consisting of residues 149 to 156 and defining the hydrophobic wall of the active site, moves considerably upon substrate binding. In particular G151 shifts about 2.5 - 3.4 Å away from the binding pocket upon interaction with prephenate or its analogs. This displacement also affects the position of E153. After substrate binding, R250 also moves ~ 1.5 Å nearer to the active site, thus allowing R250 and E153 to interact. In contrast, R250 and D247' maintain interactions before and after substrate binding (55, 63).

Our findings from site-directed mutagenesis studies do not support the premise that these residues play important roles in coordinating R250. Kinetic analysis of the E153A and D247A variants yielded only an increase in the K_m for prephenate by ~2 fold or less with a decrease of k_{cat} of approximately one-half, in agreement with a preliminary report by Bonvin (55). More importantly, there were no additive or synergistic effects in prephenate binding for the E153A/D247A variant, although k_{cat} was reduced by over 10-fold. As with other variants studied in this thesis, a decrease in K_m for NAD^+ was also observed which was magnified by the double substitutions.

The most striking observation was the effect of the double substitution in the inhibition of PD activity by L-Tyr. Although the single variants appeared markedly inhibited by the end product, the doubly substituted variant was considerably L-Tyr resistant. In fact, the enzyme reached a plateau with 70% of its activity remaining even at high concentrations of L-Tyr (Figure 13). This pattern of inhibition has also been observed for the T152P variant, a proposed key residue in L-Tyr inhibition. Kinetic inhibition data await further analysis to probe L-Tyr's interaction with the enzyme.

What the heck do these numbers mean?

In this thesis thermodynamic and kinetic solution studies were made to corroborate the results from the crystal structure of Δ19PD. ITC experiments were conducted with NAD^+ and the feedback inhibitor L-Tyr, whereas equilibrium dialysis could only be used to gain information about binding of L-Tyr to the enzyme-NAD^+-complex and the fluorescence quenching assay determined binding of the substrates and the product HPP to the free enzyme.

The dissociation constant for L-Tyr from the enzyme-NAD^+-complex of 0.5 ± 0.02 μM at 20°C and 2.4 ± 0.58 μM at 55°C obtained from ITC indicates that L-Tyr binds tightly to PD from *A. aeolicus* and is in excellent agreement with the K_d of 0.81 ± 0.21 μM obtained by equilibrium dialysis (20°C). Additionally, there was good agreement with the K_d values obtained for the interaction of free enzyme and NAD^+ using ITC (4.9 ± 1.4 μM) and fluorescence quenching (2.4 ± 0.2 μM).

The K_i (83.3 ± 16.6μM) obtained by kinetic inhibition plots for the combination of L-Tyr with the enzyme-NAD^+-complex compares reasonably well with the Michaelis-Menten constant obtained from substrate saturation curves (89.5 ± 9.7 μM) implying that substrate and inhibitor bind with approximately the same affinity to the enzyme. The K_i value determined kinetically appeared to be ~20-fold higher than determined by ITC (2.4 ± 0.58 μM) or equilibrium dialysis (0.81 ± 0.21 μM). It might be that the enzyme resides in a different conformation in the thermodynamic studies or the kinetic data is not fitted to the correct model of inhibition.

Studies in the Turnbull lab (55) and Figure 14 show that double reciprocal kinetic plots varying prephenate with increasing concentrations of L-Tyr were concave upward at lower prephenate concentrations indicating that L-Tyr binds with positive cooperativity but consistent with L-Tyr acting as competitive inhibitor. These deviations from linearity in the double reciprocal plots have also been reported for the PD of *E. coli* and are in keeping with L-Tyr promoting cooperative interactions between the subunits (42, 28, 48). It is worth noting however, that cooperative binding of L-Tyr was not observed by ITC experiments or equilibrium dialysis, but this is likely due to experimental restrictions (e.g. the range of concentrations used). It is worth noting that the crystal structure of

Δ19PD shows only one Tyr binding per monomer and not two as would be expected from the kinetic results. Thus, the solution studies and the crystal structure are not in total agreement.

Recent crystal structures of ligated Δ19PD (63) all identified one molecule of the product, the product analog or L-Tyr bound per dimer, whereas the dimer contained two molecules of NAD^+ or NADH. Christendat speculated that this was not an artefact of the crystallization process which then prompted hypothesis that perhaps NAD^+ binds first to the enzyme followed by prephenate and similarly, HPP is released before NADH leaves the active site. Therefore, the crystal structure indicates that substrate binding and product release follow an ordered kinetic mechanism. This is in contrast to the rapid equilibrium random kinetic mechanism that was proposed from the analysis of initial velocity and dead-end and product inhibition of PD from *E. coli* (42, 63). Data for fluorescence emission quenching showed that NAD^+ or prephenate can combine with the free enzyme (Figure 18) and conform to a random mechanism. However, our data are not consistent with a mechanism that assumes that such binding is in rapid equilibrium relative to a slow catalytic step as our K_m values derived for prephenate and NAD^+ (Table 6) are almost an order of magnitude higher than the K_ds determined thermodynamically. Product and dead-end inhibition studies must be performed to further decipher the kinetic mechanism of Δ19PD.

Clearly, the presence of NAD^+ promotes crystallization through structural changes as no crystal structures of apo-enzyme have been obtained (55). The idea that NAD^+ induces conformational changes in the protein can further be supported by comparing the binding isotherms for the titration of NAD^+ to the free enzyme and L-Tyr to the enzyme-

NAD^+ in which the latter yielded less scattering (Appendix 1A, 1B). We have yet to determine if L-Tyr can bind to the free enzyme. The data from ITC experiments indicate that the binding of NAD^+ and L-Tyr is enthalpy driven. Surprisingly, the enthalpy and entropy changes for L-Tyr to the enzyme-NAD^+-complex and NAD^+ to the free enzyme are similar.

Our ITC and equilibrium dialysis results do not support the crystal structure which shows a stoichiometry of 2:1 NAD^+:Tyr per dimer. The number of binding sites determined for L-Tyr and NAD^+ of 0.1 is unexpectedly low and would be explained if only one in every 10 Δ19PD molecules is in a conformation that can bind a ligand. One could speculate that at 20°C (temperature at which ITC experiments are routinely conducted) the thermophilic enzyme is not very flexible; the enzyme is also much less active at lower temperatures (30). Interestingly, increasing the assay temperature to 55°C did not result in an increase number of binding sites. Therefore, further studies concerning the solution stoichiometry have to be undertaken. It was encouraging to see that at 55°C L-Tyr binds to the enzyme-NAD^+-complex with a K_d that is 5-fold higher than obtained at 20°C. This is consistent with kinetic studies reporting the K_m for prephenate at different temperatures (30). The increase in temperature also coincides with a higher overall decrease of the enthalpy upon binding of L-Tyr to the enzyme-NAD^+-complex and less favourable entropy. Through crystallographic analysis Sun *et. al.* reported that the enzyme in complex with NAD^+ undergoes a global conformational change upon HPP or L-Tyr binding. They also reported that some residues including R250 were ordered and showed excellent electron density <u>only</u> when a second ligand (HPP or L-Tyr) was bound to the enzyme-NAD^+-complex (63). Therefore, the less favourable entropy upon L-Tyr binding could be explained in that Δ19PD's overall conformation is more ordered upon ligand binding. These conformational changes appeared to be even more prominent at higher temperatures as indicated by the differences in binding affinity and entropy obtained at different temperatures.

Chapter 5: Summary and Future Work

We found that even though the apparent binding affinity for prephenate of single replacements at positions 250 and 246 decrease only moderately, the simultaneous substitution of both residues to Ala had an additive effect and nearly eliminated prephenate binding to the variant enzyme. Furthermore, we showed through molecular docking studies that the side chain of K246’ is flexible and that the residue could participate in prephenate binding, also partially assuming the function of R250A in the variant. In addition, K246 and R250 in liaison with K239’ and K169 could help guide the negatively charged prephenate into the active site in a similar mechanism as proposed for AD of *Synechocystis* sp. (36). Site-directed mutagenesis studies also revealed that the replacements of E153 and D247’ individually or together did not disturb prephenate binding significantly, indicating that their interactions with R250 are not required to positioning R250 in a correct orientation. However, the simultaneous conversion of both, E153 and D247’ to Ala affected the enzymes sensitivity to L-Tyr. The pattern of inhibition indicates that the variant conforms to the same inhibition mechanisms as T152P. However, kinetic inhibition data await further analysis to probe L-Tyr’s interaction with the enzyme.

The results of site-directed mutagenesis studies on T152 showed that L-Tyr inhibition cannot be selectively eliminated by disrupting the backbone interaction of T152’s carbonyl group with the amine group of L-Tyr. Moreover we showed that feedback inhibition of T152P by L-Tyr can be assigned to a hyperbolic, competitive mechanism indicative of L-Tyr binding to an allosteric site. In addition, we identified S254A, a variant whose activity was feedback inhibition resistant but bound L-Tyr with similar affinity than native Δ19PD. This supports the idea that L-Tyr binds to a site other than the active site. Double inhibition studies in the presence of HPP and L-Tyr could help to decipher the correct model(s).

In contrast to what was proposed previously, we found that the ionization state of H217 is not critical for feedback inhibition by L-Tyr as our kinetic results show that the inhibition constant (K_i) describing the interaction of the enzyme-NAD$^+$-complex with L-Tyr does not vary over a broad pH range (pH 4 to 9). We, further, assigned the increase in fluorescence emission compared to native Δ19PD to complex structural perturbations, an idea that can be supported by the observed increase in K_m for prephenate and the drastically reduced k_{cat}.

Additional site-directed mutagenesis studies confirmed that the H-bonding network, including S213, H214, H147, S126 and WAT1 is important for prephenate binding as well as catalysis as shown by a decreased apparent affinity for prephenate of S213A and H214L and moderate effects on k_{cat} observed with all conversions at these positions. We also showed that W259Y was considerably less sensitive to feedback inhibition by L-Tyr. Guided by the available crystal structures (Figure 7B) we concluded that any perturbations of the H-bonding network including H217, S254, WAT2 and the amine group of L-Tyr affects the enzyme's sensitivity to feedback inhibition by L-Tyr.

Lastly, for the first time reported, we studied the roles of H205 and D206 in a TyrA protein and determined that H205 is important for the catalytic activity of the enzyme likely by positioning H147 in a correct orientation, while D206 appears critical for the structural integrity of the enzyme. We proposed that D206 is interacting with the backbone amine group of K128 which in turn sustains a H-bonding network with residues near S126 and H147 and which also includes mainly backbone interactions with G146, V127, G125, D123 and that disruption of this H-bonding network could be destabilizing the enzyme.

How is the enzyme inhibited by L-Tyr? Analysis of variant proteins indicates that this is not a simple question to answer; the solution studies and the crystallography are not in agreement. We have shown through the analysis of the variants, however, the importance of combining kinetic and thermodynamic experiments. Three models could be proposed: 1) in both the native enzyme and the variants, L-Tyr combines at an allosteric site, as evidenced through analysis of the T152P and S254A variant. An allosteric site has also been proposed for *E. coli* CM-PD through kinetic data by fitting the data to a variety of models for the interaction with L-Tyr. These models have indicated that prephenate can bind to both the active site and an allosteric site and that the binding of L-Tyr and HPP are anti-synergistic. K_d values of 4.7 ± 0.7 μM for L-Tyr binding in the active site and of 240 ± 70 μM for L-Tyr binding at the allosteric binding site have been determined by double inhibition studies with L-Tyr and HPP (43). 2) an amino acid conversion introduces an alternate binding site on the enzyme for L-Tyr. Thus, the variant could appear insensitive to L-Tyr inhibition but it could still bind L-Tyr. 3) L-Tyr binds only to the active site of one subunit which prevents binding of L-Ty but not prephenate to the other subunit. This would be in accordance with the crystal structure. In that regard, we would have observed negative cooperativity for L-Tyr binding, which our analysis currently does not show

Some immediate experiments that should be performed include: 1) purification of the enzymes by affinity chromatography step using AMP-Sepharose; this should remove a significant portion of the proteins are in a non-productive conformation, that cannot bind ligand and would enhance the stoichiometry data. 2) Kinetic double inhibition studies should be performed in the presence of HPP and L-Tyr to see if both molecules can be on the enzyme at the same time and thereby confirm the existence of an allosteric site. 3) Further ITC studies with selected variants should be performed to determine if other feedback inhibition resistant variants bind L-Tyr.

References

(1) Kaneko, M., Hwang, E. I., Ohnishi, Y., and Horinouchi, S. (2003) Heterologous production of flavanones in *Escherichia coli* : potential for combinatorial biosynthesis of flavonoids in bacteria. *J Ind Microbiol Biotechnol 30*, 456-461.

(2) Rescigno, A., Rinaldi, A. C., and Sanjust, E. (1998) Some aspects of tyrosine secondary metabolism - biochemical and immunohistochemical studies. *Biochem Pharmacol 56*, 1089-1096.

(3) Meganathan, R. (2001) Ubiquinone biosynthesis in microorganisms. *FEMS Microbiol Lett 203*, 131-139.

(4) Moller, B. L., and Conn, E. E. (1979) The biosynthesis of cyanogenic glucosides in higher plants. N-Hydroxytyrosine as an intermediate in the biosynthesis of dhurrin by *Sorghum bicolor* (Linn) Moench. *J Biol Chem 254*, 8575-8583.

(5) Memelink, J. (2004) Putting the opium in poppy to sleep. *Nat Biotechnol 22*, 1526-1527.

(6) Frick, S., and Kutchan, T. M. (1999) Molecular cloning and functional expression of *O*-methyltransferases common to isoquinoline alkaloid and phenylpropanoid biosynthesis. *Plant J 17*, 329-339.

(7) Coggins JR, Abell C, Evans LB, Frederickson M, Robinson DA, Roszak AW and Lapthorn AP, (2003) Experiences with the shikimate-pathway enzymes as targets for rational drug design. *Biochem Soc Trans 31,* 548-552.

(8) Haslam, E. (1974). *The Shikimate Pathway,* Whiley, New York.

(9) Cabrera-Valladares N, Martínez A, Piñero S, Lagunas-Muñoz VH, Tinoco R, de Anda R, Vázquez-Duhalt R, Bolívar F and Gosset G, (2006) Expression of the melA gene from Rhizobium etli CFN42 in *Escherichia coli* and characterization of the encoded tyrosines. *Enzyme and Microbial Technology 38,* 772-779.

(10) Seetharam G and Saville B, (2002) L-DOPA production from tyrosinase immobilized on zeolite. *Enzyme and Microbial Technology 31,* 747-753.

(11) Ikram, U.-H., and Ali, S. (2002) Microbiological transformation of L-Tyr to 3,4-dihydroxyphenyl L-alanine (L-dopa) by a mutant strain of *Aspergillus oryzae* UV-7. *Curr Microbiol 45,* 88-93.

(12) Bourke SL and Kohn J, (2003) Polymers derived from the amino acid L-tyrosine: polycarbonates, polyarylates and copolymers with poly(ethylene glycol). *Adv Drug Deliv Rev 55,* 447-66.

(13) Davis, B. D. (1955) Intermediates in amino acid biosynthesis. *Adv Enzymol Relat Subj Biochem 16*, 247-312.

(14) Sprinson, B. D. (1961) The Biosynthesis of Aromatic Compounds from D-Glucose. *Adv Carbohydrate Chem 15*, 235-270.

(15) Gibson, F., and Pittard, J. (1968) Pathways of biosynthesis of aromatic amino acids and vitamins and their control in microorganisms. *Bacteriol Rev 32,* 465-92.

(16) Polen, T., Krämer, M., Bongaerts, J., Wubbolts, M. and Wendisch, V. F., (2005) The global gene expression response of *Escherichia coli* to L-phenylalanine. *J Biotechnol 115,* 221-37

(17) Gorwrishankar, J. and Pittard, J., (1982) Molecular Cloning of pheR in *Escherichia coli* K-12. *J Bacteriol 152,* 1-6.
(18) Mattern, I.E. and Pittard J. (1971) Regulation of Tyrosine Biosynthesis in *Escherichia coli* K-12: Isolation and Characterization of Operator Mutants. *J Bacteriol, 107,* 8-15.
(19) Yanofsky, C, (1988) Transcription attenuation**.** *J Biol Chem 263,* 609-12.
(20) Ikeda, M., and Katsumata, R. (1992) Metabolic Engineering to Produce Tyrosine or Phenylalanine in a Tryptophan-Producing *Corynebacterium glutamicum* Strain. A*ppl Environ Microbiol 58*, 781-5.
(21) Lütke-Eversloh, T and Stephanopoulos, G, (2005) Feedback inhibition of chorismate mutase/prephenate dehydrogenase (TyrA) of Escherichia coli: generation and characterization of tyrosine-insensitive mutants *Appl Environ Microbiol 71*, 7224-7228.
(22) Patnajk, R., Zoland, R.R., Geen, D. A. and Kraynie, D. F. (2008) L-Tyr production by recombinant *Escherichia coli*: fermentation optimization and recovery. *Biotechnol Bioeng 99*, 741-52.
(23) Olson, M. M., L. J. Templeton, L. J., Suh, W., Youderian, P., Sariaslani, F. S., Gatenby, A. A. and Van Dyk, T. K. (2007). Production of tyrosine from sucrose or glucose achieved by rapid genetic changes to phenylalanine-producing *Escherichia coli* strains. *Appl. Microbiol. Biotechnol. 74*, 1031–40.
(24) Chávez-Béjar, M.I., Lara, A.R., López, H., Hernández-Chávez, G., Martinez, A., Ramírez, O.T., Bolívar, F. and Gosset, G. (2008) Metabolic engineering of Escherichia coli for L-Tyr production by expression of genes coding for the chorismate mutase domain of the native chorismate mutase-prephenate dehydratase and a cyclohexadienyl dehydrogenase from *Zymomonas mobilis*. *Appl Environ Microbiol 74,* 3284-90.
(25) Bonner, C. A., Jensen, R. A., Gander, J. E., and Keyhani, N. O. (2004) A core catalytic domain of the TyrA protein family: arogenate dehydrogenase from *Synechocystis. Biochem J 382*, 279-91.
(26) Song, J., Bonner, C. A., Wolinsky, M., and Jensen, R. A. (2005) The TyrA family of aromatic-pathway dehydrogenases in phylogenetic context. *BMC Biol 3,* 13.
(27) Sampathkumar P and Morrison JF, (1982) Chorismate mutase-prephenate dehydrogenase from *Escherichia coli*. Purification and properties of the bifunctional enzyme. *Biochim Biophys Acta 702,* 204-11.
(28) Christopherson, R. I., and Morrison, J. F. (1985) Chorismate mutase-prephenate dehydrogenase from *Escherichia coli*: positive cooperativity with substrates and inhibitors. *Biochemistry 24*, 1116-21.
(29) Christopherson, R. I., and Morrison, J. F. (1985) Chorismate mutase-prephenate dehydrogenase from *Escherichia coli*: positive cooperativity with substrates and inhibitors. *Biochemistry 24*, 1116-21.
(30) Bonvin, J., Aponte, R. A., Marcantonio, M., Singh, S., Christendat, D., and Turnbull, J. L. (2006) Biochemical characterization of prephenate dehydrogenase from the hyperthermophilic bacterium *Aquifex aeolicus*. *Protein Sci 15*, 1417-32.

(31) Xie, G., Bonner, C. A., and Jensen, R. A. (2000**)** Cyclohexadienyl dehydrogenase from Pseudomonas stutzeri exemplifies a widespread type of tyrosine-pathway dehydrogenase in the TyrA protein family. *Comp Biochem Physiol C Toxicol Pharmacol 125*, 65-83.

(32) Gaines, C. G., Byng, G. S., Whitaker, R. J. and Jensen, R. A. (1982) L-Tyrosine regulation and biosynthesis via arogenate dehydrogenase in suspension-cultured cells of *Nicotiana silvestris* Speg. et Comes. *Planta 156*, 233-40.

(33) Grinter, N. J. (1998) Developing an L-phenylalanine process. *ChemTech 28*, 33-37.

(34) Lim, S., Springstead, J. R., Yu, M., Bartkowski, W., Shroder, I. and Monbouquette, H. G. (2009) Characterisation of a key trifunctional enzyme for aromatic amino acid biosynthesis. *Extremophiles*. *13*,191-98.

(35) Bonner, C. A., Disz, T., Hwang, K., Song, J., Vonstein, V., Overbeek, R., and Jensen, R. A. (2008) Cohesion group approach for evolutionary analysis of TyrA, a protein family with wide-ranging substrate specificities. *Microbiol Mol Biol Rev 72*, 13-53.

(36) Legrand, P., Dumas, R., Seux, M., Rippert, P., Ravelli, R., Ferrer, J. L., and Matringe, M. (2006) Biochemical characterization and crystal structure of *Synechocystis* arogenate dehydrogenase provide insights into catalytic reaction. *Structure 14*, 767-76.

(37) Hyung-Keun Ku, H.K., Park, S.R., Yang, I. and Kim, S.K. (2010) Expression and functional characterization of prephenate dehydrogenase from *Streptococcus mutans. Process Biochem 45, 607–12.*

(38) Xu, S., Yang, Y., Jin, R., Zhang, M. and Wang, H. (2006) Purification and characterization of a functionally active *Mycobacterium tuberculosis* prephenate dehydrogenase. *Protein Expr Purif 49*, 151-8.

(39) Zhao, G., Xia, T., Ingram, L. O., and Jensen, R. A. (1993) An allosterically insensitive class of cyclohexadienyl dehydrogenase from *Zymomonas mobilis*. *Eur J Biochem 212*, 157-65.

(40) Chen, S., Vincent, S., Wilson, D. B., and Ganem, B. (2003) Mapping of chorismate mutase and prephenate dehydrogenase domains in the *Escherichia coli* T-protein. *Eur J Biochem 270*, 757-63.

(41) Xia, T., Zhao, G., Fischer, R. S., and Jensen, R. A. (1992) A monofunctional prephenate dehydrogenase created by cleavage of the 5' 109 bp of the tyrA gene from *Erwinia herbicola*. *J Gen Microbiol 138*, 1309-1316.

(42) Turnbull J, Cleland WW and Morrison JF, (1990) Chorismate mutase-prephenate dehydrogenase from *Escherichia coli*. 1. Kinetic characterization of the dehydrogenase reaction by use of alternative substrates. *Biochemistry 29*, 10245-54.

(43) Turnbull J, Morrison JF and Cleland WW, (1991) Kinetic studies on chorismate mutase-prephenate dehydrogenase from *Escherichia coli*: models for the feedback inhibition of prephenate dehydrogenase by L-tyrosine. *Biochemistry 30*, 7783-88

(44) Turnbull, J., Cleland, W. W., and Morrison, J. F. (1991) pH dependency of the reactions catalyzed by chorismate mutase-prephenate dehydrogenase from *Escherichia coli*. *Biochemistry 30*, 7777-82.

(45) Christendat, D., and Turnbull, J. L. (1996) Identification of active site residues of chorismate mutase-prephenate dehydrogenase from *Escherichia coli*. *Biochemistry 35*, 4468-79.
(46) Christendat, D., Saridakis, V. C., and Turnbull, J. L. (1998) Use of site-directed mutagenesis to identify residues specific for each reaction catalyzed by chorismate mutase-prephenate dehydrogenase from *Escherichia coli*. *Biochemistry 37*, 15703-12.
(47) Christendat, D., and Turnbull, J. L. (1999) Identifying groups involved in the binding of prephenate to prephenate dehydrogenase from *Escherichia coli*. *Biochemistry 38*, 4782-93.
(48) Hudson, G. S., Howlett, G. J., and Davidson, B. E. (1983) The binding of tyrosine and NAD^+ to chorismate mutase/prephenate dehydrogenase from *Escherichia coli* K12 and the effects of these ligands on the activity and self-association of the enzyme. Analysis in terms of a model. *J Biol Chem 258*, 3114-20.
(49) Hudson, G. S., and Davidson, B. E. (1984) Nucleotide sequence and transcription of the phenylalanine and tyrosine operons of *Escherichia coli* K12. *J Mol Biol 180*, 1023-51.
(50) Turnbull, J., and Morrison, J. F. (1990) Chorismate mutase-prephenate dehydrogenase from *Escherichia coli*. 2. Evidence for two different active sites. *Biochemistry 29*, 10255-61.
(51) Quashie, P. K. (2010) MSc. Thesis, Department of Chemistry and Biochemistry, Concordia University, Montreal, Canada.
(52) Hermes, J. D., Tipton, P. A., Fisher, M. A., O'Leary, M. H., Morrison, J. F., and Cleland, W. W. (1984) Mechanisms of enzymatic and acid-catalyzed decarboxylations of prephenate. *Biochemistry 23*, 6263-75.
(53) Xie G, Keyhani, N. O., Bonner, C. A. and Jensen, R. A. (2003) Ancient origin of the tryptophan operon and the dynamics of evolutionary change. *Microbiol Mol Biol Rev 67(3),* 303-342.
(54) Christopherson R.I. (1985) Chorismate mutase-prephenate dehydrogenase from Escherichia coli: cooperative effects and inhibition by L-tyrosine. *Arch Biochem Biophys 240(2)*, 646-654.
(55) Bonvin, J. (2008) PhD thesis, Department of Chemistry and Biochemistry, Concordia University, Montreal, Canada.
(56) Hassounah S. (2009) MSc. thesis, Department of Chemistry and Biochemistry, Concordia University, Montreal, Canada.
(57) Sun, W., Singh, S., Zhang, R., Turnbull, J. L., and Christendat, D. (2006) Crystal structure of prephenate dehydrogenase from *Aquifex aeolicus*. Insights into the catalytic mechanism. *J Biol Chem 281*, 12919-28.

(58) Chiub H., Abdubek P., Astakhova T., Axelrod H. L., Carlton D., Clayton T., DasD. Deller M.C., Duan L., Feuerhelm J., Grant J. C., Grzechnik A., Han G. W., Jaroszewski L., Jin K. K., Klock H. E., Knuth M. W., Kozbial P., Krishna S. S., Kumar A., Marciano D., McMullan D., Miller M. D., Morse A.T., Nigoghossian E., Okach L., Reyes R., Tien H. J., Trame C. B., van den Bedem H., Weekes D., Xu Q., Hodgson K. O., Wooley J., Elsliger M., Deacon A. M., Godzik A., Lesleyb S.A., Wilsonb I. A. (2010) The structure of *Haemophilus influenza* prephenate dehydrogenase suggests unique features of bifunctional TyrA enzymes *Acta Crystallogr F F66:* 1317–25.

(59) Deckert, G., Warren, P. V., Gaasterland, T., Young, W. G., Lenox, A. L., Graham, D. E., Overbeek, R., Snead, M. A., Keller, M., Aujay, M., Huber, R., Feldman, R. A., Short, J. M., Olsen, G. J., and Swanson, R. V. (1998) The complete genome of the hyperthermophilic bacterium *Aquifex aeolicus*. *Nature 392*, 353-8.

(60) Sitaras, N. (2009) CHEM 450 thesis, Department of Chemistry and Biochemistry, Concordia University, Montreal, Canada.

(61) Hou, W. (2009) MSc. thesis. Department of Chemistry and Biochemistry, Concordia University, Montreal, Canada.

(62) DeLano, W. L. (2002) in *The PyMOL Molecular Graphics System*, San Carlos, CA.

(63) Sun, W., Shahinas, D., Bonvin, J., Hou, W., Kimber, M.S., Turnbull, J. and Christendat, D. (2009) The crystal structure of *Aquifex aeolicus* prephenate dehydrogenase reveals the mode of tyrosine inhibition. *J Biol Chem 284(19),* 13223-32.

(64) Rieger, C. E., and Turnbull, J. L. (1996) Small scale biosynthesis and purification of gram quantities of chorismic acid. *Prep Biochem Biotechnol 26*, 67-76.

(65) Dudzinski, P. K., Morrison, J. F. (1976) The Preparation and Purification of Sodium Prephenate. *Prep Biochem 6*, 113-21.

(66) Dawson, C. M. R., Elliott, C. D., Elliot, H. W. and Jones, M. K. (1986) *Data for Biochemical Research*, 3rd edition ed., Oxford Science Publications, Clarendon Press.

(67) Turnbull, J. L. (1988), PhD thesis, Australian National University, Canberra, Australia.

(68) Rozen, S., Skaletsky, H.J. (2000) Primer3 on the WWW for general users and for biologist programmers, in *Bioinformatics Methods and Protocols: Methods in Molecular Biology* pp 365-386, Humana Press, Totowa, NJ.

(69) Bradford, M. (1976) A rapid and sensitive method for the quantitation of microgram quantities of protein utilizing the principle of protein-dye binding *Analytical Biochemistry 72*, 248-54.

(70) NCCLS Approved Standard ACS-1 (1979) *Specification for Standardized Protein Solution (Bovine Serum Albumin)*, 2nd ed., National Committee for Clinical Laboratory Standards: Villanova, PA.

(71) Sambrook, J., Russell, D. (2001) *Molecular Cloning*, 3rd ed., Cold Spring Harbor Laboratory Press, Cold Spring, New York.

(72) Besir, H. (2008) Coomassie ohne Alkohol und Essig. *Laborjournal online*, http://www.laborjournal.de/rubric/tricks/tricks/trick121.lasso
(73) Weinglass, A. B., Whitelegge, J. P., Hu, Y., Verner, G. E., Faull, K. F., and Kaback, H. R. (2003) *Elucidation of substrate binding interactions in a membrane transport protein by mass spectrometry*. *EMBO J 22*, 1467-77.
(74) Segel, I. H. (1975) *Enzyme Kinetics: Behavior and Analysis of Rapid Equilibrium and Steady-State Enzyme Systems*.John Wiley & Sons, USA.
(75) Lakowicz, J. R. (1999) *Principles of Fluorescence Spectroscopy*, Kluwer Academic/Plenum, New York.
(76) Engel, P. C. (1996) *Enzymology*, Bio Scientific Publishers, Oxford, UK.
(77) Khalil, S., and Pawelek, P.D. (2010) "A Protein-Protein Interaction Facilitates Conformational Remodeling of the *Escherichia coli* 2,3-dihydroxybenzoate-AMP ligase (EntE) Active Site by 2,3-dihydro-2,3-dihydroxybenzoate Dehydrogenase (EntA)", Manuscript in Preparation.
(78) Hardin, S.E. and Chowdhry, B.Z. (2001) *Protein-Ligand Interactions: hydrodynamics and calorimetry*, Oxford University Press Inc., New York.
(79) Lamoureux, G. (2010) CHEM 498Q / CHEM 630Q: Molecular Modeling of Proteins TUTORIAL #5: Molecular Docking, Department of Chemistry and Biochemistry, Concordia University, Montréal, Canada.
(80) Schmid, F. X. (1998) *Spectral methods of characterizing protein conformation and conformational changes*, TE Creighton edition IRL press, Oxford, UK.
(81) Harding S.E., Chowdhry B.Z., (2001) *Protein-ligand interactions: hydrodynamics and calorimetry : a practical approach*, Oxford University Press.
(82) Trott, O. and Olson, A.J. (2010) Auto-Dock Vina: Improving the speed and accuracy of docking with a new scoring function, efficient optimization and multithreading. *J Comp Chem. 31*, 455-61.
(83) Armstrong, C. (2009) CHEM 450 thesis. Department of Chemistry and Biochemistry, Concordia University, Montréal, Canada.

Appendix 1A

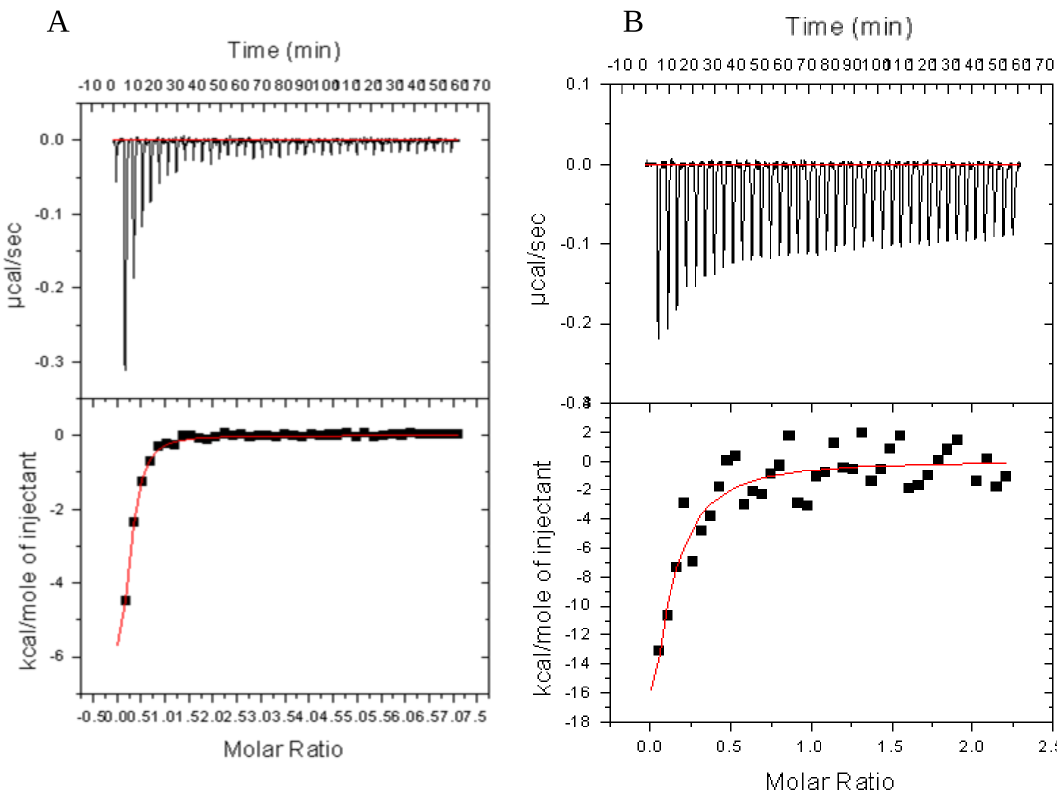

Figure 25: Isothermal titration calorimetry analysis of the interaction of (A) the S254A-NAD$^+$ -complex with L-Tyr and (B) native Δ19PD with NAD$^+$ in 50 mM KH_2PO_4 / K_2HPO_4, 75 mM NaCl, pH 7.5 at 20 °C. The initial concentration of S254A and native enzyme in the cell were 27µM and 20µM, respectively, while the initial ligand concentrations in the syringe were 250 µM. The upper panels are raw data of enthalpy changes, each peak corresponding to each injection of prephenate or NAD$^+$ (first injection 1 µl, subsequent 39 injections 7 µl) to the enzyme or enzyme-NAD$^+$-complex. The lower panels show the integrated enthalpy plot. The areas under each peak were integrated and plotted against the molar ratio. The red solid line is the best fit of the data to the one-binding-site model of the Origin® plotting software from MicroCal.

Appendix 1B

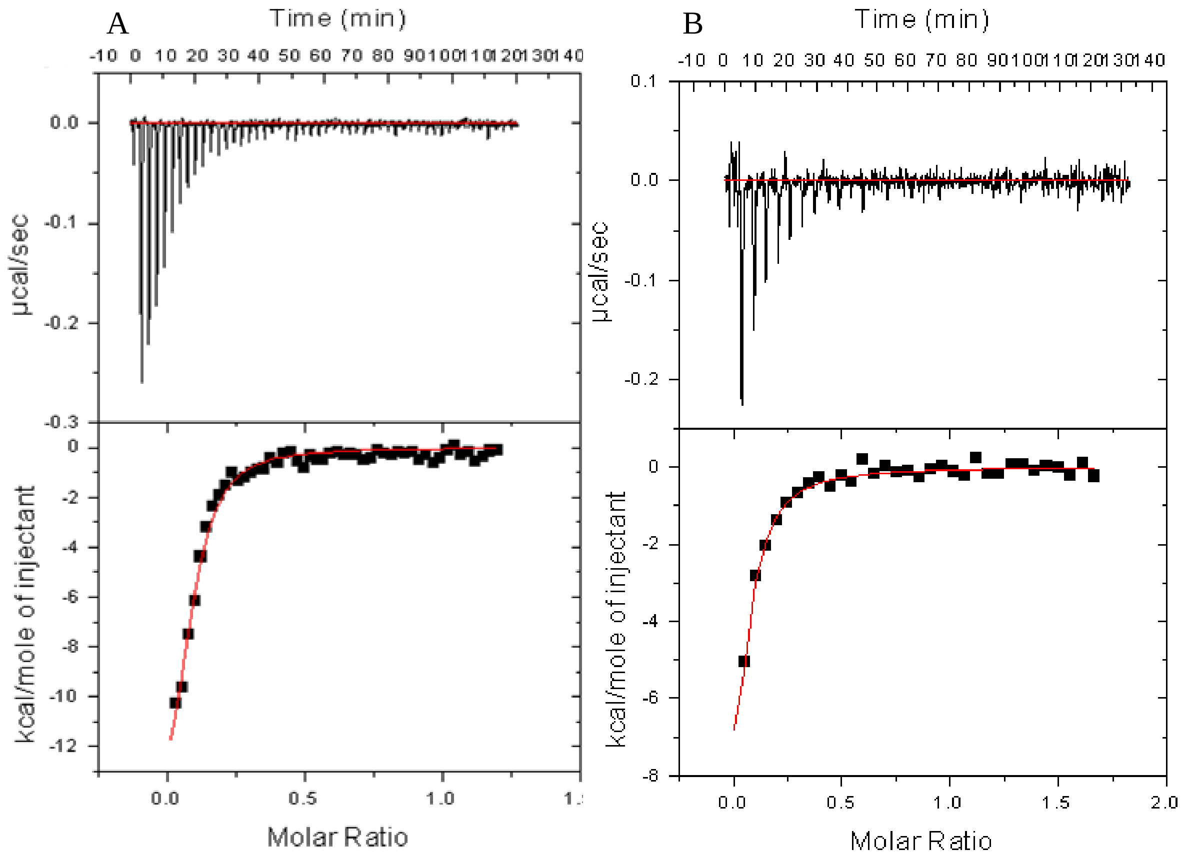

Figure 26: Isothermal titration calorimetry analysis of the interaction of the native Δ19PD-NAD$^+$ -complex with L-Tyr at (A) 20°C and (B) 55°C in 50 mM KH_2PO_4 / K_2HPO_4, 75 mM NaCl, pH 7.5. The initial concentration of native enzyme in the cell were 20µM at 20°C and 27µM at 55°C, while the initial ligand concentrations in the syringe were 500µM and 250 µM, respectively. The upper panels are raw data of enthalpy changes, each peak corresponding to each injection of L-Tyr (first injection 1 µl, subsequent 39 injections 7 µl) to the enzyme-NAD^{+-}complex. The lower panels show the integrated enthalpy plot. The areas under each peak were integrated and plotted against the molar ratio. The red solid line is the best fit of the data to the one-binding-site model of the Origin® plotting software from MicroCal.

Appendix 1C

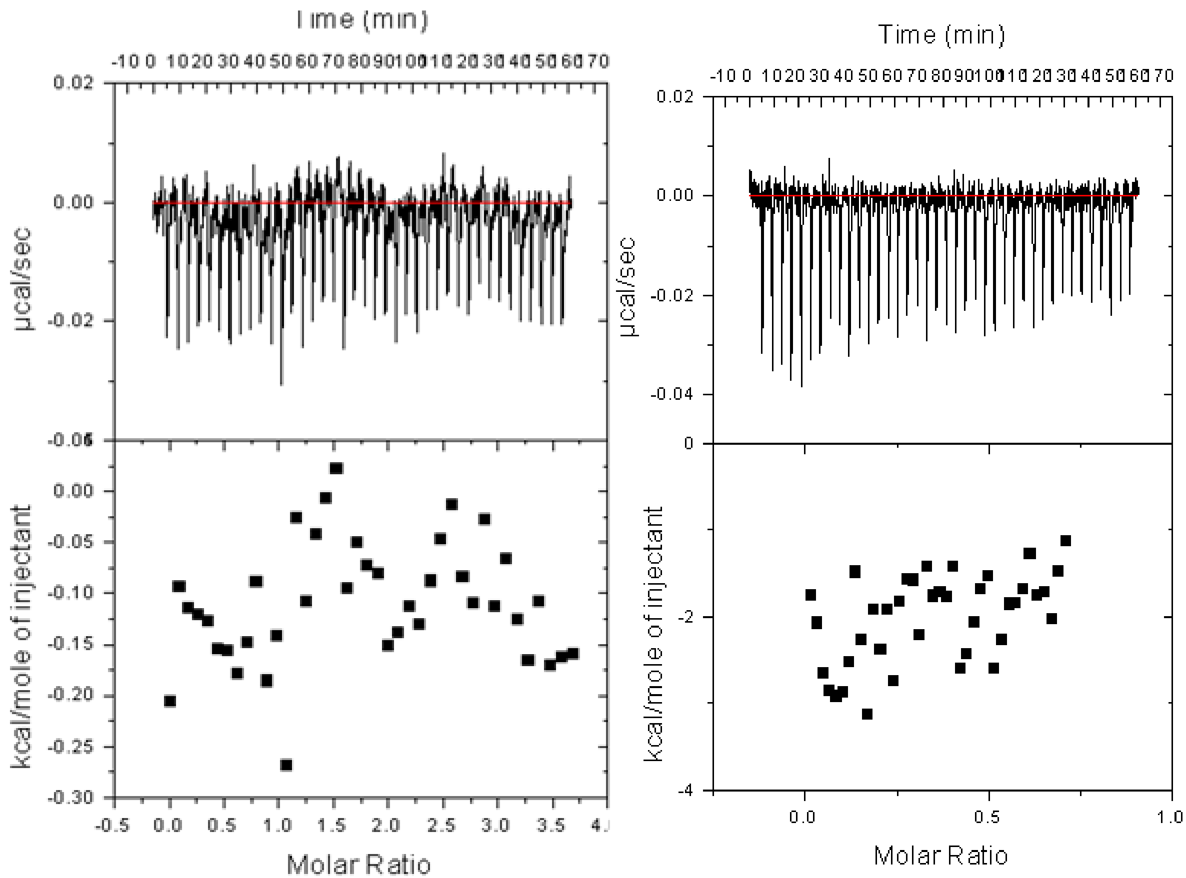

Figure 27: Isothermal titration calorimetry analysis of the interaction of (A) the Δ19PD H217A -NAD$^+$ -complex and (B) the R250A/K246A-NAD+-complex with L-Tyr in 50 mM KH_2PO_4 / K_2HPO_4, 75 mM NaCl, pH 7.5 at 20°C. The initial concentrations of R250A/K246A and H217A in the cell were 28µM and 63µM, respectively, while the initial ligand concentration in the syringe was 1000 µM for both. The upper panels are raw data of enthalpy changes, each peak corresponding to each injection of L-Tyr (first injection 1 µl, subsequent 39 injections 7 µl) to the enzyme-NAD^{+}-complex. The lower panels show the integrated enthalpy plot. The areas under each peak were integrated and plotted against the molar ratio. The red solid line is the best fit of the data to the one-binding-site model of the Origin® plotting software from MicroCal.

Appendix 1D

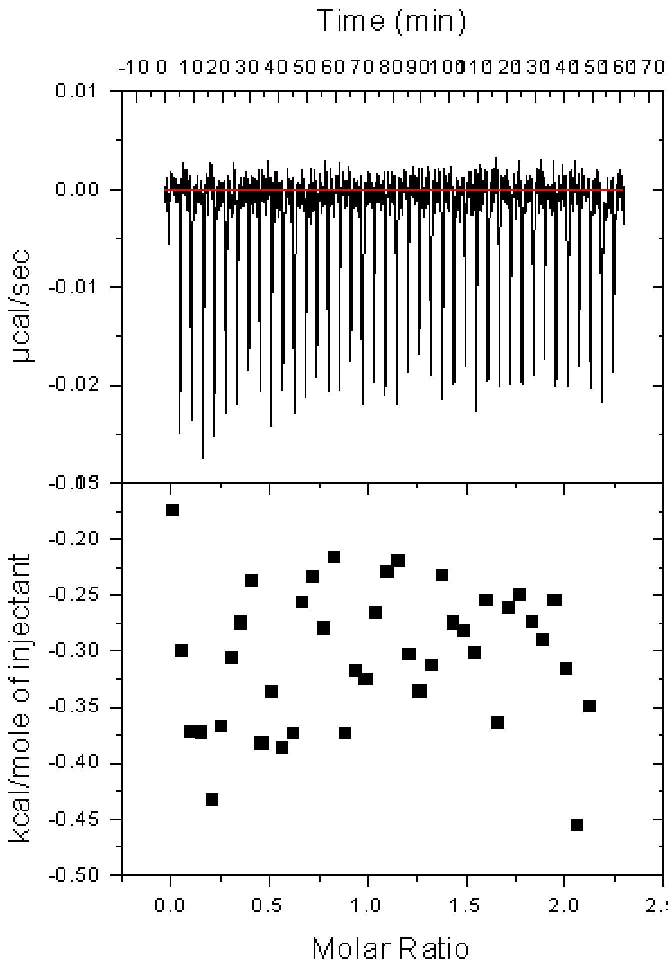

Figure 28: Isothermal titration calorimetry analysis of the interaction of the Δ19PD H147A -NAD$^+$ -complex with L-Tyr in 50 mM KH_2PO_4 / K_2HPO_4, 75 mM NaCl, pH 7.5 at 20°C. The initial concentration of H147A in the cell was 27µM, while the initial ligand concentration in the syringe was 250 µM for both.The upper panels are raw data of enthalpy changes, each peak corresponding to each injection of L-Tyr (first injection 1 µl, subsequent 39 injections 7 µl) to the enzyme-NAD^{+-}complex. The lower panels show the integrated enthalpy plot. The areas under each peak were integrated and plotted against the molar ratio. The red solid line is the best fit of the data to the one-binding-site model of the Origin® plotting software from MicroCal.